CHARACTERIZATION OF THERMAL PROPERTIES OF DEPLETED URANIUM METAL MICROSPHERES

A Thesis

by

CARISSA JOY HUMRICKHOUSE

Submitted to the Office of Graduate Studies of
Texas A&M University
in partial fulfillment of the requirements for the degree of

MASTER OF SCIENCE

May 2012

Major Subject: Nuclear Engineering

CHARACTERIZATION OF THERMAL PROPERTIES OF DEPLETED URANIUM METAL MICROSPHERES

A Thesis

by

CARISSA JOY HUMRICKHOUSE

Submitted to the Office of Graduate Studies of
Texas A&M University
in partial fulfillment of the requirements for the degree of

MASTER OF SCIENCE

Approved by:

Chair of Committee,	Sean M. McDeavitt
Committee Members,	Kenneth L. Peddicord
	Lin Shao
Head of Department,	Yassin A. Hassan

May 2012

Major Subject: Nuclear Engineering

ABSTRACT

Characterization of Thermal Properties of Depleted Uranium Metal Microspheres.

(May 2012)

Carissa Joy Humrickhouse, B.A. Physics, Whitworth University

Chair of Advisory Committee: Dr. Sean M. McDeavitt

Nuclear fuel comes in many forms; oxide fuel is the most commonly used in current reactor systems while metal fuel is a promising fuel type for future reactor systems due to neutronic performance and increased thermal conductivity. As a key heat transfer parameter, thermal conductivity describes the heat transport properties of a material based upon the density, specific heat, and thermal diffusivity. A material's ability to transport thermal energy through its structure is known as thermal diffusivity; the units for thermal diffusivity are given in area per unit time (e.g., m^2/s).

Current measurement methods for thermal diffusivity include Laser (or Light) Flash Analysis (LFA) and the hot-wire method. This study examines an approach that combines these previous two methods to characterize the diffusivity of a packed bed of microspheres of depleted uranium (DU) metal, which have a nominal diameter of 250 micrometers. The new apparatus is designated as the Crucible Heater Test Assembly (CHTA), and it induces a radial transient across a packed sample of microspheres then monitors the temperature profile using an array of thermocouples located at different distances from the source of the thermal transient. From the thermocouple data and an accurate time log, the thermal diffusivity of the sample may be calculated. Results indicate that DU microspheres have very low thermal conductivity, relative to solid uranium metal, and rapidly form an oxidation layer. At 500°C, the thermal conductivity of the DU microspheres was 0.431±13% W/m-K

compared to approximately 32 W/m-K for solid uranium metal. Characterization of the developed apparatus revealed a method that may be useful for measuring the thermal diffusivity of powders and liquids.

This thesis is dedicated to all the family members who have supported me throughout the completion of this research undertaking and have invested time in listening to science-talk. To my fiancé, Grant, thank you for being my sounding-board in and out of the lab.

ACKNOWLEDGMENTS

Dr. McDeavitt has demonstrated great skill in directing the research efforts within the FCML. His practical laboratory dexterity was essential in the design of the apparatus developed throughout this body of work; an attribute of his that I appreciate greatly. This research was supported, both financially and technically, by TerraPower, LLC through a contract with Texas A&M University. An additional thanks is due to Kevan Weaver, Josh Walter, Pavel Hejzlar, and the fuel development team at TerraPower. To Dr. Shao and Dr. Peddicord, thank you for serving on my committee, I greatly appreciate the time you've dedicated.

NOMENCLATURE

α	Thermal diffusivity (units: mm^2/s)
c_p	Specific heat (units: J/kg/K)
κ	Thermal conductivity (units: W/m-K)
ρ	Density (units: g/cm^3)
CHTA	Crucible Heater Test Assembly
DU	Depleted uranium
EU	Enriched uranium
LFA	Laser (or light) flash analysis
LFA 447	Light flash analyzer, model 447, by Netzsch Instruments
LWR	Light water reactor
ODU	Oxidized depleted uranium
PID	Proportional-Integral-Derivative controller for heater system
SS	Stainless steel, various types, commonly either 316 or 304
TWR	Travelling wave reactor
WDU	Washed depleted uranium

GLOSSARY

Band heater	An outer heater in the CHTA that clamps around the crucible.
Cartridge heater	The central heater in the CHTA; the diameter of the heater is 0.32 cm (1/8").
Microsphere	Material in ball form that has a diameter of 200-400 μm.
Test run	A single test with a sample of microspheres in the CHTA.
Test series	A collection of test runs that are related, e.g., tests performed at the same maximum temperature.

TABLE OF CONTENTS

Page

ABSTRACT iii

DEDICATION v

ACKNOWLEDGMENTS vi

NOMENCLATURE vii

GLOSSARY viii

TABLE OF CONTENTS ix

LIST OF TABLES xi

LIST OF FIGURES xii

1 INTRODUCTION 1

1.1 Scope of Work 2

2 BACKGROUND 5

2.1 Thermal Energy Transfer 6
2.1.1 Thermal Conductivity 8
2.2 Thermal Conductivity Measurement Methods 11
2.2.1 Indirect Measurement 12
2.2.2 Direct Measurement 17
2.2.3 Modeling 19
2.3 Nuclear Fuel Materials and Forms 21
2.3.1 Metal Fuel 22
2.3.2 Microspheres 23

3 EXPERIMENTAL METHOD 26

3.1 Light Flash Analysis Method 26
3.1.1 LFA Procedures 28
3.2 Crucible Heater Test Assembly 30
3.2.1 CHTA Design Details 31
3.2.2 Implementation of the CHTA 41
3.2.3 Data Analysis Method 45

Page
3.2.4 Systematic Uncertainty 48

4 RESULTS 49

4.1 Light Flash Analysis Data 49
4.2 Crucible Heater Test Assembly 50
4.2.1 Program Effects 52
4.2.2 Data from ODU Microspheres 53
4.2.3 Data from WDU Microspheres 58

5 DISCUSSION 80

5.1 Interpretation of LFA Data 80
5.1.1 LFA Challenges 81
5.2 Interpretation of the CHTA Method 82
5.2.1 Range of Analyzable Data 82
5.2.2 Interpretation of the ODU Microsphere Data 83
5.2.3 Interpretation of WDU Microsphere Data 86
5.2.4 Comparison of ODU and WDU Data from the CHTA Method 97
5.2.5 CHTA Challenges 102
5.3 Comparison of CHTA to LFA 104
5.4 Thermal Conductivity Calculations 104
5.5 Thermal Conductivity Interpretation 105
5.6 Error Sources 110

6 SUMMARY 111

REFERENCES 114

APPENDIX A OPTICAL MICROSCOPE IMAGES OF MICROSPHERES. . 117

A.1 WDU Microspheres 117
A.2 LFA Microspheres 118

VITA 122

LIST OF TABLES

TABLE Page

2.1 Literature values for thermal properties of solid uranium metal. 15

2.2 Approximate thermal conductivity values for UO_2 microspheres [30], values for solid UO_2 from [35]. 21

3.1 Products ordered for the CHTA. 36

3.2 Thermocouple placements in the CHTA. 39

4.1 Tests performed using the CHTA. 51

5.1 Key thermal properties of WDU microspheres (Series B, Test 15). 106

LIST OF FIGURES

FIGURE Page

2.1 Literature values of specific heat capacity for solid uranium metal. 13

2.2 Interpolated values of density for solid uranium metal. 14

2.3 Literature values of thermal conductivity for solid uranium metal. 16

2.4 Calculated values of thermal diffusivity for solid uranium metal. 17

3.1 A cut-away view of the LFA 447 by Netzsch Instruments [33]. 27

3.2 Powder and liquid sample holder for LFA. 28

3.3 CHTA configuration as designed in the FCML, all dimensions are in cm. 32

3.4 Outside view of the CHTA, all dimensions are in inches. 33

3.5 Photograph of the CHTA in the glovebox. 34

3.6 Assembled CHTA before installation in the glovebox. 35

3.7 Detailed CHTA schematic showing cartridge heater heated region. 37

3.8 The bottom stainless steel insert designed for the CHTA, all dimensions are in inches; also shown is cartridge heater guide tube. 38

3.9 The top stainless steel insert designed for the CHTA, all dimensions are in inches; the holes are drilled for thermocouple insertion. 39

3.10 The bottom portion of the lid with troughs designed to secure thermocouples in specified positions (see Table 3.2) all dimensions are given in cm. 40

3.11 Two part lid system designed for use with the CHTA, all dimensions are given in inches. 41

3.12 Detailed two part lid system designed for use with the CHTA, all dimensions are given in inches. 41

FIGURE Page

3.13 Photograph of the CHTA data collection sytem outside of the glovebox. . 42

3.14 Sample data test from CHTA. 45

3.15 Interpolated sample data test from CHTA. 46

4.1 Thermal diffusivity vs. temperature measurements using the LFA powder sample holder and ODU microspheres; the notable change at 125°C indicates a possible change in test material. 50

4.2 Maximum CHTA system ramp rate achievable by the central cartridge heater; data from Series B, Test 15. 53

4.3 Time dependent temperature data from CHTA testing, Series A, Test 2. 55

4.4 Time dependent temperature data from CHTA testing, Series A, Test 3. The cartridge heater temperature is shown in green, with an orange vertical dashed line signifying the point at which the cartridge heater stopped ramping at the rate of 20°C. 56

4.5 Time dependent temperature data from CHTA testing, Series A, Test 5. 57

4.6 Time dependent temperature data from CHTA testing, Series A, Test 5 with analysis regions shown. 58

4.7 Time dependent temperature data from CHTA testing, Series A, Test 6. Cartridge heater temperature is shown in green with an orange vertical dashed line when the cartridge heater stopped ramping 59

4.8 Time dependent temperature data from CHTA testing, Series A, Test 8. 60

4.9 Time dependent temperature data from CHTA testing, Series A, Test 8 with analysis regions shown. 61

4.10 Time dependent temperature data from CHTA testing, Series A, Test 9. Cartridge heater temperature is shown in green with an orange vertical dashed line when the cartridge heater stopped ramping. 62

4.11 Time dependent temperature data from CHTA testing, Series B, Test 1. 63

FIGURE Page

4.12 Time dependent temperature data from CHTA testing, Series B, Test 2. 64

4.13 Time dependent temperature data from CHTA testing, Series B, Test 3. 65

4.14 Time dependent temperature data from CHTA testing, Series B, Test 4. 66

4.15 Time dependent temperature data from CHTA testing, Series B, Test 5. 67

4.16 Time dependent temperature data from CHTA testing, Series B, Test 6. 68

4.17 Time dependent temperature data from CHTA testing, Series B, Test 7. 69

4.18 Time dependent temperature data from CHTA testing, Series B, Test 8. 70

4.19 Time dependent temperature data from CHTA testing, Series B, Test 9. 71

4.20 Time dependent temperature data from CHTA testing, Series B, Test 10. 72

4.21 Time dependent temperature data from CHTA testing, Series B, Test 11. 73

4.22 Time dependent temperature data from CHTA testing, Series B, Test 12. 74

4.23 Time dependent temperature data from CHTA testing, Series B, Test 12 with regions of data analysis shown. 75

4.24 Time dependent temperature data from CHTA testing, Series B, Test 13. 76

4.25 Time dependent temperature data from CHTA testing, Series B, Test 14. 77

4.26 Time dependent temperature data from CHTA testing, Series B, Test 15. 78

4.27 Time dependent temperature data from CHTA testing, Series B, Test 15 with regions of data analysis shown. 79

5.1 Time-Temperature information for a ramp rate of 20°C/min with a maximum temperature of 350°C. The shaded regions represent the range of analyzable (after dashed line) and questionable (before dashed line) data. 83

FIGURE Page

5.2 Time-Temperature information for a ramp rate of 10°C/min with a maximum temperature of 350°C. The shaded regions represent the range of analyzable (after dashed line) and questionable (before dashed line) data. 84

5.3 Time-Temperature information for a ramp rate of 20°C/min with a maximum temperature of 650°C. The shaded regions represent the range of analyzable (after dashed line) and questionable (before dashed line) data. 85

5.4 Time-Temperature information for a ramp rate of 150°C/min with a maximum temperature of 650°C. The shaded regions represent the range of analyzable (after dashed line) and questionable (before dashed line) data. 86

5.5 ODU data for maximum temperature of 350°C (Test Series A, Tests 2, 5, and 8). 87

5.6 ODU data for maximum temperature of 450°C (Test Series A, Tests 3, 6, and 9). 88

5.7 Extrapolation of ODU microspheres data (Series A). 89

5.8 WDU data for maximum temperature of 350°C (Series B, Tests 2, 5, and 9). 90

5.9 WDU data for maximum temperature of 450°C (Series B, Tests 3, 4, 6, and 10). 91

5.10 WDU data for maximum temperature of 550°C (Series B, Tests 7, 8, and 11). 92

5.11 WDU data for maximum temperature of 650°C (Series B, Tests 12 to 15). 93

5.12 Extrapolated thermal diffusivity for WDU. 94

5.13 WDU data for a ramp rate of 20°C/min (Series B, Test 1, 2, 3, 7, and 12). 95

5.14 WDU data for a ramp rate of 60°C/min (Series B, Test 9, 10, 11, and 14). 96

5.15 Uncertainty in thermal diffusivity measurement (Series B, Test 15). . . . 97

FIGURE Page

5.16 WDU and ODU data for a maximum temperature of 350°C (Series A, Test 5 and Series B, Tests 1 and 2). 101

5.17 WDU and ODU data for a maximum temperature of 450°C (Series A, Test 6 and Series B, Tests 3 and 4). 102

5.18 Extrapolation of data from ODU and WDU test cases. 103

5.19 Comparison of data from the CHTA and LFA methods. 105

5.20 Calculated thermal conductivity of WDU microspheres (Series B, Test 15).107

5.21 Thermal conductivity of WDU and UO_2 [29] microspheres. 108

5.22 Thermal conductivity of solid U metal [13] and UO_2 [35]. 109

A.1 Low magnification microscope image of WDU microspheres after testing was completed in the CHTA. 117

A.2 Low magnification microscope image of WDU microspheres after testing was completed in the CHTA. 118

A.3 High magnification microscope image of WDU microspheres after testing was completed in the CHTA. 119

A.4 Low magnification microscope image of ODU microspheres after testing was completed in the LFA; these microspheres were not used in any further testing. 120

A.5 High magnification microscope image of ODU microspheres after testing was completed in the LFA; these microspheres were not used in any further testing. 121

1. INTRODUCTION

Thermal transport through nuclear fuel is a key fuel performance issue in reactor design which impacts the overall capabilities of the system and limits the ultimate power output. Most reactors typically use solid fuel pellets or rods, comprised of either uranium dioxide or uranium metal alloys. These fuel materials pose challenges for the structural materials within the reactor as the operating time and power increase. Alternate fuel forms have been studied in the past and have shown promise in reducing the interactions between the uranium fuel and the reactor's structural material; one such form is particulate fuel. In the 1960's, research was conducted on uranium dioxide particulate fuel to analyze the thermal transport properties and the feasibility of this material in the reactor systems of that time period [1].

As reactor designs have improved and innovations continue to be explored, a renewed interest has been garnered in particulate fuel. A new fast reactor concept called the Travelling Wave Reactor (TWR) is under development by TerraPower, LLC (Bellevue, WA) and one of the early fuel designs under consideration was a particulate fuel comprised of packed rods of uranium alloy microspheres (!!!!!). This preliminary design of the TWR particulate pin was composed of microspheres with a nominal diameter between 200 and 500 μm, and the intent was to have a packing density between 50 and 75% with open void space either filled with liquid sodium or inert gas.

As with all nuclear fuels, it is important to characterize the thermal transport properties of the packed microspheres in order to accurately predict the thermal behavior of the fuel form and develop a well-designed reactor system. For this reason, thermal conductivity is a critical figure of merit for nuclear fuel. Thermal conductivity (typical units: W/m-K) is a measure of a material's ability to conduct thermal

This thesis follows the style of the Journal of Nuclear Materials.

energy (W) over a distance in the material (m) at a given temperature (K) and it is directly related to the thermal diffusivity, density, and specific heat of a material. Thermal diffusivity can be determined using an established method known as Laser Flash Analysis (LFA) for thin, solid samples, packed powders, and liquids with known sample dimensions. Density is readily calculated if accurate sample dimensions and mass are available, or, volumetrically by utilizing liquid displacement. There are several methods to measure the specific heat of a sample; one of which is differential scanning calorimetry.

Complications were expected with the established methods of determining thermal diffusivity, density, and specific heat, due to slight inconsistencies in packing factor and sample geometry. To overcome these complications, an alternate method was developed for this study to characterize the diffusivity of a packed bed of microspheres. A significant issue facing the use of this new method is that uranium metal will oxidize in an atmosphere containing oxygen and so the experimental development of this new method was accomplished inside of a controlled atmosphere glovebox. It was planned to use sodium metal as a liquid to fill the voids; this required the system to be maintained at a temperature greater than sodium's melting point. In order to obtain an accurate depiction of thermal transients within the system, thermocouples were needed at strategic locations. Previous methods used to determine thermal diffusivity relied upon a sudden temperature spike and the propagation of this temperature gradient across the sample. It was decided that the new system would need at least two heaters and an array of thermocouples located at precise positions (see section 3.2.1 for a description of the new experimental system).

1.1 Scope of Work

This body of work includes measurements with a Light Flash Analyzer (LFA) for depleted uranium microspheres. The LFA in the FCML is a Netzsch LFA 447 and is capable of measurements from room temperature to 300°C. Data collected

via the LFA was used solely for thermal diffusivity values. Several limitations were anticipated with use of the LFA system due to the limited temperature range and the open air atmosphere of the sample holder. Due to these limitations, the new method mentioned above was devised to measure the thermal diffusivity of uranium microspheres under an argon environment and at temperatures up to 700°C. This new system needed to have a greater temperature range than the LFA, be compatible with the insertion of microspheres, and operate under an inert atmosphere. Characterization of the apparatus was key to interpreting the meaning of the data. An analysis method was created for this new method based upon the assumption of uniform radial heat transfer through the sample. Validation of data gathered was accomplished using both LFA data and reference data (see sections 5.3 and 5.4) .

When originally received, the microspheres had developed an oxidation layer of unknown thickness. The depleted uranium microspheres had been in storage for many years, during which time an oxidation layer had developed on the surface of the microspheres. The oxidized depleted uranium (ODU) microspheres were characterized as a unique material. Following the ODU measurements, a second data series was created using the same microspheres with the oxide layer removed using a nitric acid dissolution process; the samples are designated as washed depleted uranium (WDU). Several standards were tested in addition to the ODU and WDU for verification and calibration purposes but are not included due to the limited accurate data ranges obtained.

A literature review of nuclear fuel, heat transfer, packed bed measurement methods and previous microsphere nuclear fuel research is included in Chapter 2. A detailed description of the measurement and analysis methods selected is presented as Chapter 3. Schematics of the new method developed in this study are presented in 3.2.1. Section 3.2.4 details the systematic uncertainty; which was determined to be approximately 13%. Data is displayed graphically and presented in tables in Chapter 4. Calculated thermal conductivity values of the ODU and WDU microspheres from

the new method are presented in 4.2.5. In Table 5.1 and Figure 5.21, it is shown that the thermal conductivity of WDU microspheres at 500°C was calculated to be 0.431 W/m-K. Results are interpreted in Chapter 5 and indicated that the thermal conductivity of the WDU microspheres was of the same order of magnitude as that of comparably sized UO_2 microspheres (see section 5.4).

2. BACKGROUND

The performance of any nuclear fuel is strongly related to its thermal, mechanical, and chemical properties. This present research is focused on the thermal properties of nuclear fuel. The specific fuel form of interest is a packed bed of uranium metal microspheres with a low packing density between 40 and 50% open volume to accommodate fuel swelling and gas release. This fuel configuration is one of several fuel designs under evaluation for the Travelling Wave Reactor (TWR). Using a packed bed of microspheres as a nuclear fuel form has many specific challenges, such as low thermal energy transport and fuel restructuring; this thesis is dedicated to the evaluation of basic thermal properties.

In the TWR design, fuel is to remain in the reactor for long time periods and incur a high burnup. Over time, nuclear fuel will swell which can lead to fuel failure. In an effort to prevent this from occurring, particulate fuel may be an alternative to solid monolithic fuel. Due to the structure of spherical particulate fuel, there is a significant fraction of void space (nominally greater than 30%). By building in void space, fuel swelling can be better accommodated. Unfortunately, the void space created by microspheres comes with disadvantages to heat transfer. In a sphere packed bed, heat transfer relies on point-to-point contacts which drastically decreases thermal conductivity.

In this chapter, the basic heat transfer mechanisms will be discussed and applied to different reactor fuel forms. Additionally, previous studies on the measurement of thermal conductivity of a packed bed are discussed. At the culmination of this chapter, the various heat transfer mechanisms and measurement methods will be applied to the selected fuel form, that is, microspheres of uranium metal.

2.1 Thermal Energy Transfer

Thermal energy traverses through a material as a result of phonon transport. In cases where a temperature gradient exists, a net flux of thermal energy is generated. Thermal energy may be introduced into a system through a variety of means. When this is done in a controlled manner, the basic properties of the system may be measured. Temperatures within a sample may be measured and characterized using thermocouples or other methods to monitor the temperature profile. When the temperature profile within a material is changing with time, this is known as an unsteady-state or transient system. In this condition, there are hot spots and cold spots located in the sample. In steady-state systems, sufficient thermal energy is constantly applied to the sample such that the temperature profile is constant. Three fundamental mechanisms act as the driving force for heat transfer, these are conduction, convection and radiation [5] [6].

Thermal conduction occurs when thermal energy is transferred through a material by phonon and free electron transport. Since heat is a result of energy, and high temperature regions have a higher average kinetic energy, this indicates that the atoms in a high temperature region are in an excited state. When excited, it is common for the outermost electrons, the "free" electrons, to gain energy causing the electrons to have increasingly random movements [6]. Through electrostatic repulsion, the increased path length traversed by the free electrons of one atom induce an increase in energy of the free electrons of a neighboring atom. Over time, the result is energy transfer from the excited atoms to nearby atoms. A change in temperature is the most apparent effect of the energy transfer. The unexcited atoms increase slightly in average kinetic energy whereas the originally excited atoms decrease slightly in average kinetic energy resulting in a net thermal energy transfer.

For this reason, materials with more free electrons will exhibit superior thermal conduction behavior. Ceramic materials tend to form via ionic bonds in which electrons are transferred from the anion to the cation and bound to the nucleus. This

tight bonding results in very few free electrons, which limits the ability of a ceramic to transfer heat through conduction. In metallic bonding, electrons are shared between atoms and create an electron cloud of free electrons surrounding the nucleus. Since electrons are able to move, energy is readily transferred through metals. Covalent bonds rely on the sharing of electrons between an anion and cation pair which generally allows for more electron movement than an ionic bond but less movement than a metallic bond. Due to this behavior, covalent bonds tend to have a faster heat transfer rate than ionic bonds but a slower heat transfer rate than metallic bonds [3].

Density is another material property that impacts conduction; dense materials with a high number of free electrons will generally be good conductors. For a given material, the solid phase is usually more dense than the liquid phase, which is more dense than the gaseous phase. This indicates that for most materials, heat conduction will occur more readily in the solid phase and less readily in the gaseous phase. A more dense phase of a given material will have more free electrons per a specified volume than a less dense phase of the same material. The increased number of free electrons results in an increased energy transfer which, again, allows for more rapid conduction in solids as compared to gases.

Thermal energy may also be transferred through fluid movement through a process known as convection. In convection, the circulation of hot and cold fluids creates a heat transfer path. Convection can occur naturally but is often forced in engineering applications. The general principle behind convection is that heat is transferred from a hot spot to a cooler spot by moving a fluid (either liquid or gas) across or through the warm region. As the cooler fluid intersects the warm region, heat is transferred from the surface of the warm spot to the contact fluid. This causes the fluid to increase in temperature and continue moving through either forced or natural convection.

Natural convection is driven by the temperature-dependent density variations of a material. Most materials will decrease density as temperature increases; more dense

fluid will sink and less dense fluid will rise, resulting in a natural circulation loop. This occurs at a rate determined by the heat transfer parameters for the system and the ease of heat transfer between the hot and cold regions. Pumps may be used to accomplish a similar task and control the flow rate of a cold fluid across a hot region.

A final mode of heat transfer is through electromagnetic radiation. In this process, thermal energy is radiated out of an object, typically in the form of photons (light), and into the surrounding environment. Charged particles within a hot object are excited and emit energy, in the form of photons, to reach a lower excitation level. The energy emitted is absorbed by surrounding material, causing energy, or heat, transfer. In the purest form, electromagnetic radiation is exemplified by a blackbody; that is, an object that absorbs all light (or radiation) cast upon the object's surface which then re-emits the radiation.

When a piece of metal is glowing hot, it is an example of radiative heat transfer; the metal is transferring heat from the outer layer to the surrounding environment. Another illustration of radiative thermal energy is the heat from the sun. Once away from the surface of the sun, conductive and convective heat transfer modes do not play as significant of a role in transmitting the sun's energy to earth as does radiative heat transfer. The heat of the sun is emitted from the outer layer and conveyed through the vacuum of space to earth using electromagnetic waves; a form of radiative heat transfer.

2.1.1 Thermal Conductivity

This discussion of thermal conductivity was based upon several textbook references [3], [5], [6], [7], [8], and [9].

As noted above, different materials have different thermal properties and exhibit different thermal energy transport behavior. In order to understand the thermal behavior of a material, it is essential to consider a few key material properties. In conduction, the electron density of a material is important in determining the rate of

thermal conduction. If the density of a material is high, such as in a solid, there are more free electrons per unit area. Since the electrons are exceptionally important in determining the heat transfer rate, a greater density of electrons, typically due to a greater material density, results in a more rapid energy transfer between a hot and cold region. Material density is expressed in units of mass per volume, which is reported with units of either g/cm^3 or kg/m^3.

Most solid materials are known to expand as temperature increases. This is partially due to the increased energetic movement of electrons that causes a material to expand which in turn lowers the thermal conductivity. Additionally, that expansion of a material resulting from a change in temperature, quantified via the coefficient of thermal expansion, is not typically constant for all temperatures. As a material expands it generally will reduce the rate of heat transfer. This effect can partially be attributed to increased space between nuclei resulting in fewer or slower collisions.

Another key heat transfer parameter is the rate at which thermal energy travels through a material. This property is known as the thermal diffusivity and is a measure of the amount of time required for a temperature change to propagate through a material. Thermal diffusivity is presented in units of length squared per time, with typical units of mm^2/s. The thermal diffusivity of a material is directly related to the thermal conductivity and can be calculated by dividing thermal conductivity by the product of the material density and specific heat. Thus, if a material has a high thermal diffusivity it also has a high thermal conductivity and will transmit thermal energy through the bulk of the material in a short period of time. Thermal diffusivity is used to quantify the rate of heat transfer volumetrically through the bulk of a sample. The thermal diffusivity of a material is a function of temperature and can be calculated for samples of a known geometry with an accurate temperature-time profile. Thermal energy diffuses from regions of high energy to regions of lower energy. Since temperature is a result of the average particle kinetic energy, heat tends to

diffuse from regions of high temperature to regions of low temperature; this diffusion of heat energy is termed thermal diffusivity.

Consider a pot of water on a stove top. The metal pot that contains the water is heated from beneath and acts as a heat transfer surface for the water located in the pot. As the water begins to warm, bubbles first form on the bottom surface of the pot. The location of the bubble formation indicates that the water near the pot surface is warmer than the rest of the water. At the top of the pot, the water surface is cooler since this area is not in direct contact with the heat source. Over time, the temperature throughout the pot will become uniform. The distribution of heat from the bottom surface of the pot to the top surface of the water during heating is time-dependent; over time this profile will flatten and the water will be near a uniform, steady-state, temperature profile. This time sensitive flattening effect is evidence of thermal diffusivity. If desired, an engineering model could be crafted to simulate the thermal profile in the water over time. However, for the prediction of nuclear fuel behavior, the computational requirement is much more intensive.

Different materials transfer heat at different rates due to differences in the heat capacity of the material. The thermal energy input required to change the temperature of a specific quantity of material a given amount is known as the specific heat. The units of specific heat are energy per temperature per mass; for SI units this is J/K-g. Notice that the property of specific heat does not depend on the shape (i.e. solid vs microspheres) of the material, it is simply determined on a per mass basis. However, specific heat does depend on the phase (solid, liquid or gaseous) of the material. This is related to the previous discussion of ease of electron movement through a material. In a solid, thermally excited electrons have less distance to move before exciting other electrons due to close packing. The same statement is not true for gases or liquids; both of which have a greater path length between excitable electrons. For this reason, it is expected that the specific heat of a solid will be higher

(which means it is able to increase in temperature more rapidly for a given thermal input) than that of the liquid and gaseous phases of the same material.

The combination of thermal diffusivity, specific heat, and density produces the parameter known as thermal conductivity, which allows the characterization of the heat transfer properties of a system. The SI unit for thermal conductivity is W/m-K. Thermal conductivity is a useful term to quantify the ease of heat transfer through a material. Since thermal diffusivity depends upon the form of a material while specific heat and density are intensive properties, thermal conductivity is a parameter that is sensitive to basic material properties and the form of a material. A material with many void spaces will have a lower thermal conductivity than a solid piece of the same material. If heat is easily transferred through an object it is said to be conductive. Typically, solid metals have a higher thermal conductivity due to free electrons; evidenced in copper as a common choice for electrical wires. It is relatively easy to transfer thermal energy (heat) through a copper wire due to the high mobility of the electrons, a property which also results in a higher thermal conductivity.

2.2 Thermal Conductivity Measurement Methods

Data for the specific heat, temperature-dependent density, and coefficients of thermal expansion exist for many materials. Thermal conductivity data for bulk materials such as solid uranium metal exist in literature. However, thermal conductivity is very system dependent and, therefore, literature values for solid U metal are not suitable for U microspheres. While the thermal conductivity of the bulk material remains constant regardless of the form (i.e. solid versus microspheres), the effective thermal conductivity will change drastically. There are several methods to determine the thermal conductivity of a system; either directly through precise knowledge of heater specifications or indirectly through determination of other key heat transfer properties.

2.2.1 Indirect Measurement

Specific heat is frequently measured through calorimetry, or, measuring the heat required to induce physical change. This can be accomplished through either building a reaction vessel, such as in bomb calorimetry, or through equipment in the differential scanning calorimetry method. Specific heat is dependent on material, phase, and temperature but is independent of material form; i.e. solid and powder forms of a material will have the same specific heat. Previous research [10], graphically suggested that the specific heat of solid uranium tends to decrease nearly linearly until it reaches the melting point. In the liquid phase, the specific heat undergoes highly non-linear transformation at high temperatures.

Based upon the graph contained in this study and data points for specific heat found through Kaye & Laby Tables [11], Fig. 2.1 was compiled. Similarly, the temperature-dependent density was interpolated from the density at room temperature and the density at the melting point for solid uranium using known literature values [12]. These values are shown in Fig. 2.2.

The thermal conductivity is calculated using Eq. 2.1; where k is thermal conductivity, α is thermal diffusivity, ρ is density and c_p is specific heat. Data points obtained from Kaye & Laby for uranium metal are shown in Table 2.1; obtained online [11], [12], [13], and [14]. Literature values [13] of thermal conductivity are shown in Fig. 2.3.

$$k = \alpha \rho c_p \tag{2.1}$$

Thermal diffusivity values were not supplied by the Kaye & Laby Tables but can be calculated by using the Eq. 2.1. The calculated values of thermal diffusivity for solid uranium metal range from 12.68 mm^2/s at 100°C to 12.44 mm^2/s at 600°C presented in Fig. 2.4.

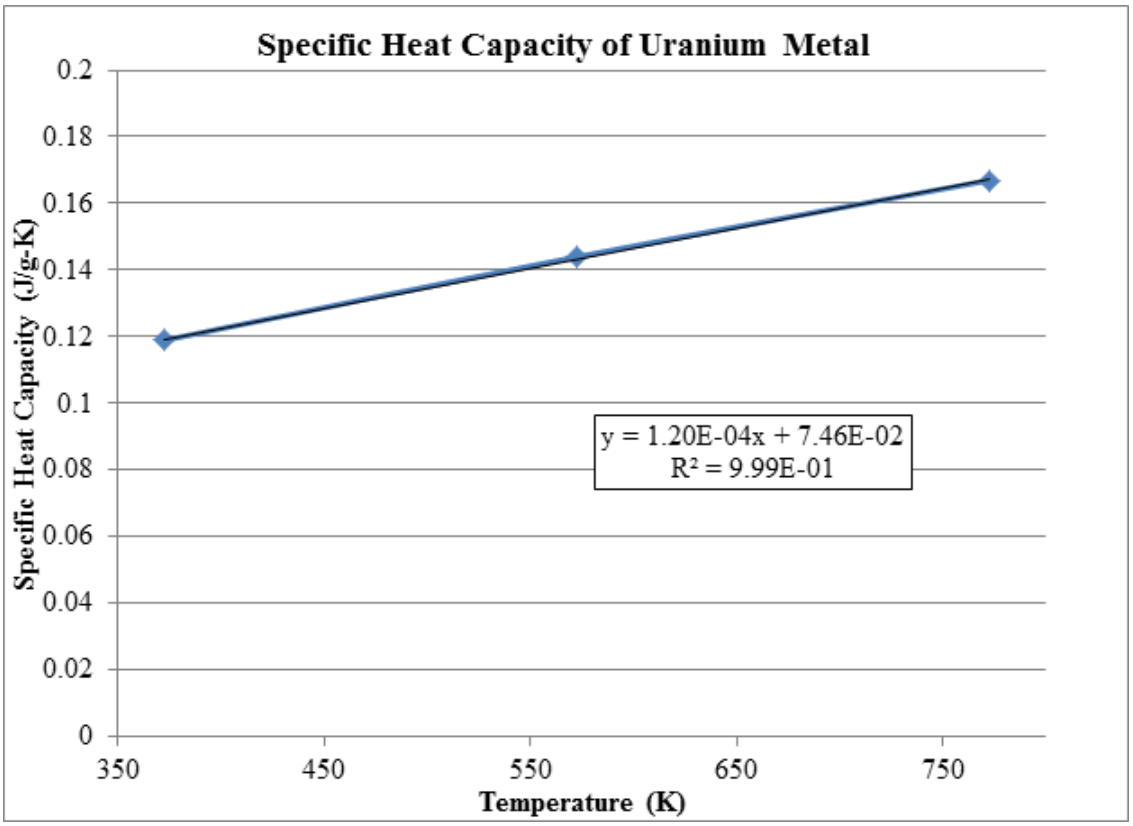

Fig. 2.1. Literature values of specific heat capacity for solid uranium metal.

If thermal conductivity values are not known due to unique composition or geometry, they may be determined through the measurement of thermal diffusivity, density, and specific heat. Frequently, literature values exist for the specific heat capacity and density of the desirable material, or a very similar material, leaving only the measurement of thermal diffusivity. One primary method, for such a measurement, uses both conductive and radiative heat transfer and is known as the LASER (or light) Flash Analysis (LFA) method. It is implemented by flashing an intense light source on one side of a sample at time zero then waiting for the temperature rise from the flash to be detected on the other side of the sample at time t. The thickness of the sample and the difference between sample temperature at time zero and time t allows for the calculation of thermal diffusivity. Generally, it is assumed

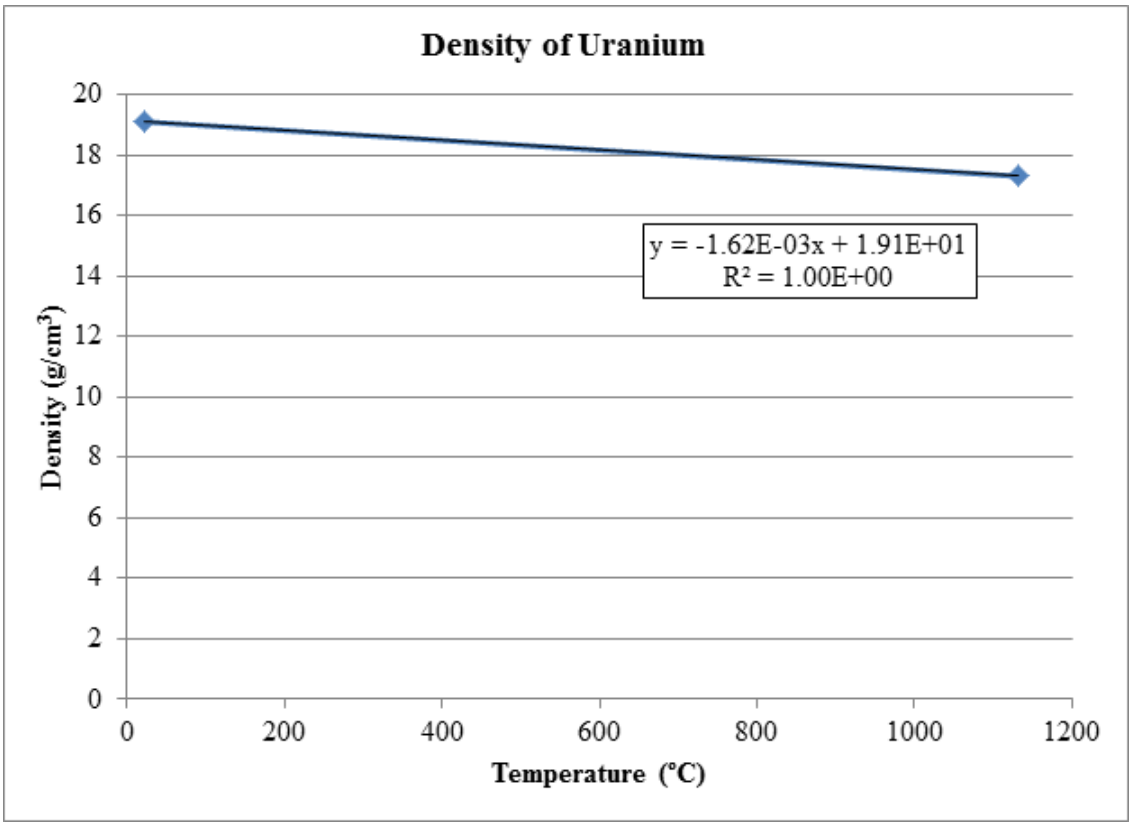

Fig. 2.2. Interpolated values of density for solid uranium metal.

that both surfaces of the sample are perfect blackbody absorbers; meaning that all of the photon energy emitted is absorbed onto the original surface of the sample. In practice, this is never an entirely accurate assumption but measures can be taken such that the sample is comparable to a blackbody. One way this is accomplished is by applying a black graphite coating to both surfaces of a thin sample.

In LFA, the light pulse is emitted on the lower surface of a flat sample with parallel top and bottom faces. The energy carried by the light pulse is absorbed into the sample and the energy (heat) is transferred through the sample until it is again emitted on the top face. There is an infrared (IR) detector located above the top face of the sample which detects the increase in heat on the top of the surface. This infrared sensor communicates with a data acquisition and control program and the

Table 2.1
Literature values for thermal properties of solid uranium metal.

Temperature (K)	Specific Heat (J/g-K)	Density (g/cm^3)	Thermal Conductivity (W/m-K)
273	-	19.1	27
373	0.119	-	29
573	0.144	-	33
773	0.167	-	-
973	-	-	43
1405	-	17.3	-

time difference between light pulse and detection, concurrently with the thickness of the sample, allows the calculation of thermal diffusivity.

The shape of the signal generated by the IR detector can vary depending on sample dimensions. For very thin, flat surfaces, there may be a sharp initial peak which is essentially the portion of the light pulse that is not absorbed by the sample. This instantaneous peak quickly fades and the real diffusivity peak emerges. The second peak is broad with a sharp increase followed by a very gradual decreasing slope after the maxima. This broad peak contains both the tail of the flash light pulse and the effects of the heat pulse through the sample. The LFA method has been published in many realms; for literature, see [15], [16], and [17].

A similar method for diffusivity measurement is possible where a thermal energy pulse is directed into a larger sample and the progression of the energy pulse can be measured and used to estimate thermal diffusivity. This method is simplest when a one-dimensional mode of heat transfer is established by the experiment geometry. The equation used to calculate thermal diffusivity for a one-dimensional system is given by Eq. 2.2 [5] where Δx is the sample thickness and Δt is the time interval

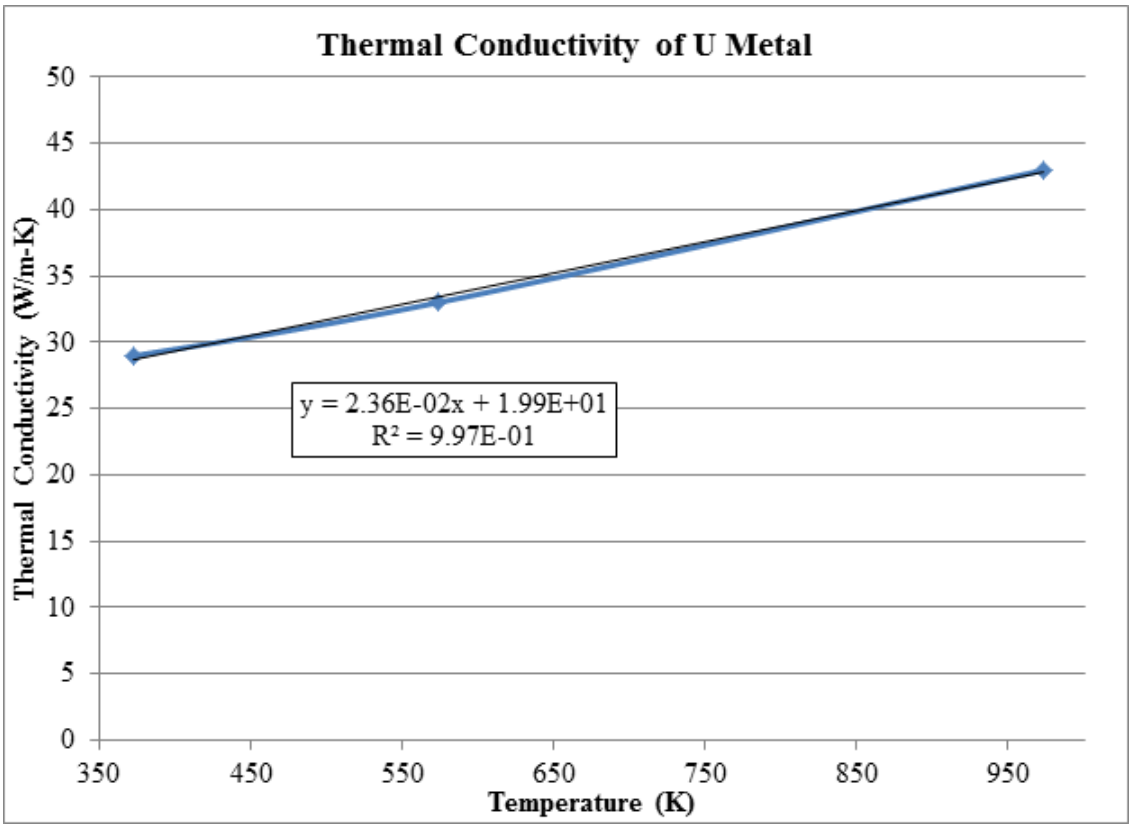

Fig. 2.3. Literature values of thermal conductivity for solid uranium metal.

for a specific temperature change to occur across distance x, the factor of 1/2 is a geometrical effect caused by the plate nature of the sample.

$$\alpha = \frac{(\Delta x)^2}{2\Delta t} \tag{2.2}$$

A flash heat source can be used to determine the thermal diffusivity of a sample, which then can be used to determine thermal conductivity. In order to minimize the error in this approach, thermocouples need to be strategically located within the sample and record exceptionally precise temperature measurements within a relatively short time step.

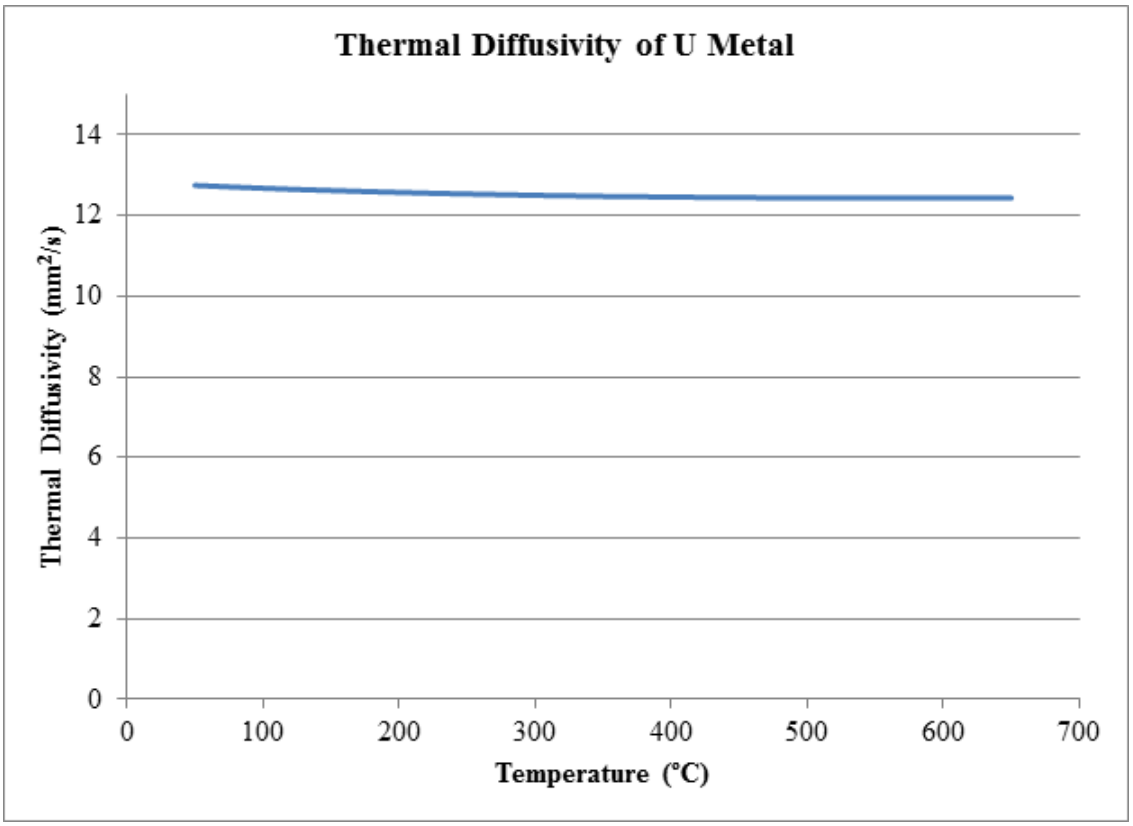

Fig. 2.4. Calculated values of thermal diffusivity for solid uranium metal.

2.2.2 Direct Measurement

Direct thermal conductivity measurement approaches tend to require very accurate information regarding the heat flux incoming to the sample. One such method uses a hot-wire or hot-plate to provide a controlled thermal flux into a well characterized sample. If the heat flux from a flash heat source is known, then the thermal diffusivity and thermal conductivity can both be directly calculated. The progression of the thermal energy through the sample is monitored at specific locations within the sample by the use of thermocouples. This accurate time-temperature log, in conjunction with the flux supplied by the heat source, is used to simultaneously calculate both the thermal diffusivity and conductivity [18]. If the flux of the heater

is not known, a standard material with known thermal properties can be used to calibrate the heat flux coming from a particular piece of equipment [19].

The hot-wire (or hot-plate) method developed in previous studies typically uses an array of thermocouples to provide accurate time-dependent temperature measurements that document the progression of the temperature rise through the sample. Using the thermocouple data, the precise position of each thermocouple, and the calibrated heat flux passing through the sample, the thermal conductivity can be directly calculated using Fourier's equation (Eq. 2.3) [19]. This equation relies upon the change of temperature with respect to axial location and the heat flux Q to calculate the effective thermal conductivity.

$$Q = -k_e \frac{\delta T}{\delta z} \tag{2.3}$$

The flow of thermal energy via phonon and electron transport is assumed to be one-dimensional and to follow parallel paths that never intersect. When applied to particle beds, studies have examined how to incorporate the contact angle, particle size, packing fraction, and fill fluid (either gas or liquid) [19]. A major limitation to the accuracy of this system is the precision in recording the temperature rise of the system. Essentially, the hot-wire acts as both the heater and as a resistance thermometer; a constant voltage is supplied across the wire and thermal conductivity is determined from the heat generation as evidenced by the temperature change in the wire [20].

The benefit to a hot-wire is that it can be embedded in the sample, allowing the use in packed beds. Similar designs have used hot-strips or hot-plates. In the hot-strip method, a constant current is supplied to a metal strip which is surrounded by the sample material. A short amount of time after the start of the experiment, the heating of the material surrounding the strip will cause a voltage increase to be noticed across the strip [21]. This allows for the calculation of the thermal transport properties of the material surrounding the strip if the sample is in intimate contact with the strip. For solids, this was accomplished by clamping the strip to the sample;

for liquids the strip could be suspended in the liquid. However, for packed particle beds this may not be the most desirable method due to the point-to-point nature of the particle contact within the packed bed.

2.2.3 Modeling

Several studies have examined modeling methods for determining the thermal conductivity of packed beds [22], [23], [24], [25], [26], [27], [28], and [29]. Some have treated microspheres as particles and have examined the heat transfer from particle-to-particle. Others have treated the sample as a bulk and examined the thermal conductivity of the bulk sample.

Heat transfer through packed beds occurs through the following three mechanisms [25]: 1) radiative and conductive transfer through the void fraction between particles, 2) conduction through point contacts between solid particles, and, 3) by convection effects of fluid. For a packed bed of particles, it has been documented that that the particle diameter is not as crucial in heat transfer as the void fraction of the packed bed and the contact angle between particles [25]. However, there are differing results that indicate that the particle diameter significantly impacts the effective thermal conductivity of a packed bed [26]. Methods to increase the thermal conductivity resulting from these models include increasing the pressure of the system [25] and [27] and using particles with a rough outer surface [28] to increase the number of contact points between particles may increase, thus increasing the rate of heat transfer.

Previous studies have made the assumption that thermal diffusivity does not depend on temperature and have used equations similar to Fick's Law of Diffusion in the analysis of heat transfer. The assumption of thermal diffusivity not dependent on temperature may be valid for non-conductive materials, such as ceramics [22] but is not true in the case of metals. Another method is the parabolic heat conduction equation which assumes an infinite thermal propagation speed; an assumption known to be invalid. The challenges to the parabolic heat conduction equation are

partially mitigated by a generalized Fourier's Law which, leads to the hyperbolic heat conduction equation [23].

The previous model has been extended to a porous medium filled with a fluid [24]. In this study, it was assumed that the only mode of heat transfer was conduction through the solid and the fluid. This approach uses known values for specific heat, density, and the bulk mean voidage (of both the solid and liquid) to model the behavior surrounding the pores. As long as the values for the previously mentioned parameters are known, this model allows for the calculation of the system's effective thermal conductivity for any porous material within a fluidized bed.

Heat transfer experiments were conducted with vibro-compacted microspheres of uranium dioxide (UO_2) [29]. In this study, a model was developed that accounted for heat effects known to occur within particle beds. These effects include the distortion of heat flux path directions to the point-to-point contacts between particles, low ambient pressure, and differing particle size. The resulting model was tested using an apparatus similar to the hot-wire method, with an external cylindrical heater that supplied a known heat flux. Additionally, there was an inner core heater and thermocouples placed along the outermost edge of the sample. The assumptions made in this model assume linear heat transfer and uniform powder packing. The results from this apparatus [30], indicated that the thermal conductivity increased as nominal particle size increased. It was also noticed after a sample cooled that sintering had occurred during the heating phase resulting in a greater surface contact angle. Also of interest, was that the packing fraction for the 200 μm spheres was near 67%. The study included an evaluation of pressure and fill-gas variables. It was found that the effective thermal conductivity of the spheres was greatest in a helium filled bed, followed by argon, and lastly krypton. At 400 K, values obtained for argon and krypton were within 20% of each other while helium was nearly four times greater. At atmospheric pressure, the approximate values for 200 μm are listed in Table 2.2 [30].

Table 2.2
Approximate thermal conductivity values for UO_2 microspheres [30], values for solid UO_2 from [35].

Temperature (K)	Helium (W/m-K)	Argon (W/m-K)	Krypton (W/m-K)	Solid UO_2 (W/m-K)
400	1.1	0.3	0.2	7
1000	1.0	0.4	0.3	3

2.3 Nuclear Fuel Materials and Forms

Nuclei have varying probabilities of fission based on the ease of the nuclei to interact with an incident neutron; this probability is represented as a cross-section and is generally described in barns or 10^{-24} cm^2. The primary selection mechanism for nuclear fuel isotopes is the size of the fission cross-section; the greater the cross-section, the more likely fission is to occur resulting in energy release. Uranium has been the most commonly selected nuclear fuel due to the large cross-section of U-235.

Most reactors in operation currently use uranium fuel that is enriched to 3-5% of U-235, known as low-enriched uranium (LEU). Natural uranium is composed nominally of U-238 (about 99.3%) and U-235 (0.7%). Enrichment methods are used to increase the U-235 content of uranium for fuel applications. In the process of enrichment, there is a feed stream, a product stream and a waste stream. The feed stream is natural uranium, the product stream is generally LEU and the waste stream is depleted uranium (DU). Typically, a composition of 0.3% U-235 is considered DU. Due to the continual need to enrich uranium for the reactor designs currently in operation, a large amount of DU has accumulated.

Generation IV (Gen-IV) reactor designs have been proposed that use the DU to breed fissile isotopes; meaning that over time the U-238 captures a neutron and transmutes to fissile plutonium, specifically Pu-239. As a fissile material, Pu-239 is

similar to U-235 in regards to the fission cross-section and is therefore quite useful as fuel for reactors. These reactor designs then burn the Pu-239 as fuel and are commonly known as breed-and-burn reactors.

The primary types of fuel previously studied are oxide in the form of uranium dioxide (UO_2), uranium metal, uranium carbide, and, to a lesser extent, uranium nitride. Currently, the reactor design most commonly used is a light water reactor (LWR) that uses UO_2 fuel which has U-235 enriched to 3-5%. The LWR design uses a thermal spectrum meaning that the average speed of the neutrons in the reactor is slow. Uranium metal alloys are commonly considered for Gen-IV designs that rely on fast spectrum neutrons, meaning that the neutrons are very energetic (1 to 2 MeV). Uranium carbide and nitride fuels have also been suggested as alternatives for both UO_2 and U metal due to increased thermal conductivity compared to UO_2 and decreased swelling compared to U metal.

2.3.1 Metal Fuel

In many of the previous fast reactor and developing Gen-IV reactor designs, metal alloy fuel is considered the fuel form of choice. One reason for the interest in metal fuel is the higher thermal conductivity of the fuel resulting in lower reactor operating temperatures and greater efficiency transmitting the heat from fission from inside the fuel to coolant channels. There are, however, some negative characteristics associated with metal fuel.

One of the main issues of metal fuel is the inevitable swelling due to high temperatures within an operating reactor. The operating temperature range of a reactor is high enough that any metal will incur drastic swelling, an attribute that is further augmented by the radioactive environment. For nuclear fuel, this requires that there must be some void space for the fuel to swell into in order to protect the cladding in the reactor. Cladding is essentially a narrow tube (about 1 cm in diameter) that is used to encase fuel to limit the release of fission products to the reactor coolant

and to provide structural integrity. If fuel swells to such a point that the cladding ruptures, for any reason, then the operation of the reactor is compromised [2].

In the case of uranium metal, swelling can primarily be attributed to the anisotropic grain growth in alpha phase uranium caused by the buildup of fission products along the long axis of the orthorhombic structure. As the time in the reactor increases, swelling will also increase. This phenomena supports the practice of alloying uranium metal for use as reactor fuel. With alloying, the anisotropic swelling of uranium metal can be mitigated.

2.3.2 Microspheres

In practice, nuclear fuels are monolithic solid pieces of material (i.e. pellets for UO_2 or pins for U metal). Alternative fuel designs have examined the use of particle fuels due to several proposed benefits such as reduced fuel cladding interactions and additional empty volume to accommodate swelling [31]. Throughout this section, particle fuel will be defined as spherical, sub-millimeter microspheres between 100 and 500 μm in diameter. Previous studies on particle fuel have suggested several benefits but these benefits come at the cost of reduced heat transfer properties [4] and [32]. Interest in particle fuel was bolstered in the 1980's by the ability to produce the fuel remotely and without dust, resulting in a facility that may be more easily safeguarded [1].

From previous testing, it has been suggested that microspheres reduce the chemical interaction between fuel and cladding that occurs within a reactor [31]. A common phenomenon observed in a nuclear fuel pin is an interaction layer between the fuel and the cladding that forms due to chemical penetration of fission products into the cladding, more generally called Fuel-Cladding Chemical Interaction (FCCI). This FCCI reduces the strength of the cladding and will eventually lead to cladding failure. In some reactor designs, FCCI serves as a limiting factor for the lifetime of a fuel in the reactor and the resulting burnup of the fuel. It is theorized that due to the

point contacts inherent to particle fuel, FCCI would be reduced as compared to that which occurs with solid fuel pellets, slugs or pins. The idea is that since particle fuel would only be in point contact with the cladding, the diffusion of destructive FCCI inducing components such as lanthanides into the cladding would be minimized due to the initial reduction in contact due to the point contacts.

It has also been observed that particle fuel rapidly undergoes restructuring and sintering during reactor operation, which results in the loss of most of the particle structure (including the point-to-point contact discussed above). In previous studies, the particle fuel densified and formed an annular structure composed of sintered low density fuel [31]. After densification, the contact between the fuel and cladding increases. This has the impact of improving thermal conductivity while exacerbating FCCI and swelling challenges.

An additional proposed benefit of particle fuel is the increased void space to accommodate both swelling and fission gas release. To reach high burnups, the smear density of the fuel needs to be such that temperature and transmutation swelling effects can be accommodated without exerting too much pressure on the cladding. The increased void porosity may result in decreased fuel-cladding mechanical interaction (FCMI), again extending the life of the cladding. If the spheres are all of one size, a smear density of approximately 60% of the theoretical fuel density may be achievable since the closest packing of monosized spheres is approximately 72% [3]. This amounts to a large fraction of open porosity and leaves necessary space for fuel swelling to occur.

A downside to the point-to-point contacts that reduce FCCI and FCMI is evidenced in the thermal conductivity of the fuel. Thermal transport paths also utilize the point-to-point contacts in order to transfer heat from the fission reactions within the fuel to the coolant. In solid fuel, this heat transfer path is accessible due to the continuous nature of the fuel. Prior to sintering and densification in particle fuel, the thermal conductivity of the fuel is severely inhibited by the reduced heat transfer

pathways due to the reliance of point-to-point contacts. During sintering and fuel restructuring, the point-to-point contacts flatten out a bit allowing for a greater heat transfer path and increasing the thermal conductivity [32]. This increase in thermal conductivity would occur to a lesser extent in solid fuel during restructuring.

3. EXPERIMENTAL METHOD

Two primary methods of data collection were explored. The first method was Laser (Light) Flash Analysis (LFA), and the system used was limited to relatively low temperatures. To augment the data collected by using LFA, a custom-designed apparatus was developed based partially on the hot-wire method described in Section 2.2.2. The new apparatus was called the Crucible Heater Test Apparatus (CHTA) and was utilized to measure the thermal diffusivity of a packed bed sample of depleted uranium metal microspheres after a test procedure had been established using standard materials. The uranium spheres were naturally coated with an oxide layer and are designated as the Oxidized Depleted Uranium (ODU) microspheres. An acid washing procedure was established to remove existing surface oxidation from the ODU microspheres so that a pure uranium metal sample could be tested. After the washing process the microspheres were termed Washed Depleted Uranium (WDU). Tests with the WDU were impossible in the LFA because an inert atmosphere was required to minimize the effects of oxidation at elevated temperatures. Both ODU and WDU were tested in the CHTA. Since the samples used were of microspheres, there was a significant void fraction within the sample. The desire to develop the capability to test with different fill gases or liquids was fundamental in the designing of a second apparatus.

3.1 Light Flash Analysis Method

A Light Flash Analyzer 447 (LFA 447) manufactured by Netzsch Instruments N.A. LLC (Burlington, MA) is installed in the Fuel Cycle and Materials Laboratory (FCML) at Texas A&M University and was used for this research. This machine enables the measurement of thermal diffusivity from room temperature to 300°C utilizing programmable test parameters. There is a plate-style sample holder in the center of the machine designed for a maximum of four thin samples up to 12

mm in diameter. A xenon flash lamp is installed, within the machine, below the sample tray and emits rapid light pulses directly below the bottom surface of each sample independently. The sample tray slides along a lateral plane such that the desired sample is positioned directly above the flash lamp prior to the light pulse being emitted. A schematic of the LFA interior is provided in Fig. 3.1; this figure is available through a Netzsch Instruments brochure [33].

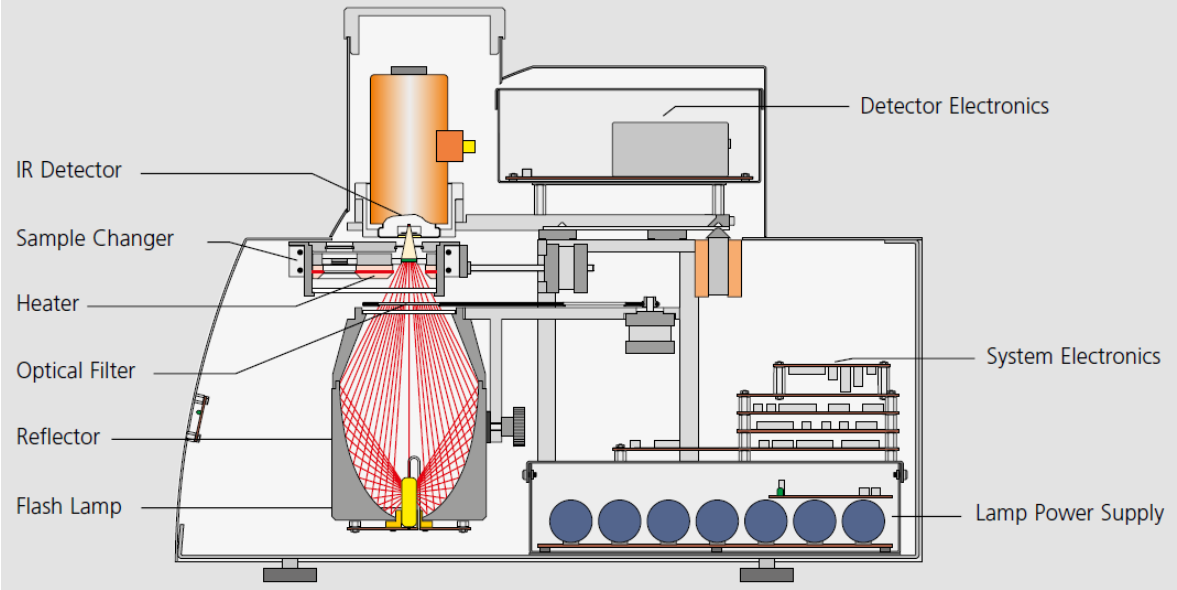

Fig. 3.1. A cut-away view of the LFA 447 by Netzsch Instruments [33].

After a pulse has been triggered by the lamp, the machine records the time until an energy shift, in the form of temperature rise in the top surface of the sample, is observed using an infrared detector. This heat shift peaks at a maximum and then steadily decreases. Due to internal variations within the sample and the capabilities of the flash lamp, the original detection peak follows the trend of a photon Bragg Peak. The maximum of the Bragg Peak corresponds to the time at which the maximum heat shift was noticed by the infrared detector on the top surface of the sample.

3.1.1 LFA Procedures

Typically, LFA is accomplished using solid samples with surfaces perpendicular to the flash lamp and the detector. When using a disk-shaped sample, this is readily achievable. For powder samples, it is challenging to achieve this condition due to the many edges of the particles. Netzsch manufactures a powder and liquid sample holder which presents a flat transparent sapphire surface to both the flash lamp (bottom) and detector (top). This sample holder has a metal outer ring very similar to that of the disk-type LFA sample holders. However, there is a sapphire pan that sits within the sample holder and an accompanying sapphire lid, both of which serve to contain the powder or liquid sample throughout the duration of the test run. See Fig. 3.2 for a photograph of the sample holder used throughout the testing of the microspheres in the LFA.

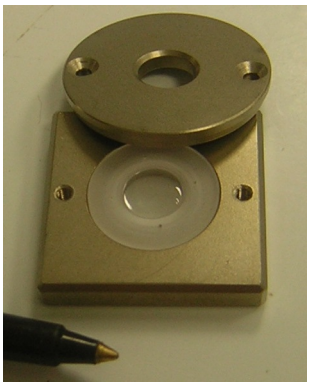

Fig. 3.2. Powder and liquid sample holder for LFA.

It is recommended to pack the powder lightly such that as smooth of a surface as possible is presented to both the flash lamp and the detector. When the powder shape is microspheres, this is not feasible to achieve because the surface will always be rough with texture and not smooth. For solid samples, both sides of a sample generally were thinly coated with graphite spray such that the emitted pulse was nearly completely absorbed on the surface of the sample. This task was much more

difficult for microspheres. Using a small fraction of the microspheres of standard materials, a graphite coating was sprayed using a swirling motion inside of a petri dish. Another attempt at implementing this coating procedure with the microspheres was to spray the bottom and top surfaces of the sapphire pan and lid instead of the microspheres directly.

The data collected via LFA was designed to provide a baseline database to benchmark the new system (CHTA) described in the next section. The LFA has a lower temperature range than the CHTA. For the microsphere samples, the voltage of the machine was consistently at the maximum value and the duration was typically above 30 seconds. The duration is the time between flash and detection by the infrared sensor; a long duration is used when the measured thermal diffusivity is expected to be low. The flash length was also set to the longest setting; this is the duration of the light flash from the flash bulb. For solid materials, the flash length is typically set to the medium setting. A longer flash length compensates for increased energy leakage due to the non-perpendicular surfaces and non-linear heat transfer of the microspheres. Materials were tested in the LFA multiple times in order to maximize data collection and to establish a robust data series.

The experiments conducted with the LFA followed the same general test plan; beginning at 25°C, flashes were performed at increasing set-point values with 25°C increments up to 300°C. Liquid nitrogen was used to cool the infrared detector and a water chiller was used to cool the flash lamp and instrumentation in the LFA lower chamber underneath the sample holder. Multiple flashes, usually five, were recorded at each temperature for every sample in order to allow for better averaging and error analysis. One major disadvantage to the LFA is that it is not configured for inert atmosphere operation and therefore samples are open to air during measurements. Since uranium metal rapidly oxidizes in air, it was difficult to test within the LFA at temperatures greater than 125°C. Because of this only the ODU microspheres were tested in the LFA.

3.2 Crucible Heater Test Assembly

In order to record higher temperature diffusivity data in an inert atmosphere, the Crucible Heater Test Assembly (CHTA) was designed and installed in an inert atmosphere glovebox (manufactured by Ionex in Denver, CO). The designed apparatus intended to be able to operate with liquid sodium surrounding the microspheres, but that option was never utilized. Since the melting point of sodium metal is approximately 100°C, the baseline operating temperature of the apparatus needed to be slightly above this value. Also, data points below the melting point of sodium would be unnecessary since a sodium cooled fast reactor would invariably use liquid sodium coolant and would require temperatures significantly greater than 100°C.

Due to a limited quantity of uranium microspheres, a small cylindrical yttrium oxide (Y_2O_3) crucible was selected to contain the sample. An outer band heater was selected to heat the entire system; the band heater clamped on to the outer circumference of the crucible. Additionally, a small diameter cartridge heater was selected to supply a heat flux from the center of the apparatus. The design was based on a combination of the hot-wire and LFA concepts. Both heaters were controlled by separate proportional-integral-derivative (PID) controllers that were programmed and tuned for the unique heating requirements of the attached heater.

The ambient system temperature was controlled by the outer band heater and the transient heat pulse was controlled by the inner cartridge heater. Using a thermocouple array with precise locations, the progression of the thermal energy through the sample could be monitored using a multi-channel data logger. After the transient was completed, the temperature of the cartridge heater was held constant as the radial temperature profile equilibrated; temperature measurements from the thermocouples were recorded throughout this entire process. The data obtained was used to calculate the thermal diffusivity which in turn allowed for the calculation of the thermal conductivity. Thermal diffusivity was calculated during the transient initiated by the cartridge heater immediately following the heat pulse. Since the thermocouples

were at specified locations across the sample and detailed time measurements were recorded, radial disks of material could be analyzed to determine the time required for the heat to progress through a specific surface area. The calculation was completed by taking the difference between surface areas for the measurement points of the outermost thermocouples and the innermost thermocouple then dividing by the difference in time required for a specific temperature to be reached at the outermost thermocouple relative to the innermost thermocouple. The resulting value had the units of length squared over time, or thermal diffusivity. Additionally, the geometry of the system needed to be considered. The thermal energy was traversing a cylindrical volume, not a straight line; this caused a factor of $1/(2\pi)$ to compensate for the dispersion of the thermal energy.

The nominal procedure for the CHTA method starts by loading the sample into the test apparatus (described in the following section); powder samples may be easily poured into the system, but solid samples must be carefully machined. The first step of operation was to establish a uniform radial temperature profile across the sample. After the initial temperature profile was stable and centered between 115 and 125°C, the cartridge heater would be rapidly heated up to a specified temperature at an experiment specific rate, in °C/min. After the maximum temperature was reached, the system power would be held constant for at least one hour. Then both heaters would simultaneously be turned off allowing the system to cool. This basic procedure was used for various maximum hold temperatures and cartridge heater ramp rates.

3.2.1 CHTA Design Details

Initial design considerations were driven by the size of the crucibles available. The CHTA design was based on a 7.6 cm (3 in) tall cylindrical yttrium oxide crucible with an outer diameter of 5 cm (2 in) and wall thickness of 0.2 cm (0.06 in). The outer band heater was selected due to the ability to tighten on to the crucible to provide maximum contact heat transfer. Dimensions for the band heater were

customized such that the crucible was easily placed within the heater then tightened to specification via two clamps. The area with the clamp was a vertical strip that was approximately 1.5 cm wide; this area was not heated as it contained no heating elements. A coil heater was also considered for the outer heater but was rejected due to the vertical variations in heat applied and the lack of ability to tightly connect to the crucible; the curved surface of the coil would only make good contact at the crucible once per loop.

A design schematic is shown in Fig. 3.3 and 3.4.

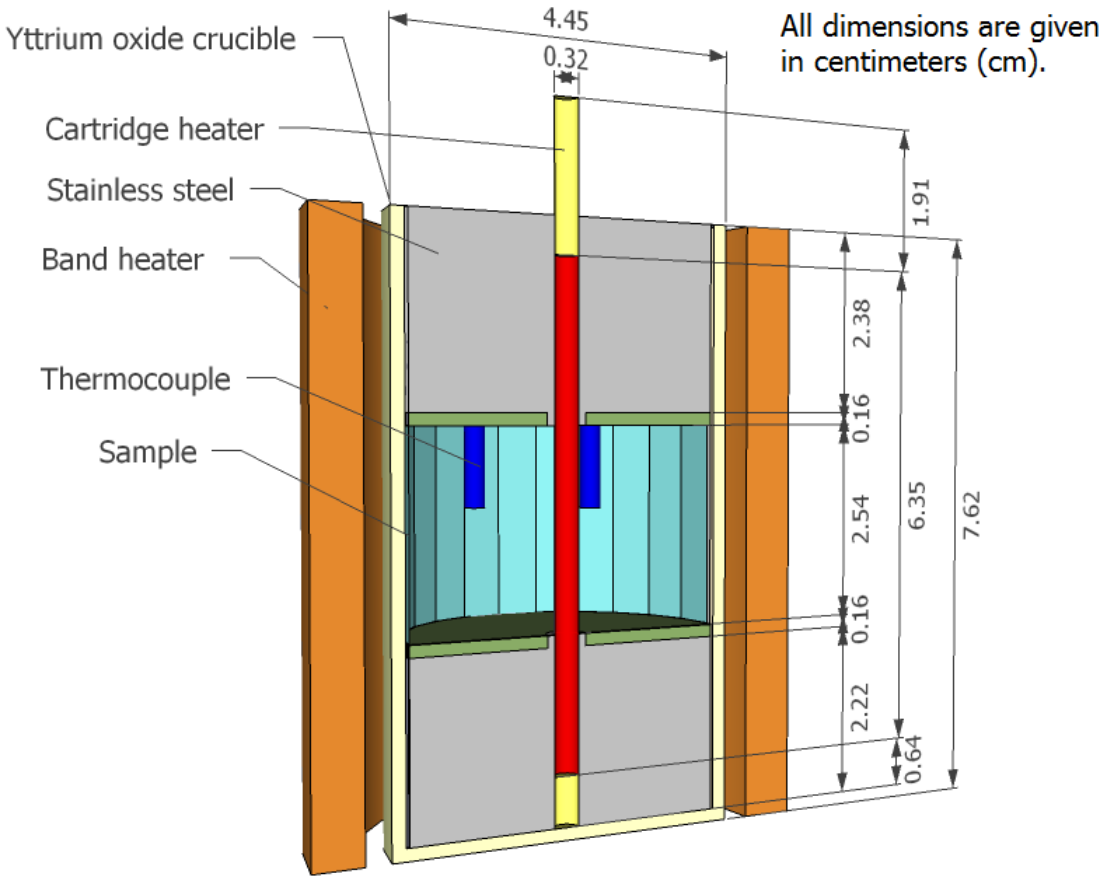

Fig. 3.3. CHTA configuration as designed in the FCML, all dimensions are in cm.

Pictures of the setup are included as Fig. 3.5 and 3.6. A complete list of all ordered and custom-made components for this system is presented in Table 3.1.

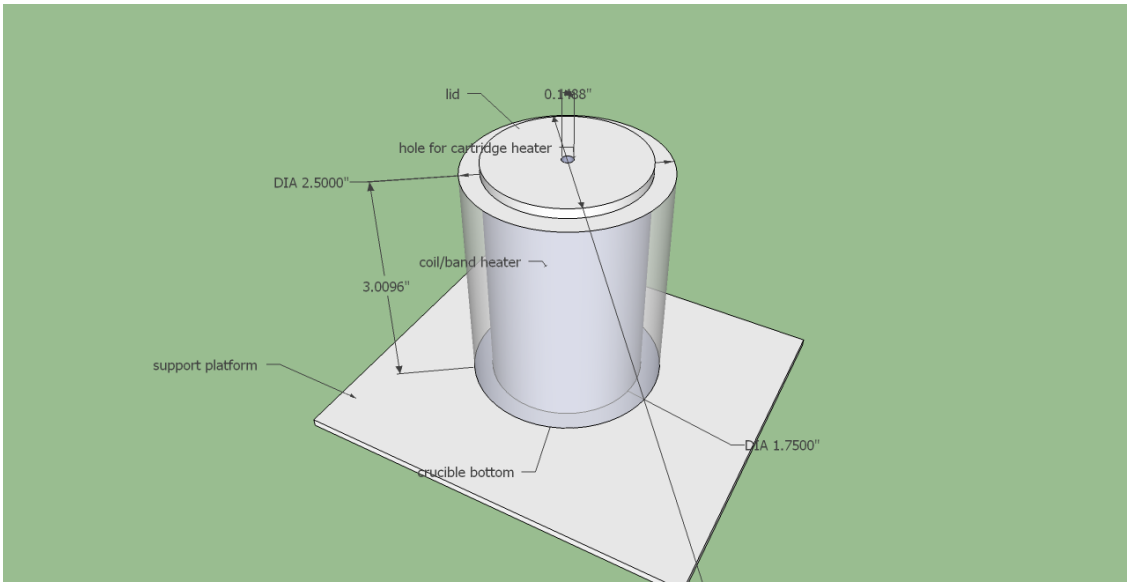

Fig. 3.4. Outside view of the CHTA, all dimensions are in inches.

In an effort to approximate the hot-wire method, the smallest diameter cartridge heater that could be located was custom designed. The cartridge heater was 8.25 cm long (3.25 in) and 0.32 cm (0.125 in) in diameter. It was designed such that there was a no-heat tip approximately 0.6 cm long (0.25 in) located at the insertion end and a second no-heat region about 2 cm (0.75 in) long at the lead end of the cartridge heater, shown in Fig. 3.7. Sandwiched between these regions was a heated region approximately 5.7 cm (2.25 in) in length. The heated region length was selected to maximize the available power across the cartridge heater which, in turn, allowed a quick heating ramp rate and a high maximum temperature.

In order to maximize the efficacy of the radial heat transfer, two custom-machined stainless steel (type SS304) blocks were placed inside of the CHTA on either side of the microsphere sample. These blocks were 2.5 cm (1 in) in thickness and 4.4 cm (1.75 in) diameter. The lower block had only a central hole drilled in it for the cartridge heater while the upper block had holes drilled for the cartridge heater and

Fig. 3.5. Photograph of the CHTA in the glovebox.

seven holes for the thermocouples to penetrate through the block into the sample. Figures 3.8 and 3.9 show these inserts.

In an effort to minimize vertical heat transfer from the stainless steel blocks into the sample, a thin sheet of insulation was placed between the block and the sample on both the top and the bottom of the sample. This was assembled by stacking the following components from the bottom of the crucible to the top of the crucible: 1) the bottom stainless steel block, 2) a sheet of insulation, 3) the sample material, 4) a sheet of insulation, 5) the top stainless steel block, and 6) the CHTA cover with thermocouple guides. The insulation was Fiberfrax 970 paper that was 0.159 cm (0.0625 in) thick and cut to fit the stainless steel block. A stainless steel tube

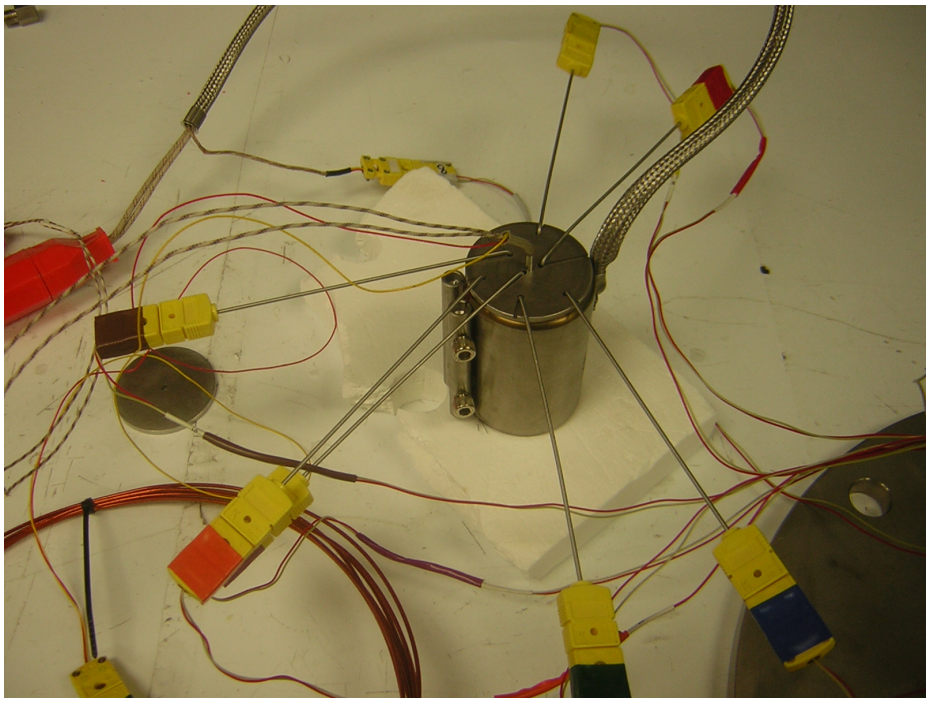

Fig. 3.6. Assembled CHTA before installation in the glovebox.

protected the cartridge heater and provided a channel for the cartridge heater to slide into; this tube was cut to be the length of the crucible.

The CHTA had a two part lid system, shown in Fig. 3.10, 3.11, and **??**. The first lid had a raised lip that fit loosely around the crucible in order to prevent it from sliding. The upper lid was a flat thin piece of metal. Both pieces were fabricated from stainless steel 304 and had a central hole drilled in order to allow the cartridge heater to slide in and out of the system. The lower lid had channels fabricated for the thermocouples to fix the position of each thermocouple in the sample. Thermocouples were secured into the lower lid and the upper lid rested on top as a secondary containment system.

The placement of the thermocouples was determined such that a complete radial temperature profile could be generated without disturbing the heat flux through the system too drastically. The thermocouple placements are listed in Table 3.2. One

Table 3.1
Products ordered for the CHTA.

Item Name	Supplier	ID Number	Amount
MI Band Heater	Watlow	1901	2
Firerod Cartridge Heater	Watlow	19012	3
Control Console	Watlow	50201	1
Fiberfrax Paper 970F	Unifrax	PS-3350	0.1 m^2
Stainless Steel Rod	McMaster-Carr	1305T351	1
Stainless Steel Tubing	McMaster-Carr	6100K192	1
TC Feed-Through	Conax Technologies	HD25-450(12K)PG2AT	1
Power Feed-Through	Conax Technologies	PL-16-A4-T, 120/84	1
TC Data Logger	Omega Engineering	OM-CP-OCTTEMP2000	1
Data Analysis Software	Omega Engineering	OM-CP-IFC110	1
Sub-mini Connectors	Omega Engineering	SMPW-K-M-ROHS	8
Sub-mini TC, K	Omega Engineering	KMQXL-062G-6	40

thermocouple was placed adjacent to the cartridge heater to verify the heater temperature and record the ramp rate during heat up. Three thermocouples were evenly spaced throughout the sample to illustrate the progression of the heat wave from the cartridge heater to the outermost band heater. More importantly, these central thermocouples were also used to determine if a near uniform radial temperature

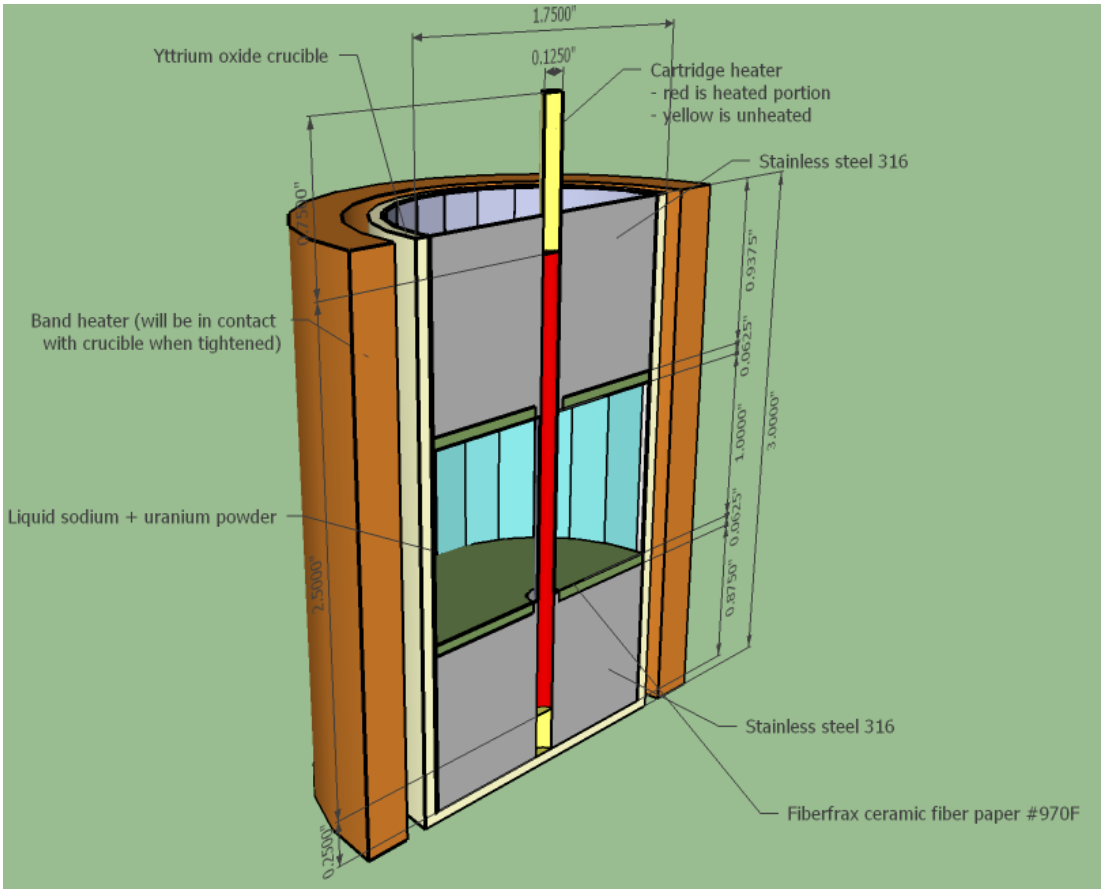

Fig. 3.7. Detailed CHTA schematic showing cartridge heater heated region.

profile had been established across the sample. Since the outermost and innermost thermocouples were privy to the response of the heaters directly, these alone would not have accurately conveyed if the entire radial temperature profile had reached steady state. Lastly, there were three thermocouples at the outermost band heater all equidistant from the central cartridge heater but offset by 120°. Together, these three thermocouples indicated if the temperature was uniform azimuthally. In total the thermocouple array included seven thermocouples each penetrating a depth of approximately 1.25 cm (0.5 in) into the powder sample. Additionally, all of the thermocouples were on different radial slices of the system; for any given thermocouple, if a radian was taken across the sample through the central cartridge heater, no other

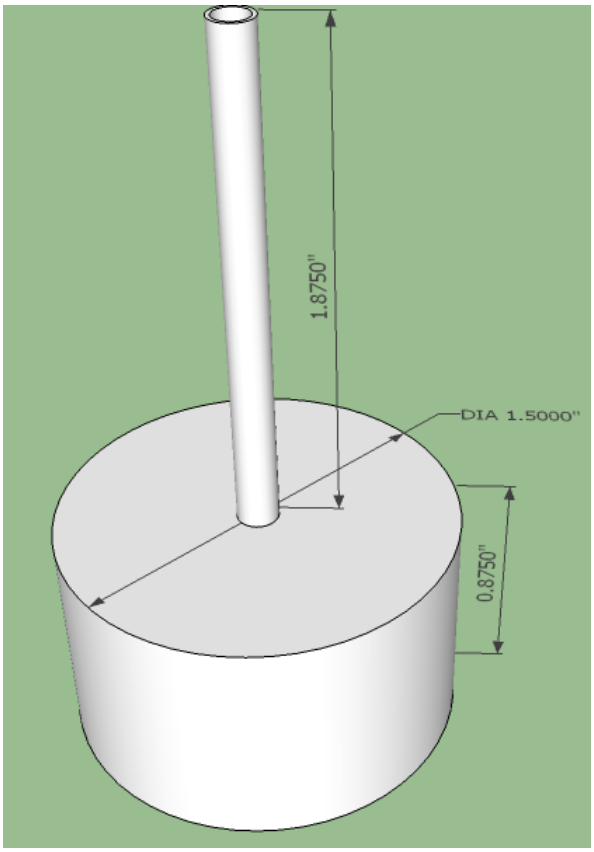

Fig. 3.8. The bottom stainless steel insert designed for the CHTA, all dimensions are in inches; also shown is cartridge heater guide tube.

thermocouples would fall on the same line. Type K thermocouples of 0.16 cm (0.0625 in) diameter were selected for all positions.

All thermocouple data was collected via a digital data logger. The data logger had the capability for eight input channels and an adjustable sampling rate. Each channel was set to record a new temperature measurement every second. Additionally, the data logger had the capability to interface directly with a computer and display real-time results on screen. Due to ease of navigation, the data logger was primarily used in conjunction with a laptop for all test runs. The data logger was purchased through Omega and came with calibration certification.

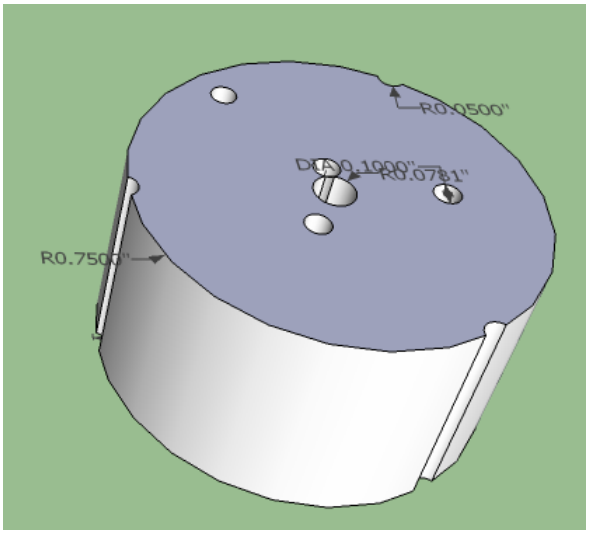

Fig. 3.9. The top stainless steel insert designed for the CHTA, all dimensions are in inches; the holes are drilled for thermocouple insertion.

Table 3.2
Thermocouple placements in the CHTA.

Thermocouple Number	Distance from Cartridge Heater (mm)
1	3.1
2	5.1
3	10.3
4	15.5
5, 6, 7	19.3

The CHTA was installed in a glovebox with a recirculating argon atmosphere. This glovebox operated with an argon atmosphere maintained below 50 ppm throughout this set of experiments and was regenerated regularly using a Dri-Train (manufactured by Vacuum Atmospheres Company model number MO 40-1). Initially, steel

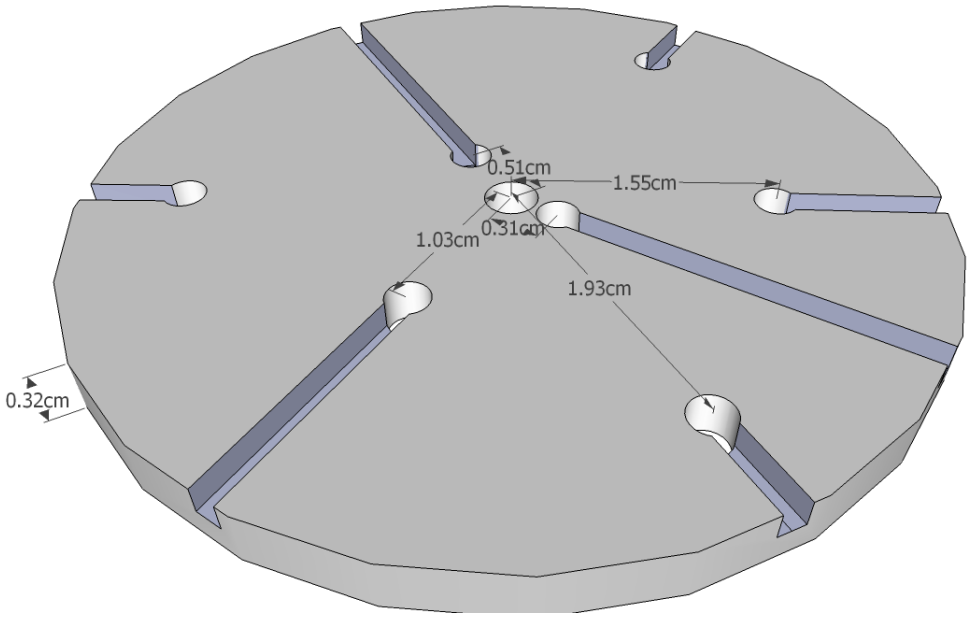

Fig. 3.10. The bottom portion of the lid with troughs designed to secure thermocouples in specified positions (see Table 3.2) all dimensions are given in cm.

microsphere samples[1]were tested in the CHTA outside of the glovebox in air. An oxidation layer was noticed to form on the outside of the steel microspheres after the CHTA had been tested up to 400°C. At this point, the apparatus was installed in the glovebox via a wire feed-through port located on the side wall of the glovebox, see Fig. 3.13. The feed-through ports were welded into a stainless steel plate. One feed-through contained 12 thermocouple pair wires; the other allowed for four power lead wires. Thermocouple or power lead connections were then installed on the ends of the wires to create a circuit. The use of feed-throughs allowed for power to be supplied to the heaters through a control console and for the thermocouple data to be collected and analyzed outside of the glovebox.

[1]Courtesy of M. Hash, Ervin Industries, MI

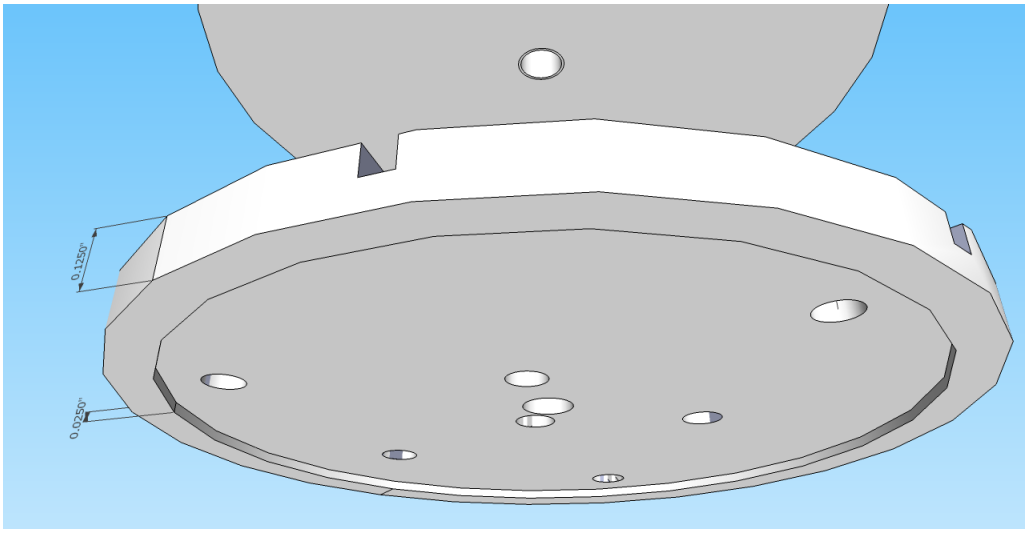

Fig. 3.11. Two part lid system designed for use with the CHTA, all dimensions are given in inches.

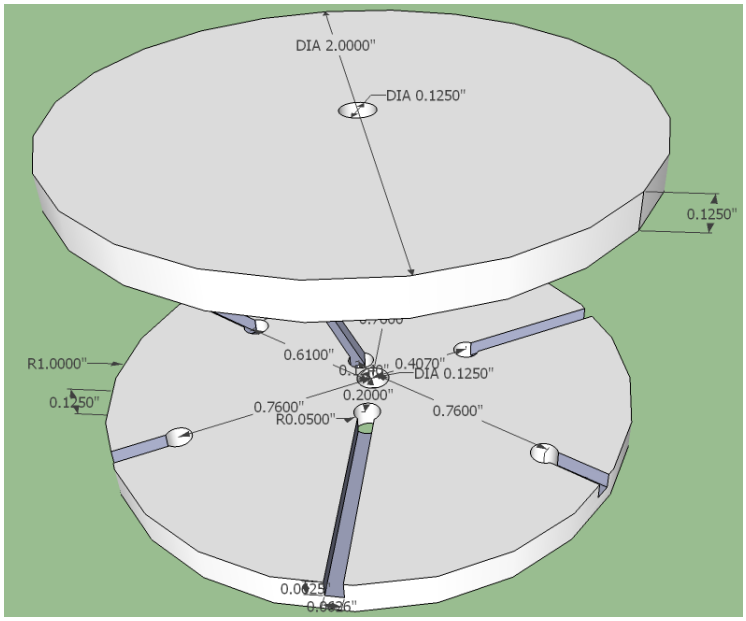

Fig. 3.12. Detailed two part lid system designed for use with the CHTA, all dimensions are given in inches.

3.2.2 Implementation of the CHTA

Benchmark testing was completed in air with two different steel microsphere samples. Initial hold times ranging from 30 minutes to 3 hours were tested after

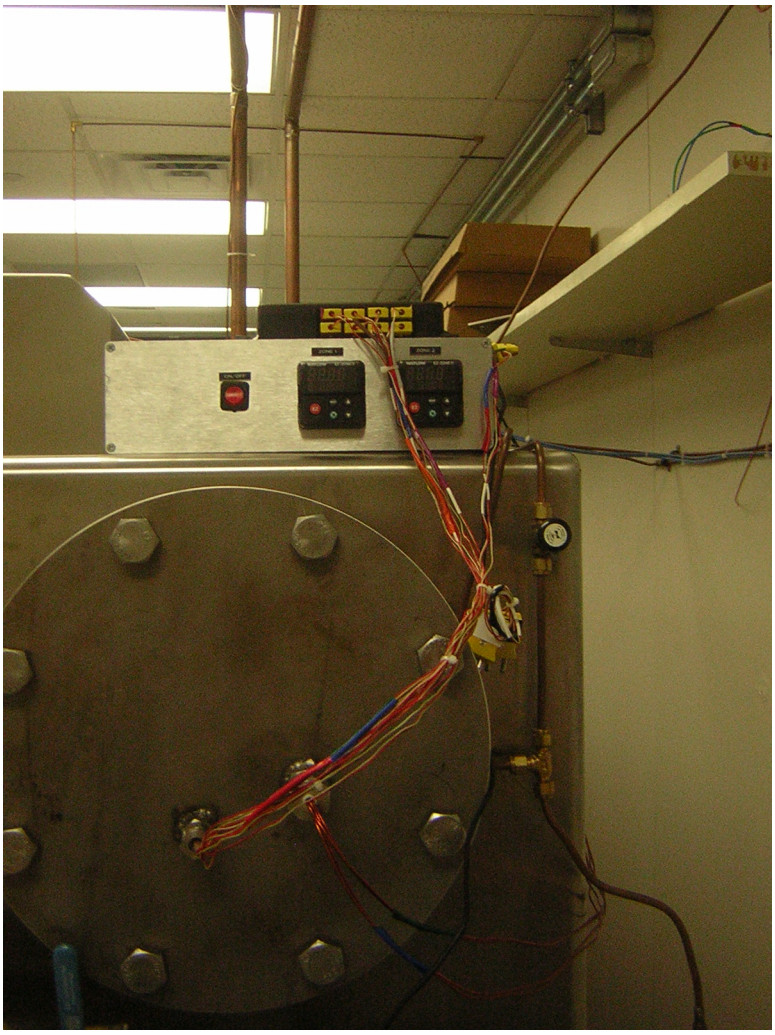

Fig. 3.13. Photograph of the CHTA data collection sytem outside of the glovebox.

the outer band heater had been heated to 100°C to determine how long it took for the radial temperature profile to equilibrate. Heating scenarios with and without the cartridge heater engaged were examined to determine if a uniform radial temperature profile could be established by the band heater alone or if a combination effort from the band and cartridge heaters was optimal. The cartridge heater used for this preliminary testing had poor calibration with the control console and would regularly exceed the programmed temperature. Settings on the PID were adjusted and tuned

to optimize the performance of both heaters. The cartridge heater was regularly plugged into input one and the band heater in input two due to calibration settings. Following this initial benchmark testing, the apparatus was installed in the glovebox.

To initiate a test, the lower stainless steel block and insulation layer were placed in the crucible before being loaded into the glovebox. The crucible was allowed to off-gas under a rough vacuum in the airlock of the glovebox for at least 24 hours to reduce the impurities in the glovebox and limit the amount of oxygen introduced. A stainless steel tube that was approximately 5 cm (2 in) in length was inserted into the center hole of the lower block to serve as a guide for cartridge heater insertion. The tube stretched from the bottom of the crucible, through the first block, and through the sample. Dimensions of the tube were selected to optimize heat transfer away from the cartridge heater, i.e. the tube was very thin-walled (about 1 mm). The guide tube served to protect the cartridge heater from burning out by providing a solid heat transfer surface as opposed to the point contacts that would have resulted from the microspheres. It also ensured that the top stainless steel block was aligned with the bottom stainless steel block by forcing the cartridge heater to be inserted perpendicular to both blocks. The tube remained in the crucible for the duration of the test run.

After the tube was set, the crucible was placed into the band heater which was then loosely tightened. Once stable, the cartridge heater was temporarily inserted into the tube to prevent microspheres from pouring down the tube to the bottom of the crucible. After this, microspheres may be successfully poured into the crucible on top of the lower piece of insulation. Microspheres were poured until the crucible was filled to near the top of the tube. At this point, the cartridge heater was removed. The upper piece of insulation was placed on top of the sample followed by the top stainless steel block. The lower lid, with thermocouples troughs upward, was placed on the top of the crucible. Thermocouples were then placed individually through the lid, into the sample at previously determined depths (about 4 cm) to penetrate the

sample. Once all seven thermocouples were placed, the second lid was added to the system and the cartridge heater was reinserted into the center hole.

The temperature control programs were set using the control console and began with a preliminary heating up step. In this step, the system was heated to 125°C in 20 minutes using both the band and cartridge heaters. After the set point was reached, the temperature was held for 1 hour to allow the radial temperature profile to equilibrate. The band heater remained at this set point throughout the remainder of the run to provide a constant ambient temperature. The heat pulse from the cartridge heater occurred after the one hour hold time. Each test run had a constant ramp rate and a programmed maximum hold temperature; once the maximum temperature was reached, to was maintained for one hour. After the hour hold, the cartridge and band heaters simultaneously disengaged and the system cooled without a control program. A typical heating profile is shown in Fig. 3.14; this test run was completed with ODU microspheres, with a ramp rate of 20°C and a maximum temperature of 450°C. The innermost and outermost thermocouple placements are indicated on the figure, in addition, the time interval for an isotherm to traverse from the innermost thermocouple to the outermost thermocouple is indicated.

An expanded version of the temperature profile in Fig. 3.14 is shown in Fig. 3.15; this data was collected for a test run with ODU, a ramp rate of 20°C and a maximum temperature of 450°C. Thermocouple measurements with known radial positions, were plotted and the temperature was interpolated between thermocouples to create a smooth temperature distribution. This figure is included to demonstrate the progression of the heat pulse through the sample.

Each powder sample was planned to be tested with a starting hold temperature of 125°C and maximum temperatures of 250, 350 and 450°C. The oxidized depleted uranium microspheres were measured with ramp rates of 10, 15 and 20°C/min. Various ramp rates were tested to determine if the ramp rate altered the calculation of the thermal diffusivity. Ramp rates were set using the PID controller for the car-

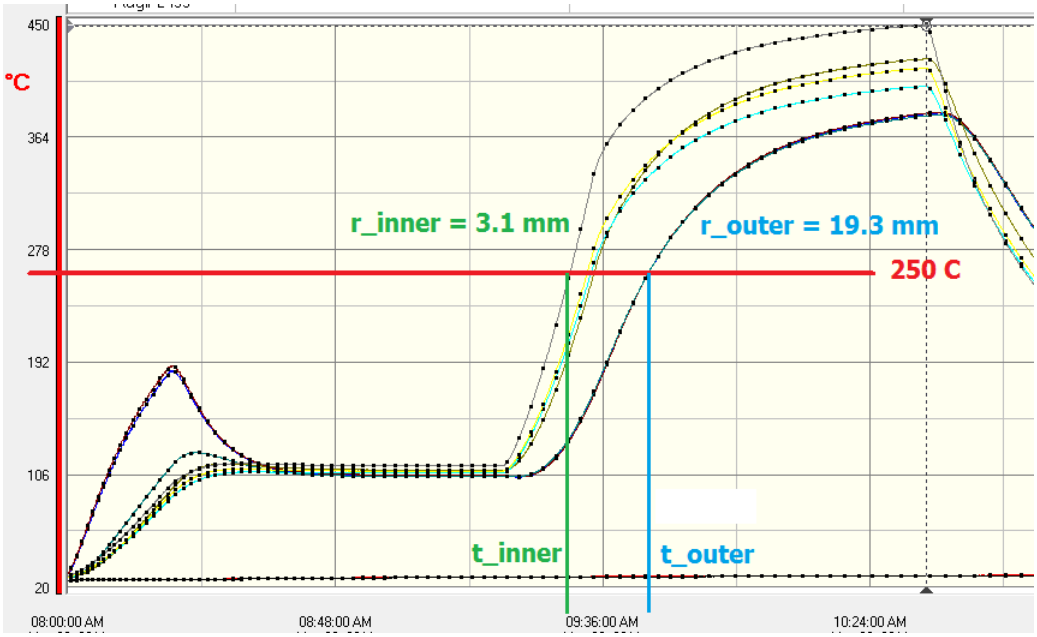

Fig. 3.14. Sample data test from CHTA.

tridge heater. This was accomplished by changing the amount of time allowed for the cartridge heater to complete the pulse.

3.2.3 Data Analysis Method

A few different transient state analysis methods were considered during the design of the CHTA system. The foundation of the transient analysis was the establishment of a temperature change across the sample. This was considered from three different perspectives. After a near steady-state was achieved across the sample, the cartridge heater was pulsed and a thermal transient was initiated, which created a temperature transient that was recorded by the thermocouple array. This was the first transient in the system. After the peak temperature of the cartridge heater was reached, the system equilibrated without heat flux changes supplied through either the cartridge or band heaters; however, the temperatures were still changing across the sample material. During this second transient phase, no changes were made to the external

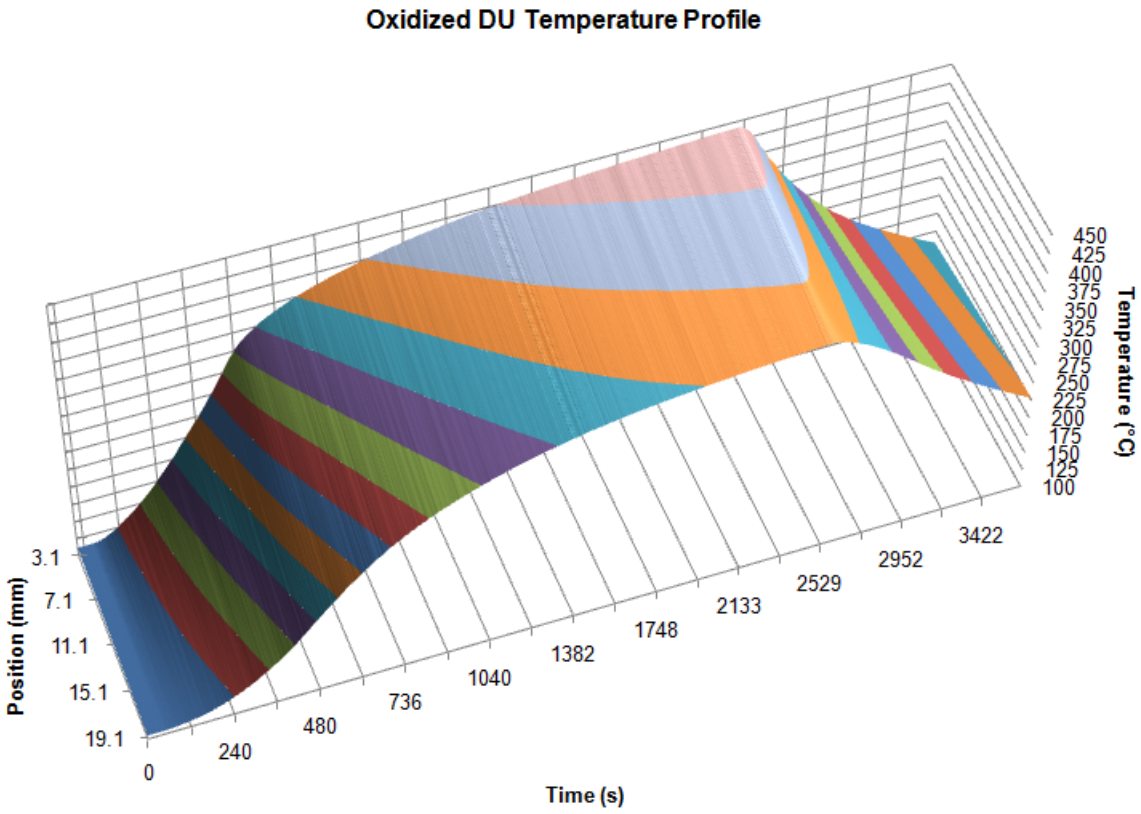

Fig. 3.15. Interpolated sample data test from CHTA.

heat flux and the changes were driven by thermal diffusion. After the hour hold time, both heaters were turned off and the system was allowed to cool naturally to room temperature. This cool down period was the third transient. The difference in dimensions of the band and cartridge heaters allows the band heater to retain heat more easily than the cartridge heater.

Hot-wire analysis methods were also examined in the design process, however, the implementation of such equations proved tricky since the heat source was not well characterized. In order to properly analyze the system, the heat flux into the system at all points must be well known. This requires precision that is not available in the selected laboratory equipment and heaters. As another alternative, a Fick's Law of

Diffusion type approach was examined for analysis but this required the assumption that thermal diffusivity was not a function of temperature; an assumption known to be false. For this reason, a system was designed that allowed for calculation of thermal diffusivity using transient state analysis.

In order to calculate the thermal diffusivity, the time required for a certain temperature to progress through a specified surface area had to be known. In the LFA method, the sample has a known thickness, the furnace is well controlled at a constant temperature and the time required for effects of the light flash to be detected on the top surface of the sample was recorded. A similar approach was taken in the design of the CHTA. The system was controlled at a constant temperature then a thermal transient was introduced and progressed across the sample and the rate at which a specific temperature progressed indicated the thermal diffusivity for that temperature. Similar methods were used to calculate the time required for the wave to progress through known surface areas as those used to model the data obtained through LFA.

$$\alpha(T) = \frac{1}{2\pi} \frac{A_{outer} - A_{inner}}{t_{outer} - t_{inner}} \tag{3.1}$$

Shown in Eq. 3.1 is the method utilized to calculate the apparent thermal diffusivity. The A values in the equation were the surface areas of the innermost and outermost thermocouples when examined as a planar slice of a cylinder with the radius equivalent to the location of the thermocouple. The t terms indicated the time required for a heat pulse to be recorded at the inner and outer thermocouples. A factor of $\frac{1}{2\pi}$ appeared due to the radial geometry. As a result, the units of the equation work properly to determine apparent thermal diffusivity which was then evaluated to determine thermal conductivity. This equation was derived based upon that presented as Eq. 2.2 [5]. As test parameters were altered, the calculated apparent thermal diffusivity approached the actual thermal diffusivity for the sample.

3.2.4 Systematic Uncertainty

Equipment for the CHTA was selected with consideration of uncertainty minimization. A data logger that interfaces with the computer was used for accurate collection of time-temperature data. While the time log on this device has a negligible uncertainty, the accuracy in the measurement of temperature data is ±0.5°C for type K thermocouples. This is compounded to the uncertainty of the type K thermocouple, which is the greater of either 2.2°C or 0.75% of the measured value. This source of uncertainty is relatively insignificant due to the frequency of measurements; the interval between measurements was typically two to five seconds.

A non-trivial source of uncertainty can be attributed to the thermocouple positions. Partially to encourage ease of operation in a glovebox, the bore holes for the thermocouples in the lid and upper stainless steel block were drilled to be 2.54 mm (0.1 in) in diameter while the thermocouples were 1.59 mm (0.0625 in) in diameter. When propagated through the calculation of the inner and outer surface areas, a relative error of approximately ±13% resulted in all calculations of thermal diffusivity. At a given temperature, the density and specific heat were regarded as constants. For this reason, thermal conductivity values also contained a ±13% uncertainty.

Uncertainty that cannot be quantified resulted from assumptions made in the design of the apparatus. These assumptions that may contribute uncertainty were that the heat flux from the central cartridge heater during the pulse travels radially outward and is constant along the length of the heated region. Also, the insulating papers between the stainless steel blocks and the uranium metal sample were assumed to effectively block all heat transfer from the stainless steel into the uranium. To compensate for heat transfer effects near the stainless steel blocks, thermocouple placement was established in the vertical mid-plane of the sample cylinder.

4. RESULTS

4.1 Light Flash Analysis Data

The oxidized depleted uranium microspheres were loaded into the sapphire LFA sample holders within the large glove box and then transferred through the airlock to the system for analysis. Microspheres were closely monitored at room temperature to observe any signs of oxidation (for example, heat). Samples showed no signs of further oxidation at room temperature and were loaded into the LFA for testing. The LFA was programmed to flash every 25°C from room temperature to 300°C; each individual flash of the lamp is known as a shot. Each shot had a duration of at least 30 s between the firing of the flash lamp and the detection of the heat pulse on the top surface of the sample.

At 150°C, the thermal diffusivity data began to decrease in an unusual manner, indicating that a change might be occurring within the sample holder. This drop-off occurred until 225°C, at which point the system forced a test shut down. Thermal diffusivity values obtained from this LFA test are presented in Fig. 4.1.

After cooling to room temperature, the LFA was opened to view the samples. It was immediately apparent that the sapphire sample pans had shattered causing the uranium microspheres to drop off the sample platform onto the lower plate immediately above the flash lamp. Due to the failure of the sapphire pans, the unwashed depleted uranium microspheres were only tested once within the LFA. Since unwashed microspheres with a significant oxidation layer caused failure of the sapphire pans, it was decided that testing within the LFA would not be used for the WDU microspheres. The interpretation of these results is discussed in Section 5.1.

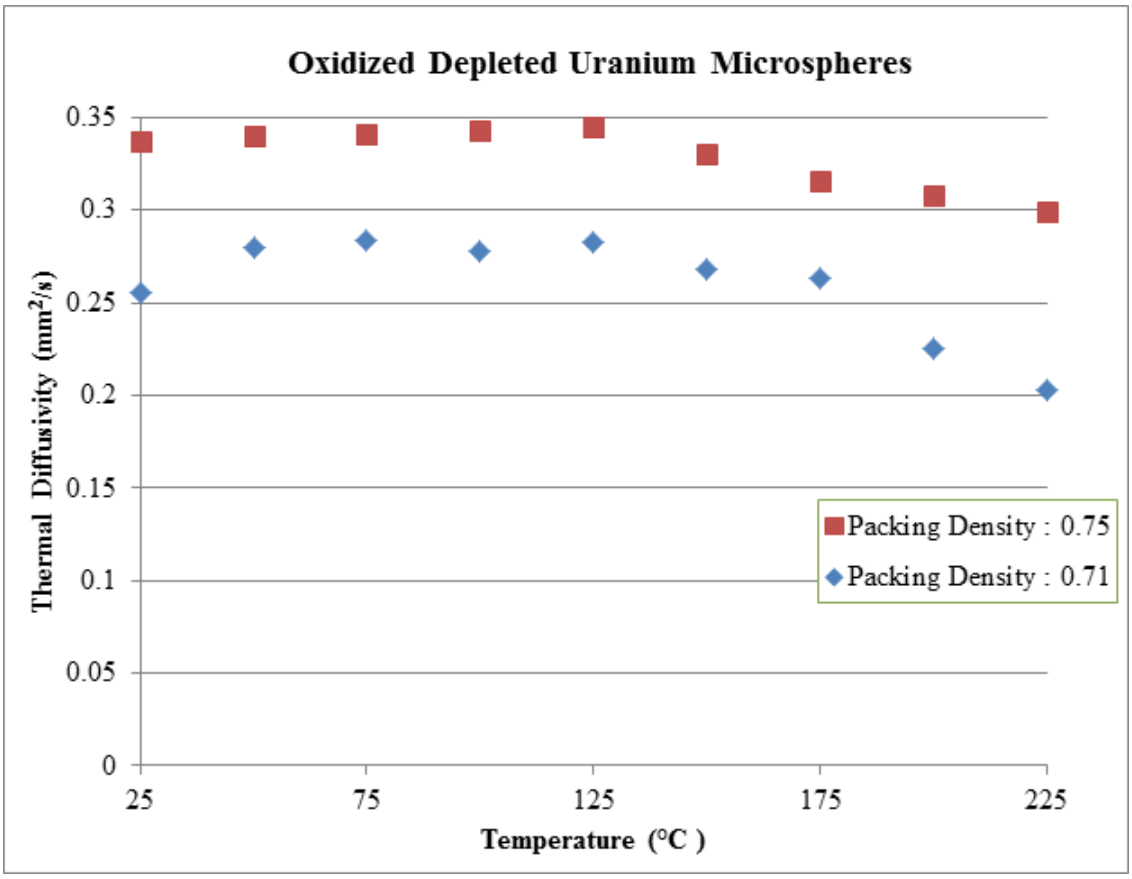

Fig. 4.1. Thermal diffusivity vs. temperature measurements using the LFA powder sample holder and ODU microspheres; the notable change at 125°C indicates a possible change in test material.

4.2 Crucible Heater Test Assembly

Testing within the Crucible Heater Test Assembly (CHTA) was completed with the ODU and WDU microspheres. Table 4.1 details each individual CHTA test and pertinent parameters for the heaters. Data collected from Test Series A was utilized to establish test parameters in Test Series B. Each test series was completed using a single sample of microspheres in the same packing arrangement without external disruption to the system. Therefore, systematic errors in thermocouple position and packing efficiency are maintained identical throughout each series.

Table 4.1
Tests performed using the CHTA.

Test Series (Material)	Test Number	Band Heater Temperature (°C)	Cartridge Heater Set Point (°C)	Ramp Rate (°C/min)
A (ODU)	1	125	250	15
A (ODU)	2	125	350	15
A (ODU)	3	125	450	15
A (ODU)	4	125	250	20
A (ODU)	5	125	350	20
A (ODU)	6	125	450	20
A (ODU)	7	125	250	10
A (ODU)	8	125	350	10
A (ODU)	9	125	450	10
B (WDU)	1	25	350	20
B (WDU)	2	125	350	20
B (WDU)	3	125	450	20
B (WDU)	4	25	450	20
B (WDU)	5	25	350	40
B (WDU)	6	25	450	40
B (WDU)	7	50	550	20
B (WDU)	8	50	550	40
B (WDU)	9	50	350	60
B (WDU)	10	30	450	60
B (WDU)	11	50	550	60
B (WDU)	12	50	650	20
B (WDU)	13	50	650	40
B (WDU)	14	50	650	60
B (WDU)	15	50	650	200

Microspheres other than the depleted uranium were originally tested to characterize the CHTA and determine appropriate operating conditions. These microspheres were used solely for programming the heaters and, as such, the test parameters were highly variable leading to inconsistent data.

4.2.1 Program Effects

For consistency, it was determined that all experiments should follow the same procedure with the initial temperature of 125°C. The band and central cartridge heaters were set to 125°C in order to create a uniform radial temperature profile in a shorter period of time. Various experiments were subjected to different ramp rates to reach the maximum set point of the cartridge heater. The ramp rate was programmed into the control box as the length of time desired for the cartridge heater to reach the maximum set point from the 125°C hold temperature. The maximum set point temperatures were 250, 350, and 450°C; each with ramp rates of 10, 15, and 20°C/min. Analysis of the data gathered from the ODU samples in Test Series A suggested changes for Test Series B and the maximum temperatures for WDU were changed to 350, 450, 550, and 650°C. Also, the ramp rates were changed to 20, 40, and 60°C/min. Tests in Series B were completed with an outer band heater temperature from 25 to 50°C, as opposed to the previous 125°C established in Matrix A. Two tests were run with WDU identical to the tests completed with ODU; with ramp rates of 20°C/min, maximum cartridge heater set points of 350 and 450°C and an initial hold temperature of 125°C.

One test was completed with a programmed ramp rate of 200°C/min to test the cartridge heater limitations. The cartridge heater ramp rate maxed out at 150°C/min, per measurements on the heater control thermocouple, without burning out or causing system damage to the CHTA. Fig. 4.2 illustrates the programmed ramp rate, achieved ramp rate and the innermost thermocouple temperature mea-

surement during the cartridge heater pulse from this test. This information characterizes the maximum ramp rate the cartridge heater was able to successfully maintain.

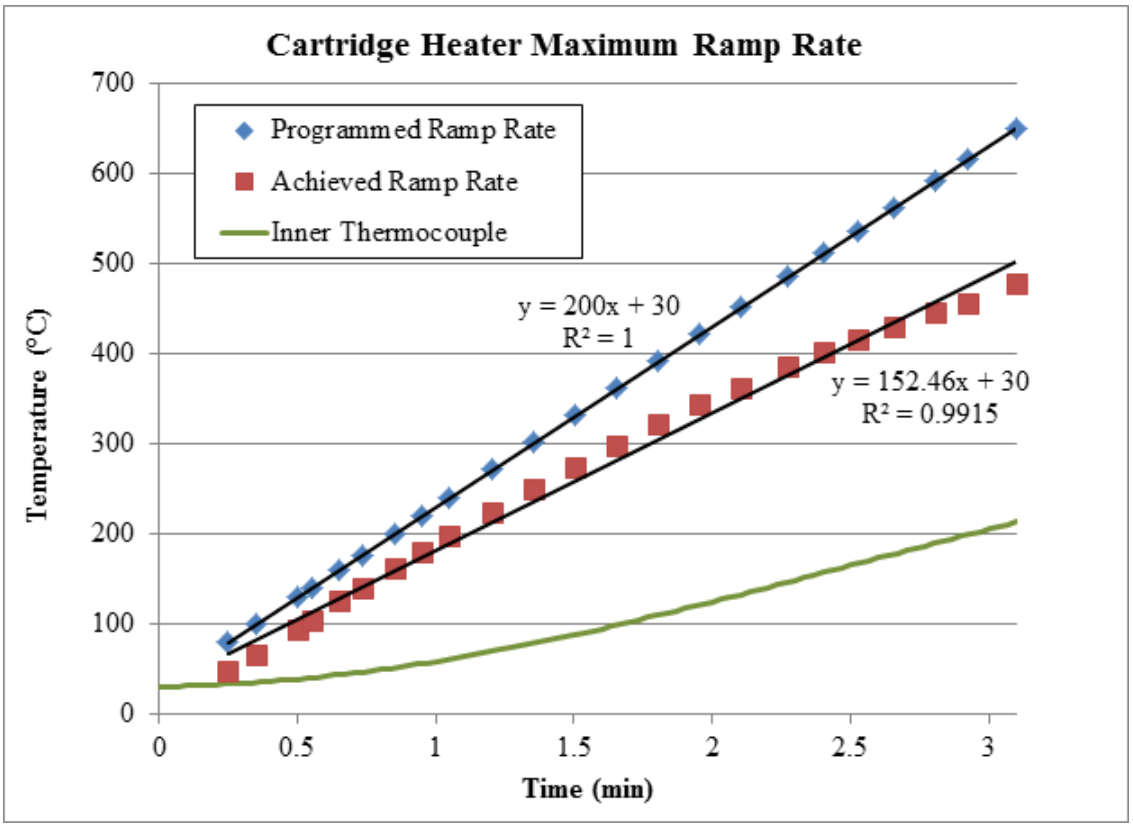

Fig. 4.2. Maximum CHTA system ramp rate achievable by the central cartridge heater; data from Series B, Test 15.

4.2.2 Data from ODU Microspheres

Results from Series A are presented in this section. In the case of all of the runs with a maximum cartridge heater temperature of 250°C, the data range that was analyzable was too small to be worthwhile due to the format of the thermal diffusivity equation (which is why 250°C was omitted from Test Series B). By the time the cartridge heater disengaged, the innermost thermocouple reading was greater than that achieved by the outermost thermocouple at any point during the test run. Since

the data was only analyzable after the cartridge heater pulse disengaged but before a steady-state was achieved at the innermost thermocouple, the high temperature at the innermost thermocouple as compared to that at the outermost thermocouple presented an insurmountable analysis challenge.

Data from tests 1, 4, and 7 from Series A were not useful for analysis because the change in temperature between the initial hold temperature and the maximum cartridge heater temperature was only 125°; a range which proved too narrow to analyze.

Figure 4.3 is data collected for the second test with the ODU microspheres. The heater settings for this test were the band heater set initially to 125°C, the cartridge heater maximum temperature set to 350°C by ramping 15°C/min. This data test was completed to analyze the effect of ramp rate on the calculated apparent thermal diffusivity. The glovebox oxygen level was 5.47 ppm.

Figure 4.4 is data collected for the third test with the ODU microspheres. The heater settings for this test were the band heater set initially to 125°C, the cartridge heater maximum temperature set to 450°C by ramping 15°C/min. This data test was completed to compare differences in maximum temperature on the calculated apparent thermal diffusivity. The glovebox oxygen level was 5.93 ppm.

Figure 4.5 is data collected for the fifth test with the ODU microspheres. The heater settings for this test were the band heater set initially to 125°C, the cartridge heater maximum temperature set to 350°C by ramping 20°C/min. This data test was completed to analyze the effect of ramp rate on the calculated apparent thermal diffusivity. The glovebox oxygen level was 15.36 ppm. Shown in Fig. 4.6, is the A5 test data with the addition of the regions of best analyzable data (top shaded region) and limited analyzable data (bottom shaded region). The lower shaded region is during the cartridge heater ramping stage and is during the first transient in the system; the upper shaded region is during the maximum temperature hold and illustrates the second transient region.

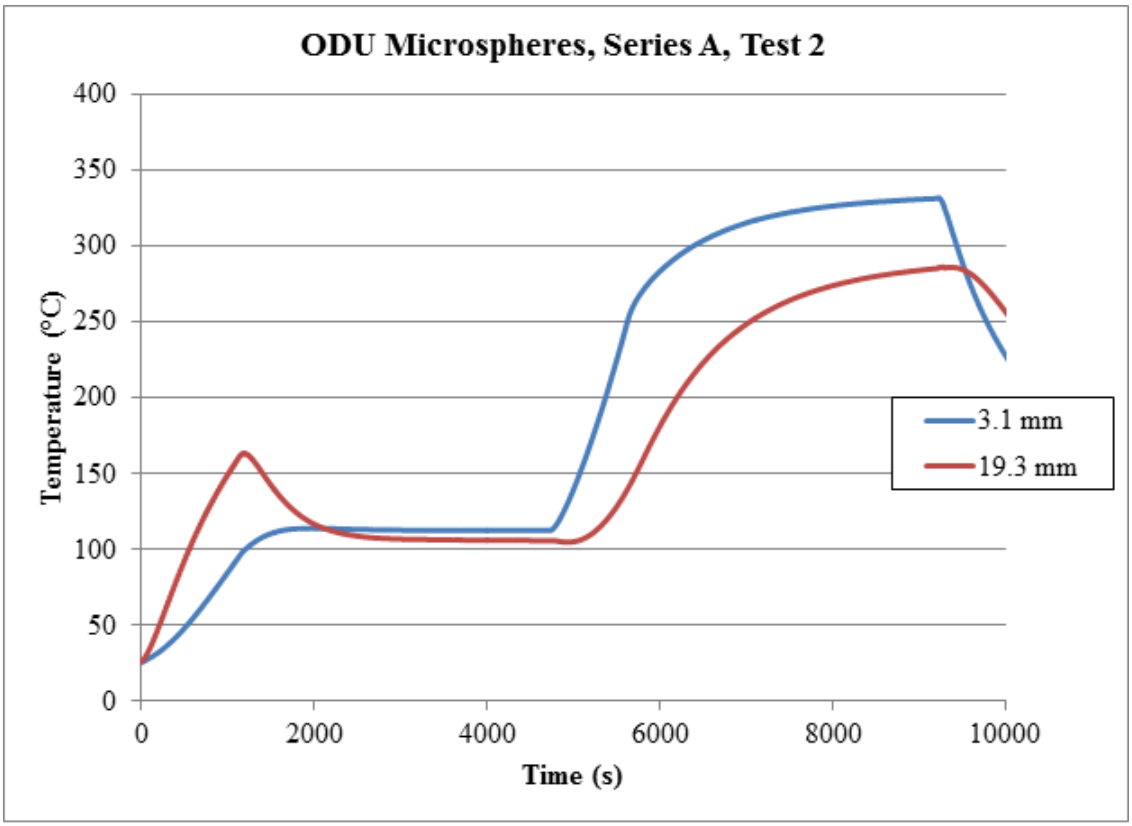

Fig. 4.3. Time dependent temperature data from CHTA testing, Series A, Test 2.

Figure 4.7 is data collected for the sixth test with the ODU microspheres. The heater settings for this test were the band heater set initially to 125°C, the cartridge heater maximum temperature set to 450°C by ramping 20°C/min. This data test was completed to compare differences in maximum temperature on the calculated apparent thermal diffusivity. Shown in Fig. 4.7 is the temperature of the cartridge heater as programmed during the ramping stage; the orange vertical line represents the point at which the system transitions to the second transient phase. The glovebox oxygen level was 20.72 ppm. In this test, it appears an error was made and the maximum temperature was actually set to 400°C instead of the intended 450°C.

Figure 4.8 is data collected for the eigth test with the ODU microspheres. The heater settings for this test were the band heater set initially to 125°C, the cartridge

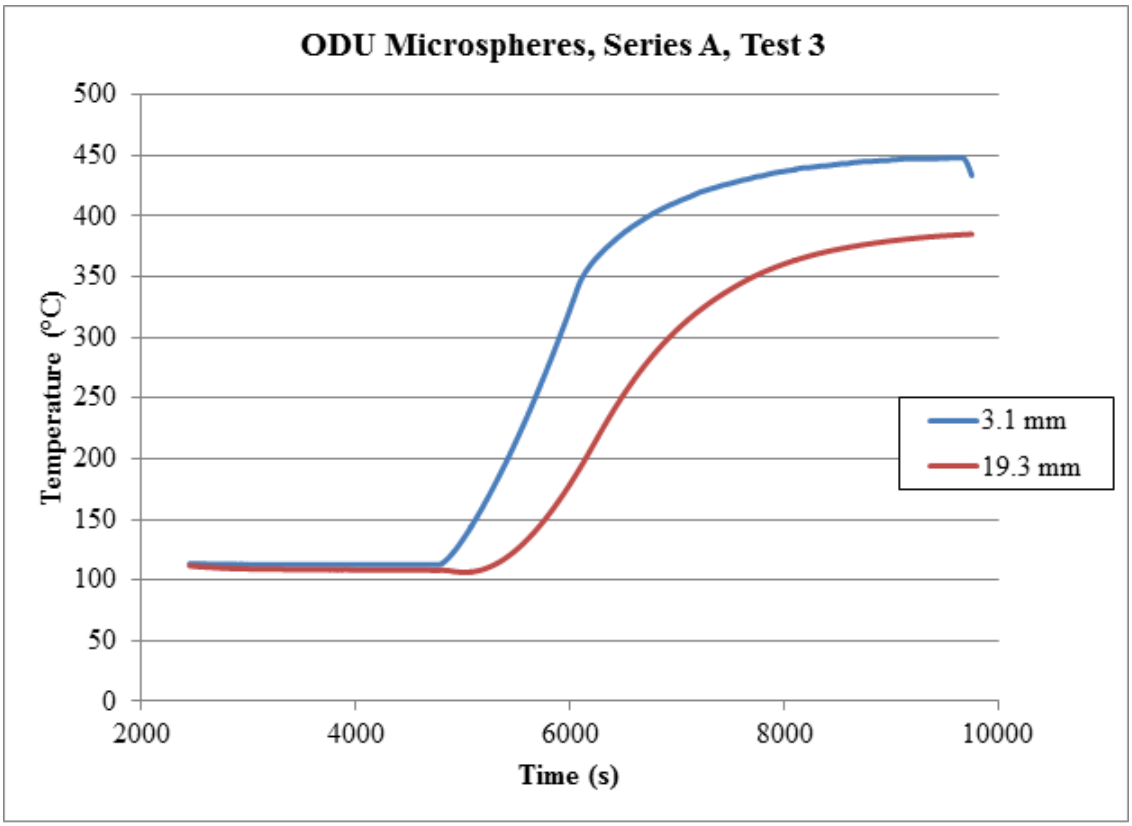

Fig. 4.4. Time dependent temperature data from CHTA testing, Series A, Test 3. The cartridge heater temperature is shown in green, with an orange vertical dashed line signifying the point at which the cartridge heater stopped ramping at the rate of 20°C.

heater maximum temperature set to 350°C by ramping 10°C/min. This data test was completed to analyze the effect of ramp rate on the calculated apparent thermal diffusivity. The glovebox oxygen level was 28.07 ppm. Shown in Fig. 4.9, is the A8 test data with the addition of the regions of best analyzable data (top shaded region) and limited analyzable data (bottom shaded region). The lower shaded region is during the cartridge heater ramping stage and is during the first transient in the system; the upper shaded region is during the maximum temperature hold and illustrates the second transient region.

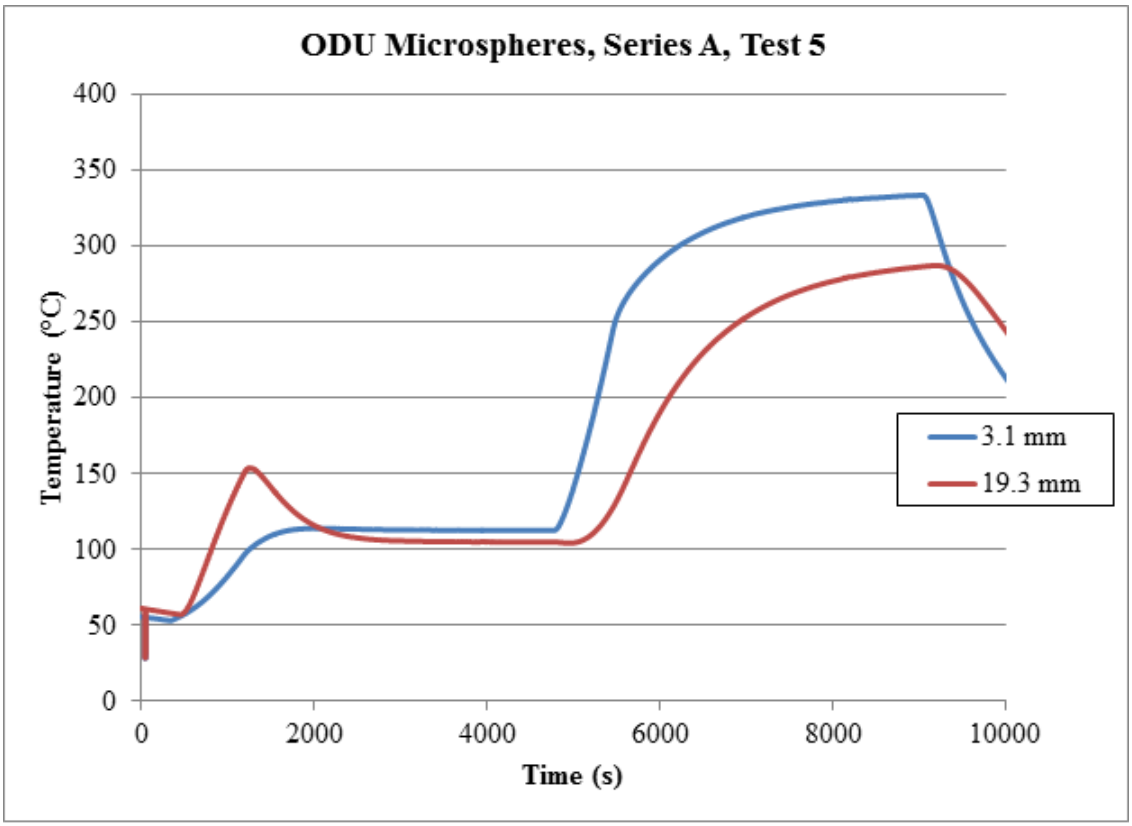

Fig. 4.5. Time dependent temperature data from CHTA testing, Series A, Test 5.

Figure 4.10 is data collected for the ninth test with the ODU microspheres. The heater settings for this test were the band heater set initially to 125°C, the cartridge heater maximum temperature set to 450°C by ramping 10°C/min. In Fig. 4.10, the cartridge heater temperature is plotted in addition to the temperatures recorded at the inner and outer thermocouples. Also indicated is the point at which the cartridge heater switched from the first transient to the second transient, as discussed in Section 3.2.3. This data test was completed to analyze the effect of ramp rate on the calculated apparent thermal diffusivity. The glovebox oxygen level was 32.52 ppm.

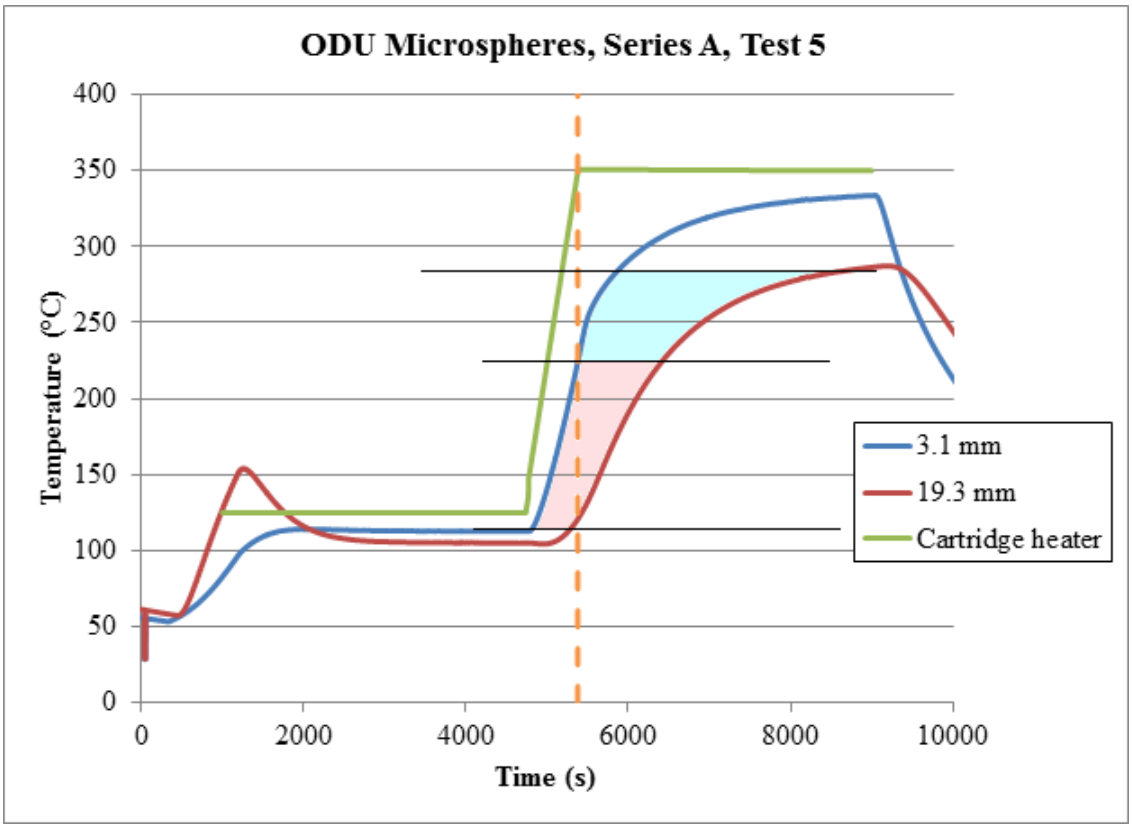

Fig. 4.6. Time dependent temperature data from CHTA testing, Series A, Test 5 with analysis regions shown.

4.2.3 Data from WDU Microspheres

Uranium was initially washed with nitric acid in a glovebag within a fume hood. In the glovebag, the uranium turned a bright silver hue while in the nitric acid solution. It was noticed that the nitric acid washing solution created an exothermic reaction and the wash beaker became warm to the touch. As the microspheres were poured out of the nitric acid solution, heat was rapidly released and the uranium turned a very dark brown color within the glove bag. It was hypothesized that the key issue was oxygen contamination within the glove bag. The small glovebox was configured for washing the uranium microspheres. Again, while in solution, the microspheres were a bright silver hue. While still in solution, the microspheres

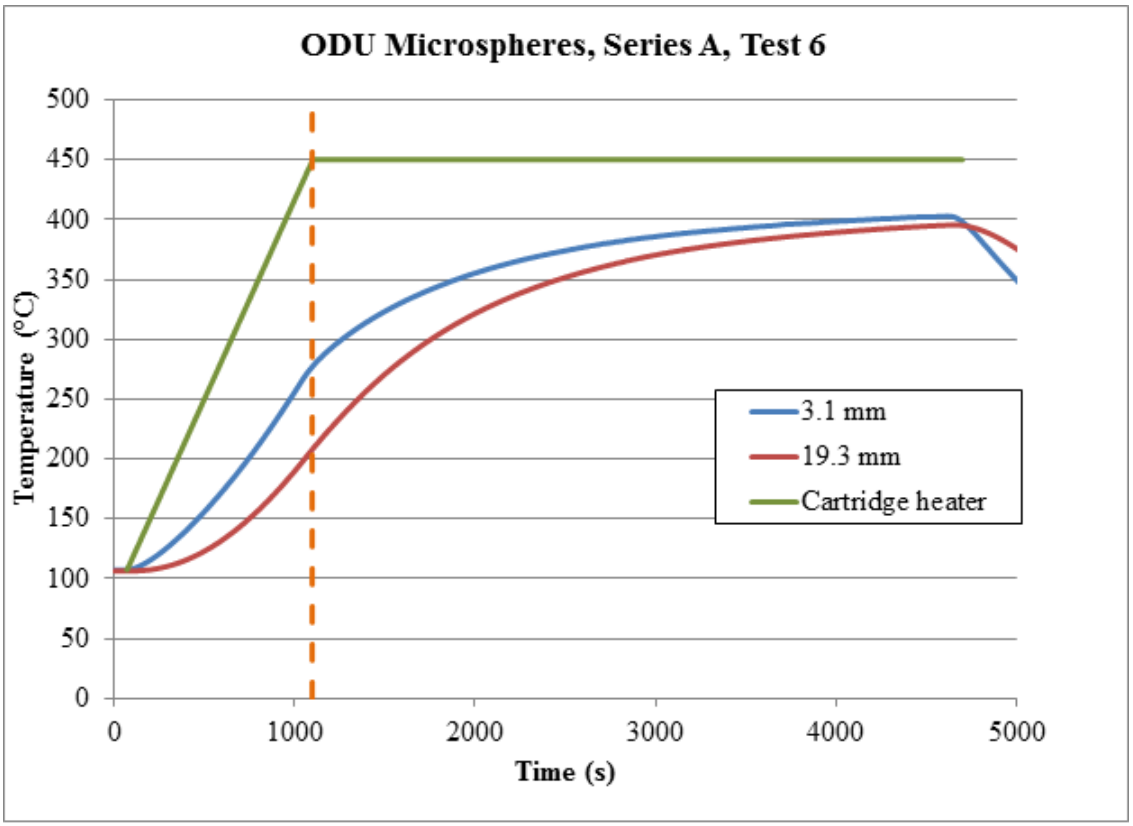

Fig. 4.7. Time dependent temperature data from CHTA testing, Series A, Test 6. Cartridge heater temperature is shown in green with an orange vertical dashed line when the cartridge heater stopped ramping

began to shift to a darker color with a slight brown hinge. Since the microspheres were entirely submerged in solution, it was suspected that either a thin uranium nitride or uranium oxide layer formed on the exposed surface of the microspheres; with uranium nitride seeming more feasible. Due to the inability to remove this surface contamination, the WDU microspheres were tested in the CHTA with a newly formed layer of surface oxidation or nitridation.

Based on the data collected for the ODU microspheres, test settings were altered for the WDU microspheres in an effort to approximate the actual thermal diffusivity as opposed to the apparent thermal diffusivity. These changes were elimination of

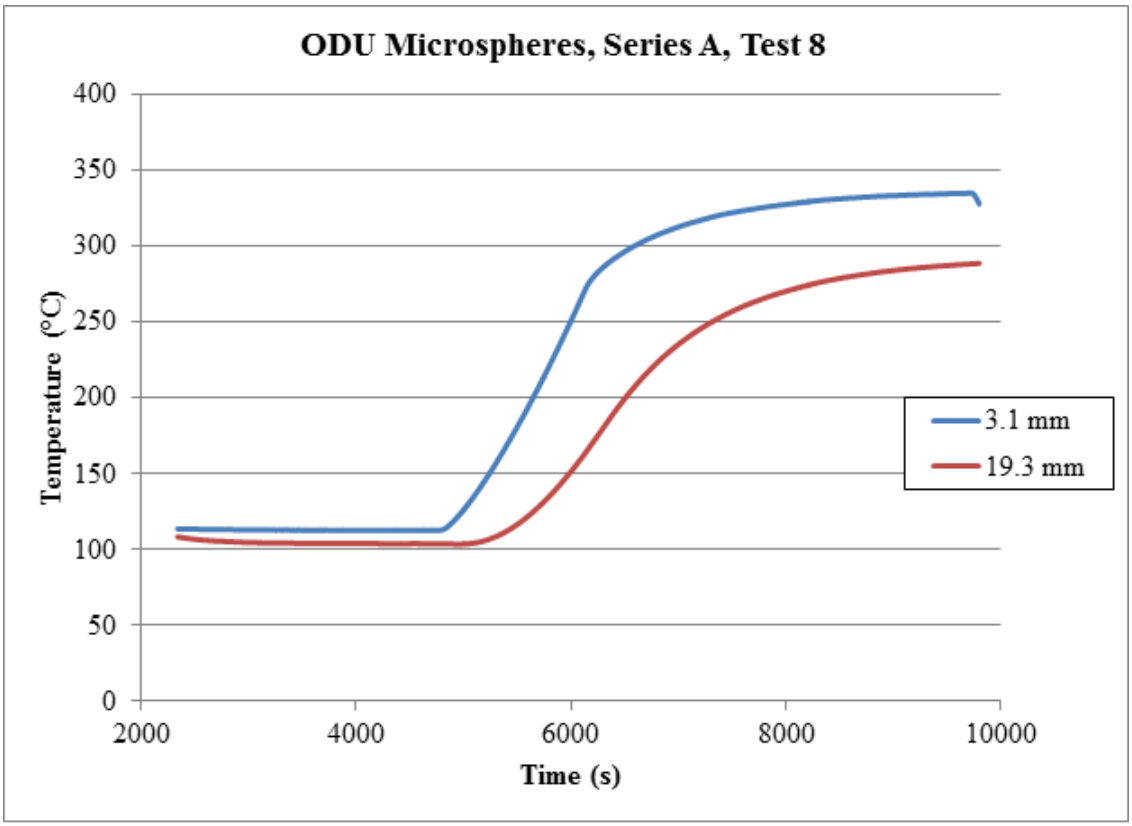

Fig. 4.8. Time dependent temperature data from CHTA testing, Series A, Test 8.

the initial elevated hold temperature, ramping rates of 20, 40 and 60°C/min, and increased maximum temperatures of 450, 550, and 650°C. The parameters for each test are presented with a time-temperature plot and the glovebox oxygen levels. In order to clearly present data, only temperature records for the innermost thermocouple (located at 3.1 mm) and the average of the outermost thermocouples (located at 19.3 mm) are shown.

Figure 4.11 is data collected for the first test with the WDU microspheres. The heater settings for this test were the band heater set initially to 25°C, the cartridge heater maximum temperature set to 350°C by ramping 20°C/min. This test was completed for comparison to Series A, Test 5. The glovebox oxygen level was 21.22 ppm, despite frequent purity regeneration cycles.

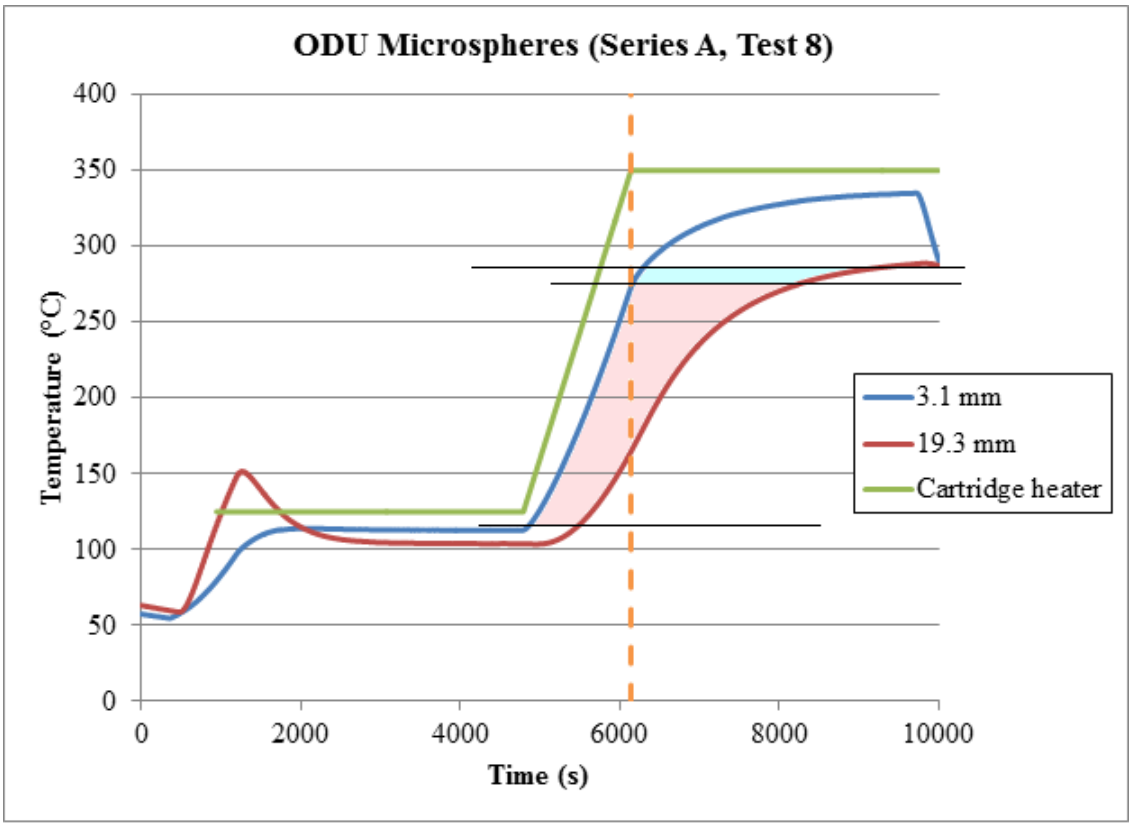

Fig. 4.9. Time dependent temperature data from CHTA testing, Series A, Test 8 with analysis regions shown.

Figure 4.12 is data collected for the second test with the WDU microspheres. The heater settings for this test had the band heater initially at 125°C and the cartridge heater maximum temperature set to 350°C by ramping 20°C/min. Series B, Tests 1 and 2 were both completed to compare to data from Series A, Test 5. The difference between these tests was the initial temperature set by the band heater. The goal was to verify that the initial ambient temperature did not have an effect on the calculated apparent thermal diffusivity. This data test has a longer initial hold time in order to establish a uniform initial radial temperature profile. The glovebox oxygen level was 21.71 ppm.

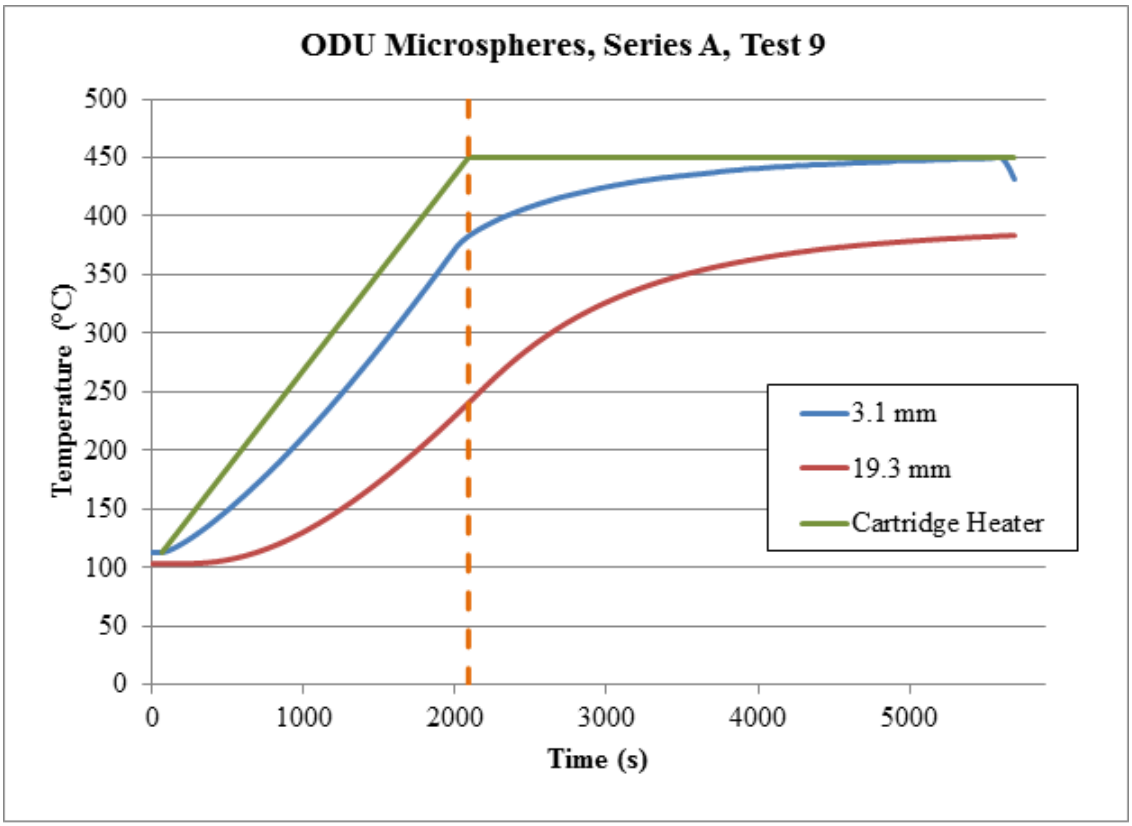

Fig. 4.10. Time dependent temperature data from CHTA testing, Series A, Test 9. Cartridge heater temperature is shown in green with an orange vertical dashed line when the cartridge heater stopped ramping.

Figure 4.13 is data collected for the third test with the WDU microspheres. The heater settings for this test had the band heater initially at 125°C and the cartridge heater maximum temperature set to 450°C by ramping 20°C/min. This test was completed for comparison to Series A, Test 6. This data test has a longer initial hold time in order to establish a uniform initial radial temperature profile. The glovebox oxygen level was 22.21 ppm.

Figure 4.14 is data collected for the fourth test with the WDU microspheres. The heater settings for this test had the band heater initially at 125°C and the cartridge heater maximum temperature set to 450°C by ramping 20°C/min. Series B, Tests 3

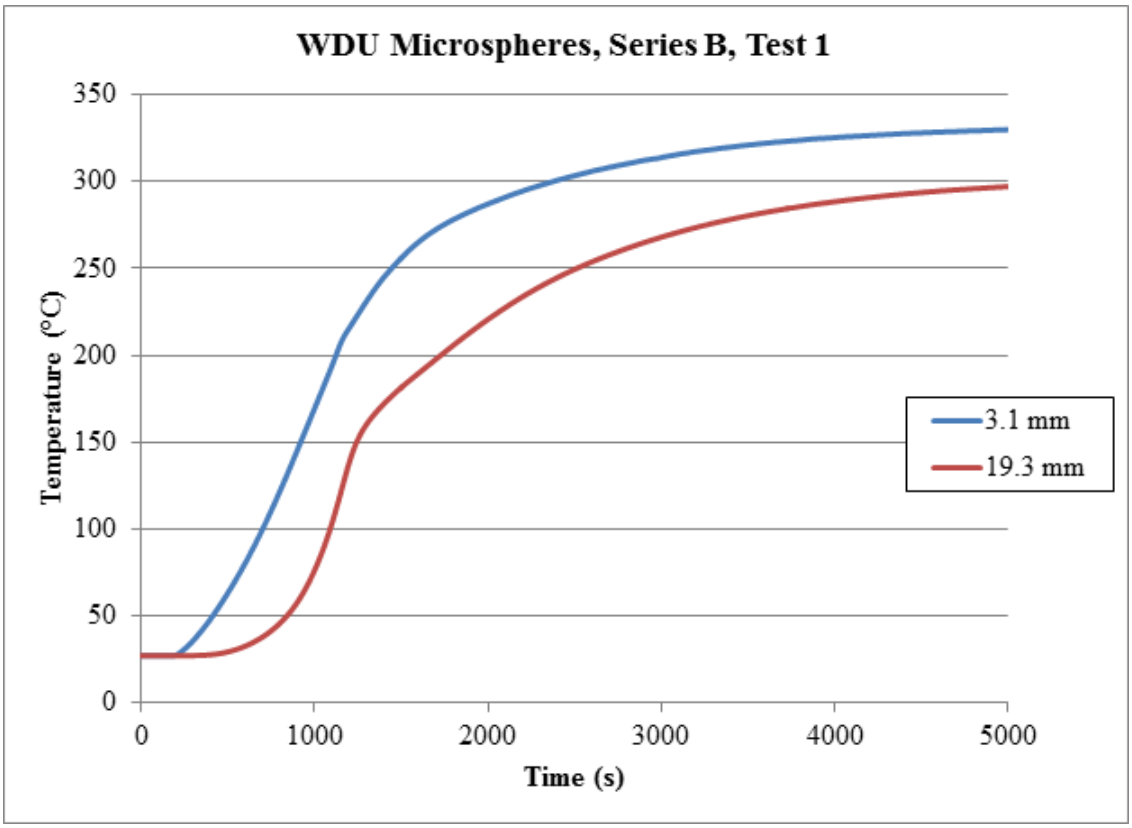

Fig. 4.11. Time dependent temperature data from CHTA testing, Series B, Test 1.

and 4 were completed to compare to Series A, Test 6 to determine if the initial hold temperature impacted the CHTA analysis method. The glovebox oxygen level was 24.83 ppm.

Figure 4.15 is data collected for the fifth test with the WDU microspheres. The heater settings for this test had the band heater initially at 25°C and the cartridge heater maximum temperature set to 350°C by ramping 40°C/min. Prior to the start of this test run, the powder was inspected and was determined to have shifted in color from a brown-green hue to black suggesting further oxidation had occurred. This test was the beginning of tests intended to determine if the ramping rate of the cartridge heater influenced the calculation of thermal diffusivity in the CHTA

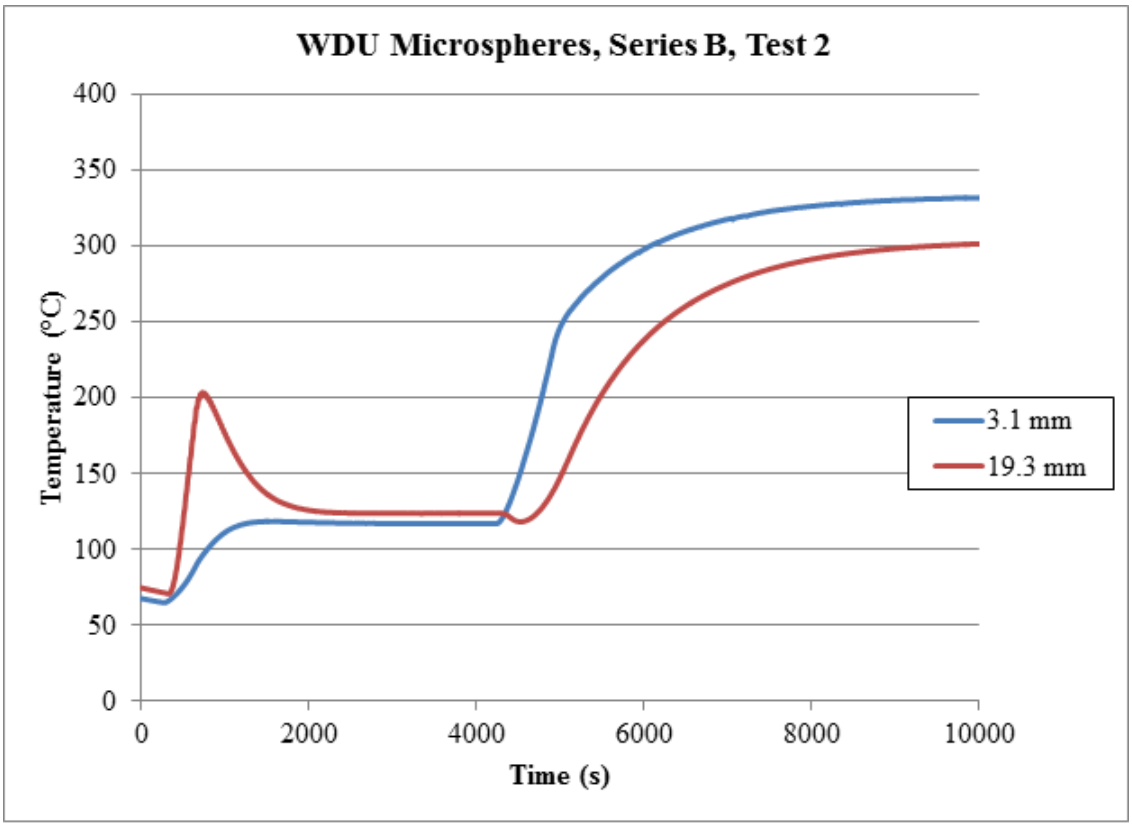

Fig. 4.12. Time dependent temperature data from CHTA testing, Series B, Test 2.

analysis method. The glovebox oxygen level was 56.8 ppm. This spike was attributed to a different project occurring in the glovebox. In an effort to lower the oxygen level, zirconium hydride was heated in the glovebox using the furnace well set to 400°C.

Figure 4.16 is data collected for the sixth test with the WDU microspheres. The heater settings for this test had the band heater initially at 25°C and the cartridge heater maximum temperature set to 450°C by ramping 40°C/min. This test was a continuation of the ramping rate analysis. The glovebox oxygen level was 15.92 ppm at the start of the test and 8.63 at the end of the test; this was assumed to be due to the heating of zirconium hydride. The hydrogen level was 2.267 ppm.

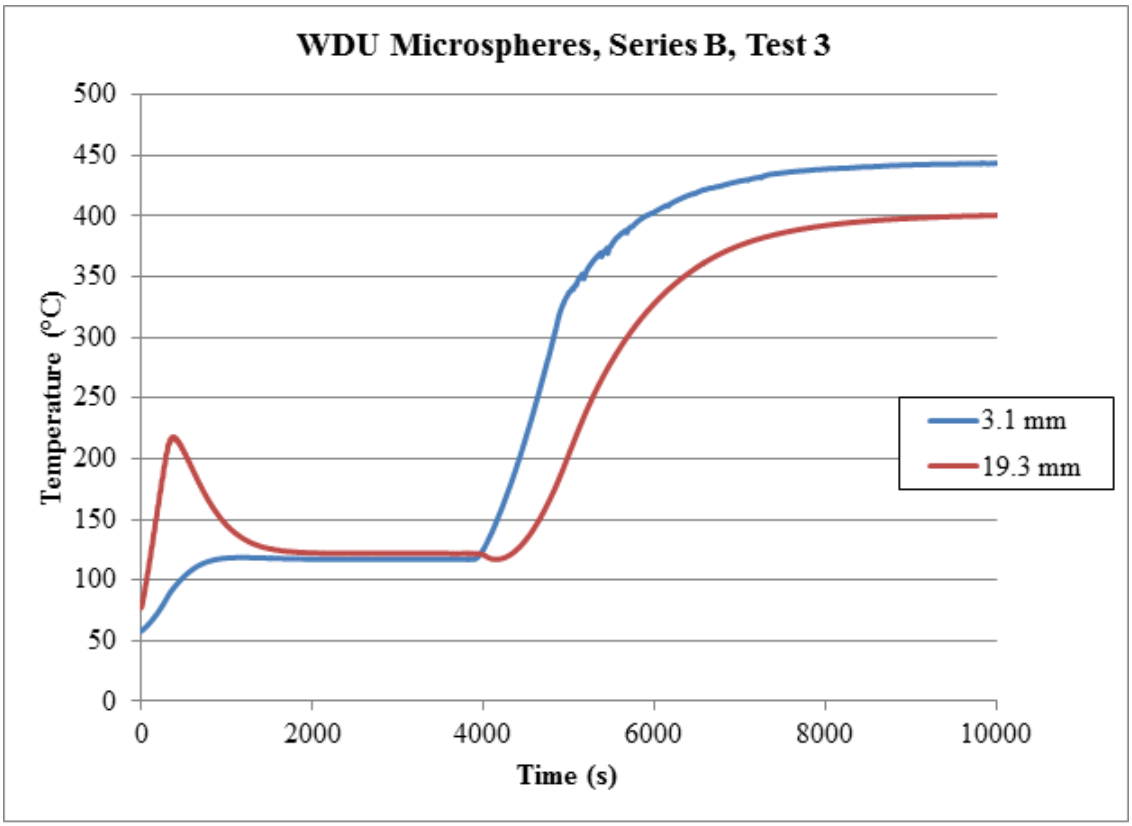

Fig. 4.13. Time dependent temperature data from CHTA testing, Series B, Test 3.

Figure 4.17 is data collected for the seventh test with the WDU microspheres. The heater settings for this test had the band heater initially at 50°C and the cartridge heater maximum temperature set to 550°C by ramping 20°C/min. This test was part of the series of testing to determine if changing the maximum temperature of the cartridge heater impacted the calculated apparent thermal diffusivity. The glovebox oxygen level was 8.47 ppm.

Figure 4.18 is data collected for the eighth test with the WDU microspheres. The heater settings for this test had the band heater initially at 50°C and the cartridge heater maximum temperature set to 550°C by ramping 40°C/min. This test was a continuation of the ramping rate analysis. The glovebox oxygen level was 7.99 ppm.

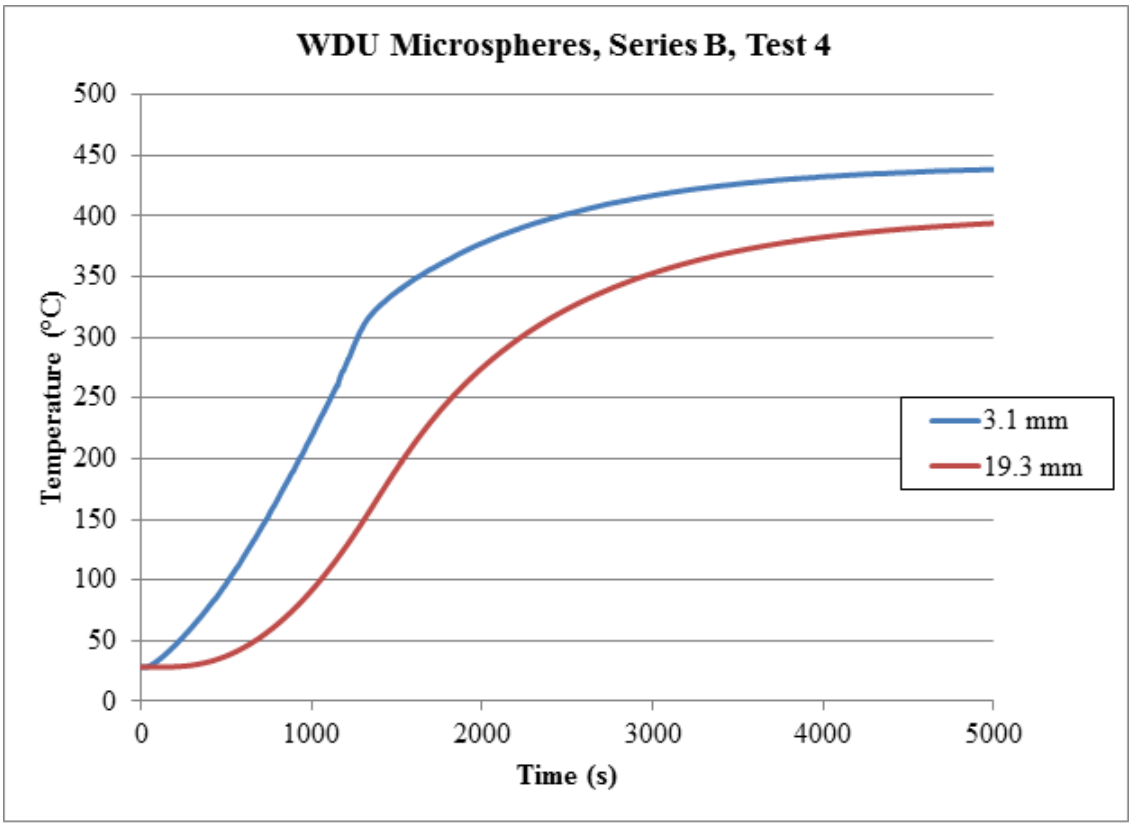

Fig. 4.14. Time dependent temperature data from CHTA testing, Series B, Test 4.

Figure 4.19 is data collected for the ninth test with the WDU microspheres. The heater settings for this test had the band heater initially at 50°C and the cartridge heater maximum temperature set to 350°C by ramping 60°C/min. This test was a continuation of the ramping rate analysis. The glovebox oxygen level was 8.22 ppm.

Figure 4.20 is data collected for the 10^{th} test with the WDU microspheres. The heater settings for this test had the band heater initially at 30°C and the cartridge heater maximum temperature set to 450°C by ramping 60°C/min. This test was a continuation of the ramping rate analysis. The glovebox oxygen level was 8.27 ppm.

Figure 4.21 is data collected for the 11^{th} test with the WDU microspheres. The heater settings for this test had the band heater initially at 50°C and the cartridge

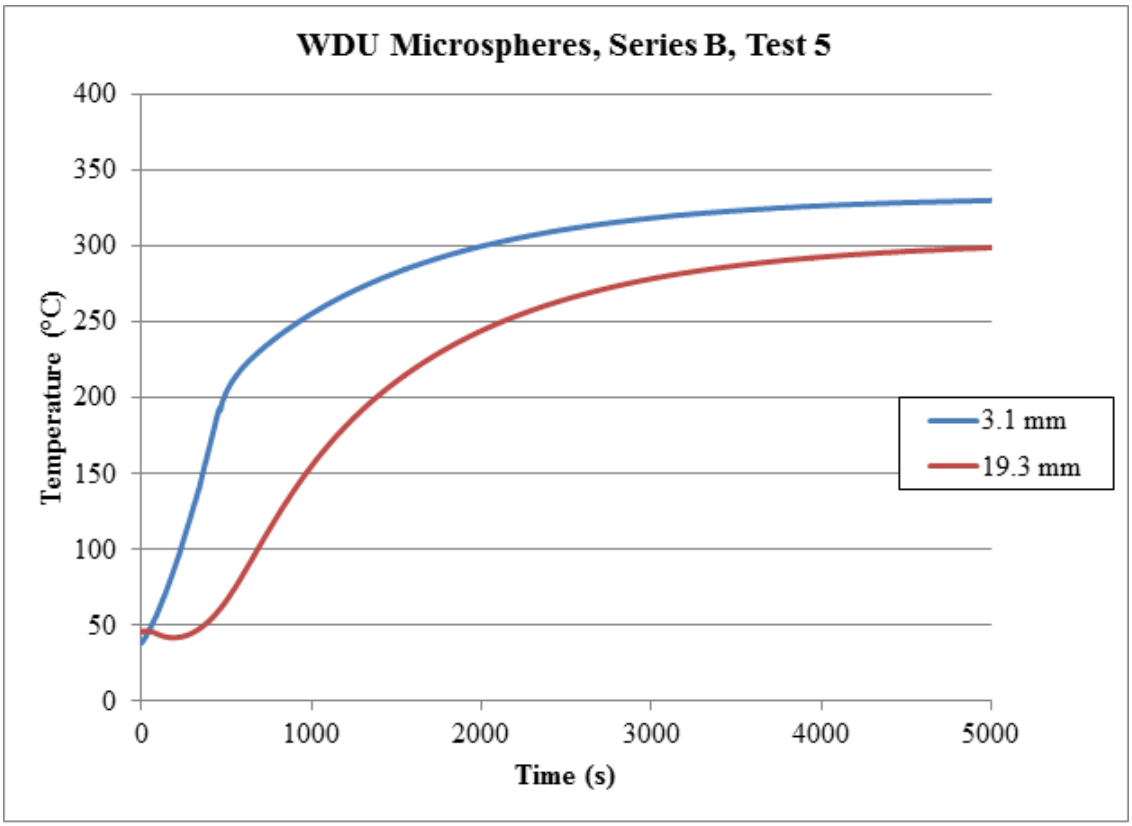

Fig. 4.15. Time dependent temperature data from CHTA testing, Series B, Test 5.

heater maximum temperature set to 550°C by ramping 60°C/min. This test was a continuation of the ramping rate analysis. The glovebox oxygen level was 8.12 ppm.

Figure 4.22 is data collected for the 12^{th} test with the WDU microspheres. The heater settings for this test had the band heater initially at 50°C and the cartridge heater maximum temperature set to 650°C by ramping 20°C/min. This test was a continuation of the maximum temperature analysis. In Fig. 4.22, communication was briefly interrupted between the data logger and the channels containing the outermost thermocouples as evidenced by the vertical lines after 4000 s. The glovebox oxygen level was 8.28 ppm. Shown in Fig. 4.23, is the B12 test data with the addition of the regions of best analyzable data (top shaded region) and limited analyzable

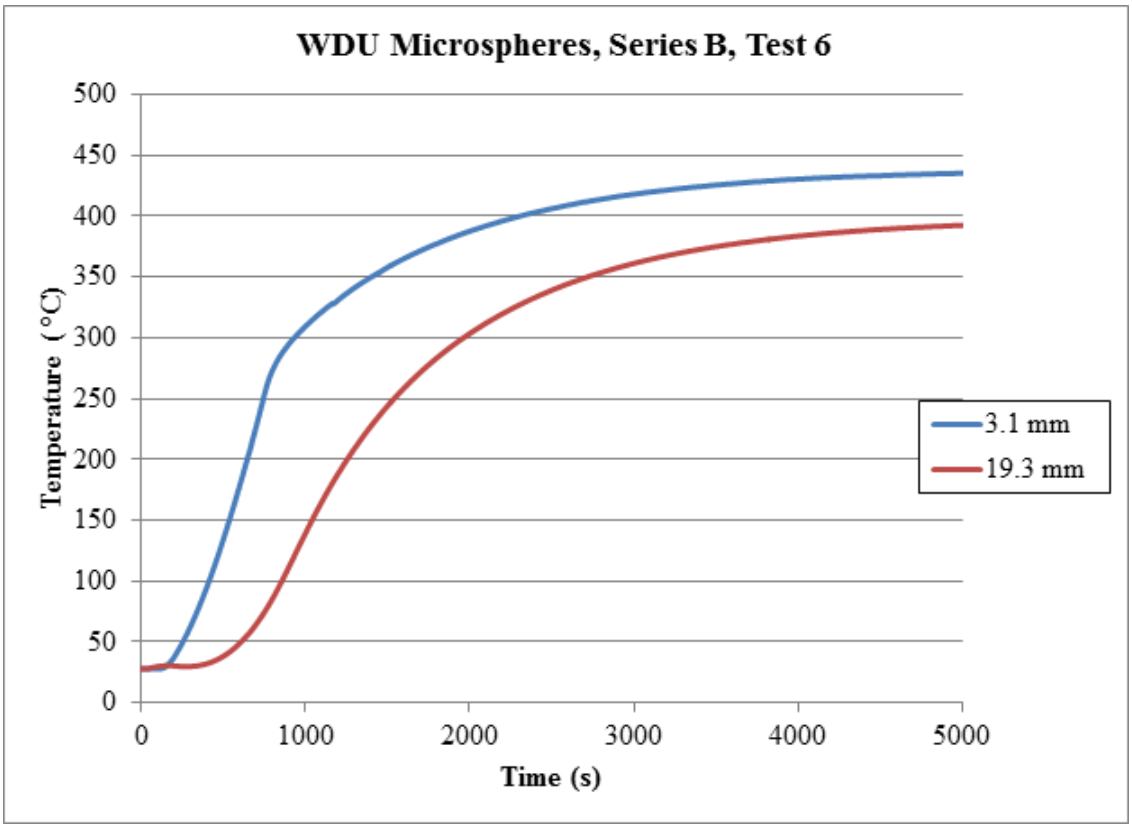

Fig. 4.16. Time dependent temperature data from CHTA testing, Series B, Test 6.

data (bottom shaded region). The lower shaded region is during the cartridge heater ramping stage and is during the first transient in the system; the upper shaded region is during the maximum temperature hold and illustrates the second transient region.

Figure 4.24 is data collected for the 13^{th} test with the WDU microspheres. The heater settings for this test had the band heater initially at 50°C and the cartridge heater maximum temperature set to 650°C by ramping 40°C/min. This test was a continuation of the ramping rate analysis. The glovebox oxygen level was 8.15 ppm.

Figure 4.25 is data collected for the 14^{th} test with the WDU microspheres. The heater settings for this test had the band heater initially at 50°C and the cartridge heater maximum temperature set to 650°C by ramping 60°C/min. This test was a

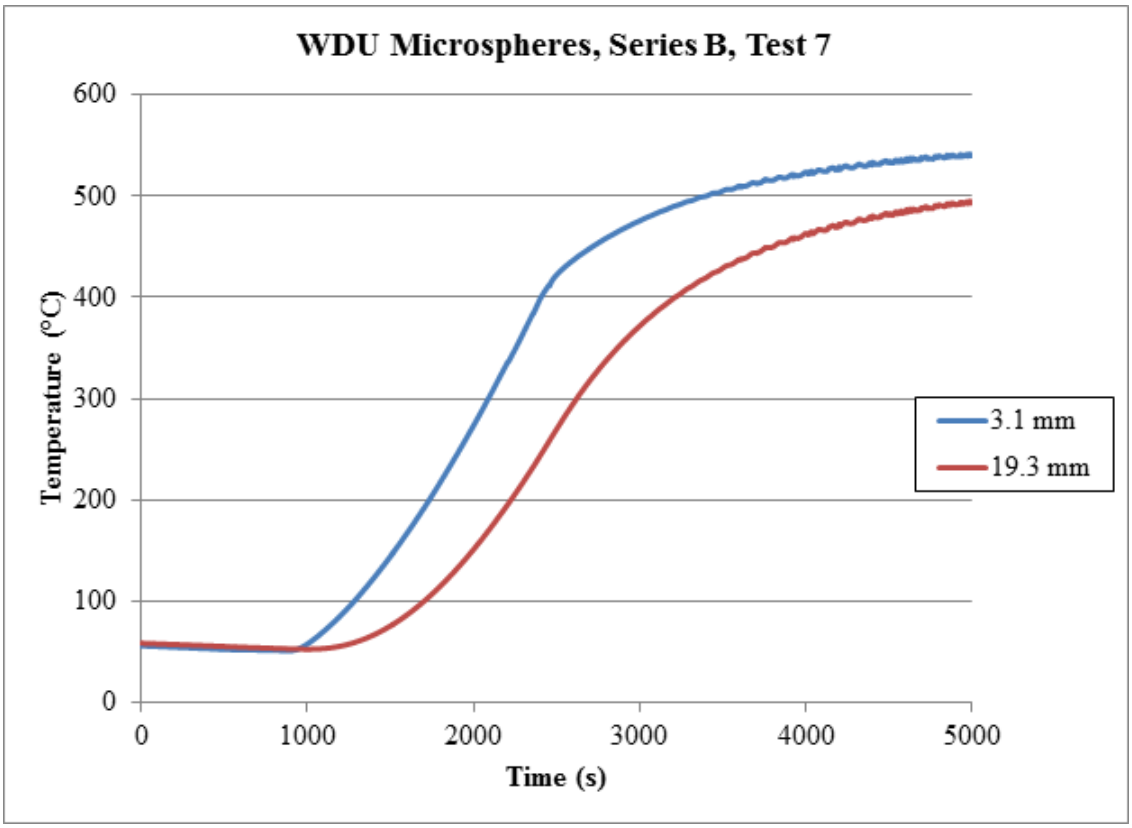

Fig. 4.17. Time dependent temperature data from CHTA testing, Series B, Test 7.

continuation of the ramping rate analysis. In Fig. 4.25, the vertical line is a momentary disconnect or malfunction between the thermocouples and the data logger. The glovebox oxygen level was 8.21 ppm.

Figure 4.26 is data collected for the 15^{th} test with the WDU microspheres. The heater settings for this test had the band heater initially at 50°C and the cartridge heater maximum temperature set to 650°C by ramping 200°C/min. This test was a continuation of the ramping rate analysis. For additional information on this test, see Section 4.2.1. The glovebox oxygen level was 8.12 ppm. Shown in Fig. 4.27, is the B15 test data with the addition of the regions of best analyzable data (top shaded region) and limited analyzable data (bottom shaded region). The lower

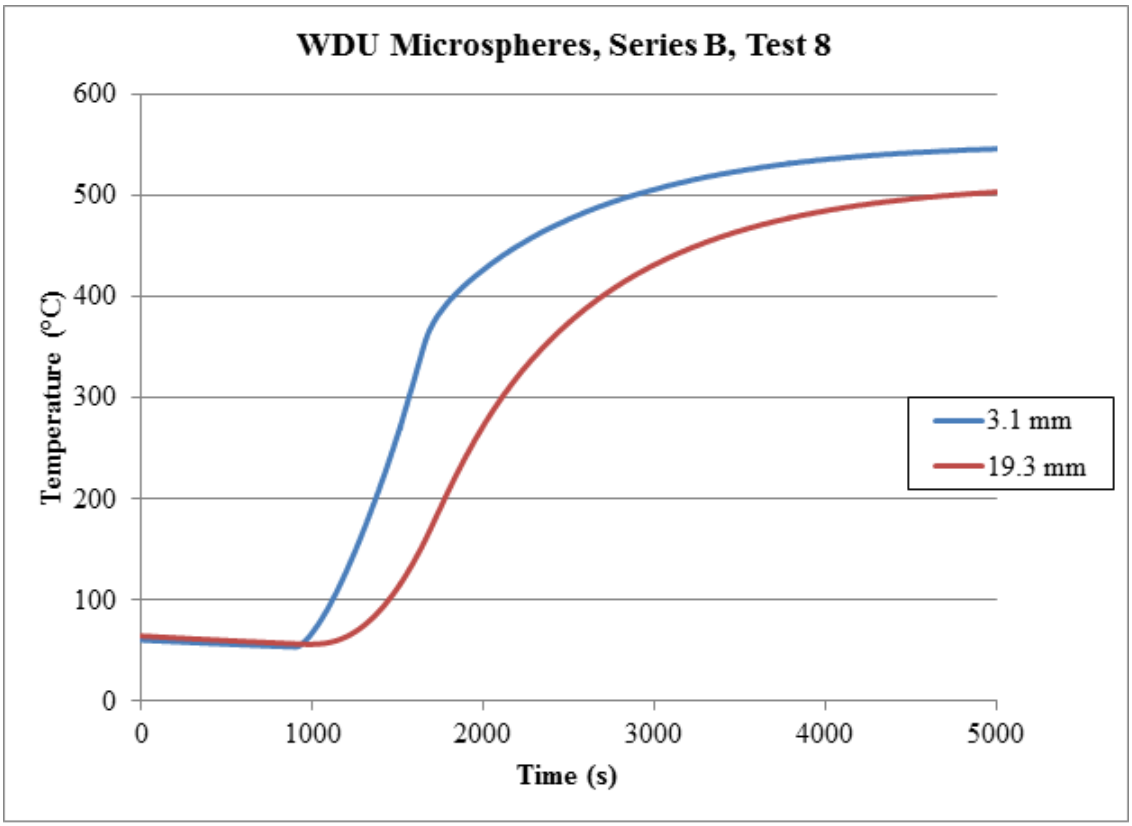

Fig. 4.18. Time dependent temperature data from CHTA testing, Series B, Test 8.

shaded region is during the cartridge heater ramping stage and is during the first transient in the system; the upper shaded region is during the maximum temperature hold and illustrates the second transient region.

Tests 1 to 5 had a high oxygen contamination level regardless of frequent regeneration cycles using the Dri-Train. In order to lower the glovebox level, zirconium hydride was continuously heated from tests 6 through 15 in the glovebox furnace well. The zirconium hydride functioned well to lower the oxygen level in the glovebox but at this point, oxidation effects (e.g. color change) were already noted on the WDU microspheres.

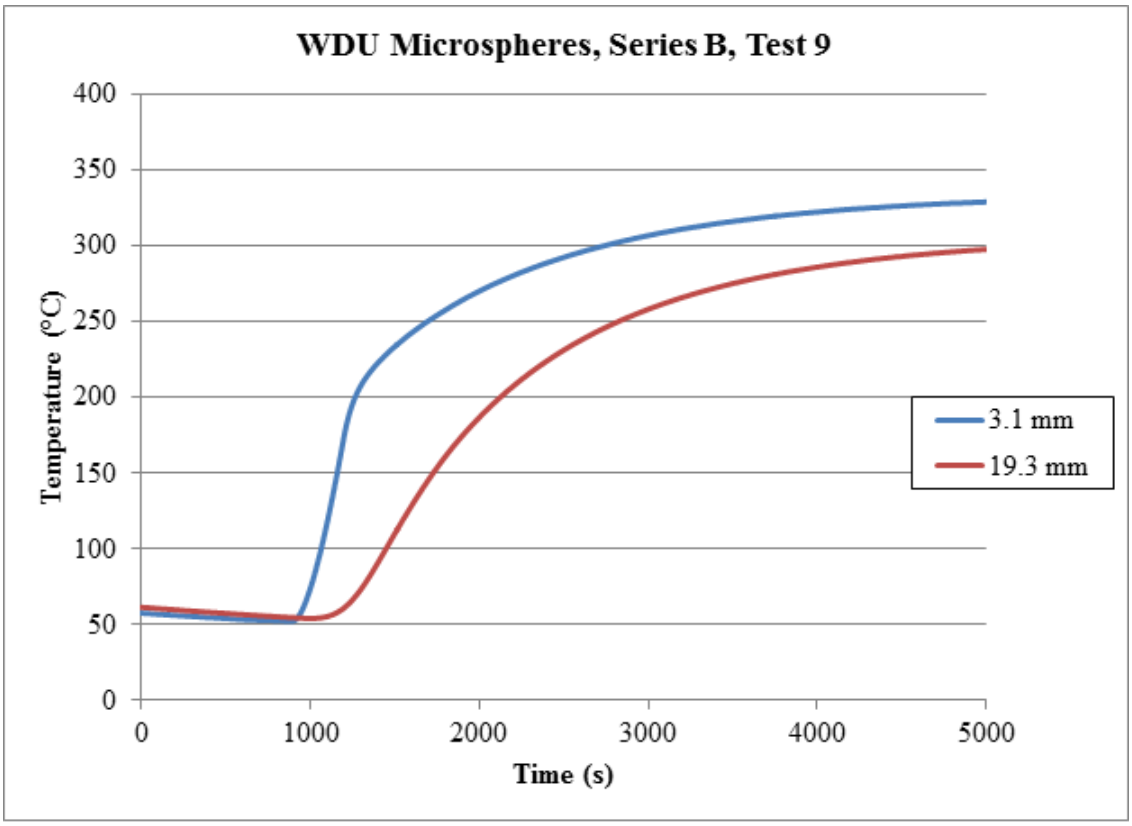

Fig. 4.19. Time dependent temperature data from CHTA testing, Series B, Test 9.

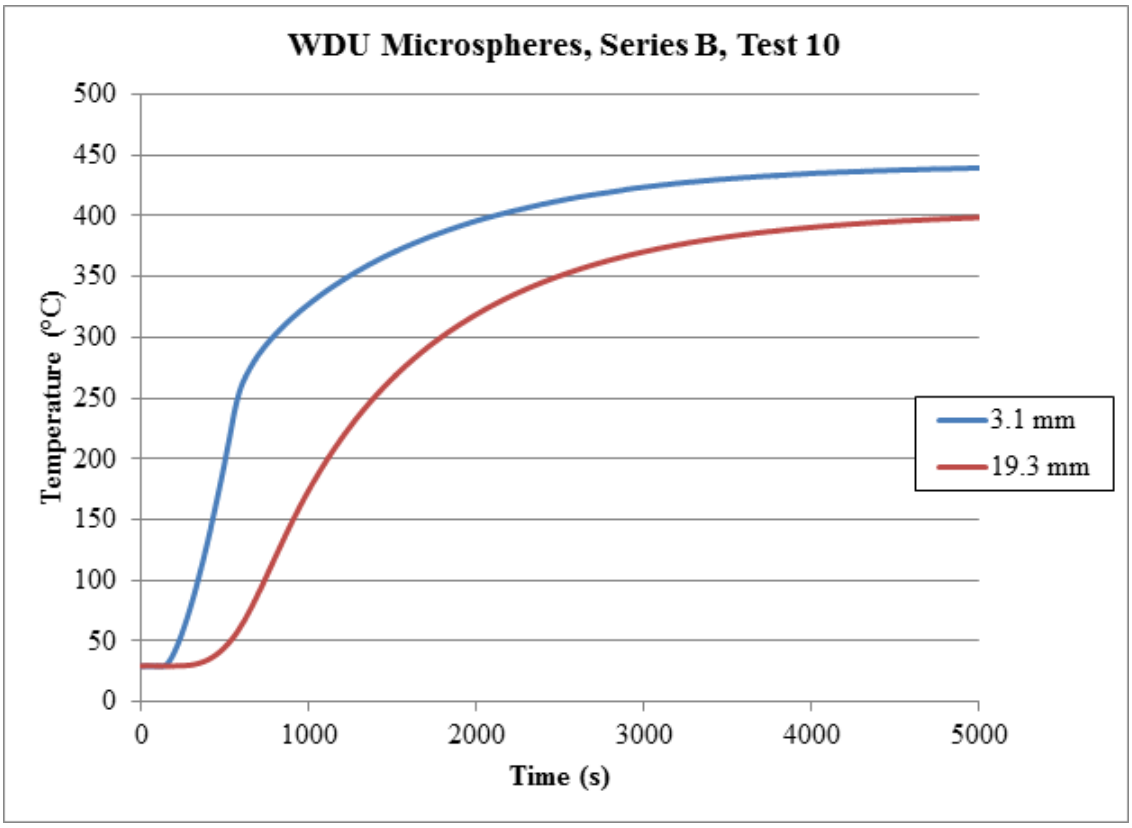

Fig. 4.20. Time dependent temperature data from CHTA testing, Series B, Test 10.

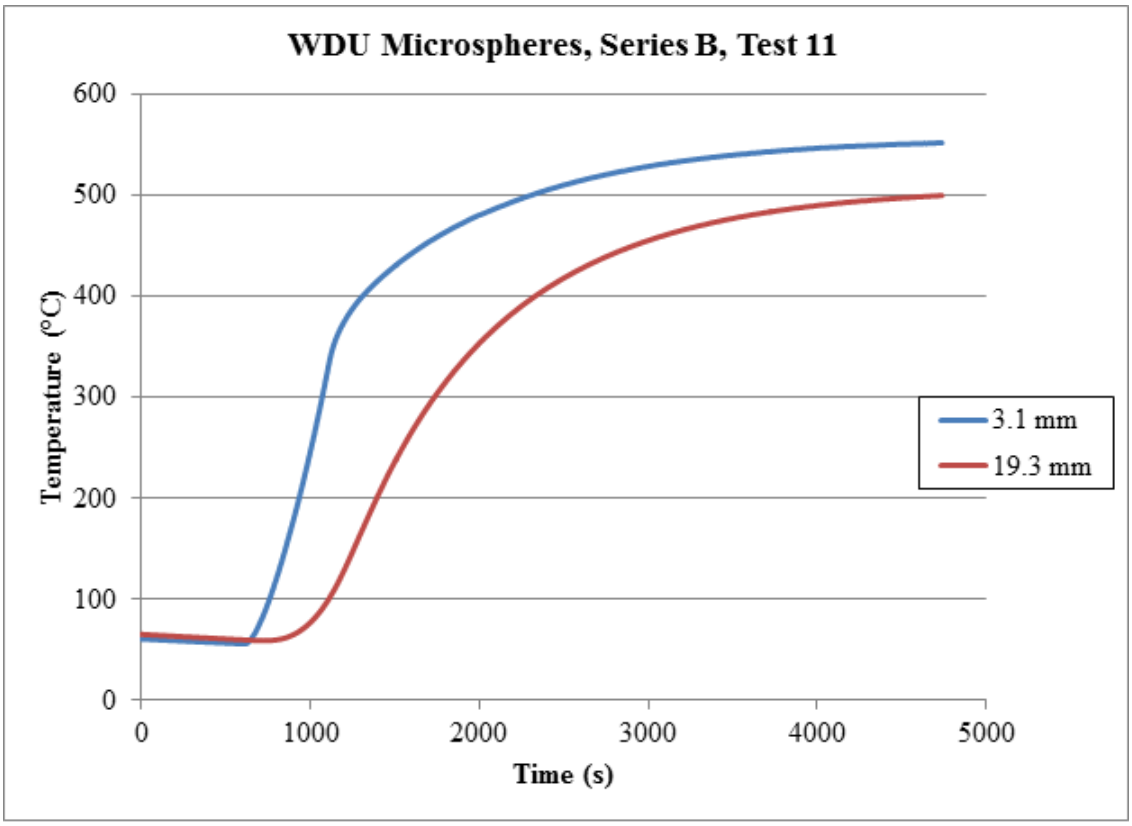

Fig. 4.21. Time dependent temperature data from CHTA testing, Series B, Test 11.

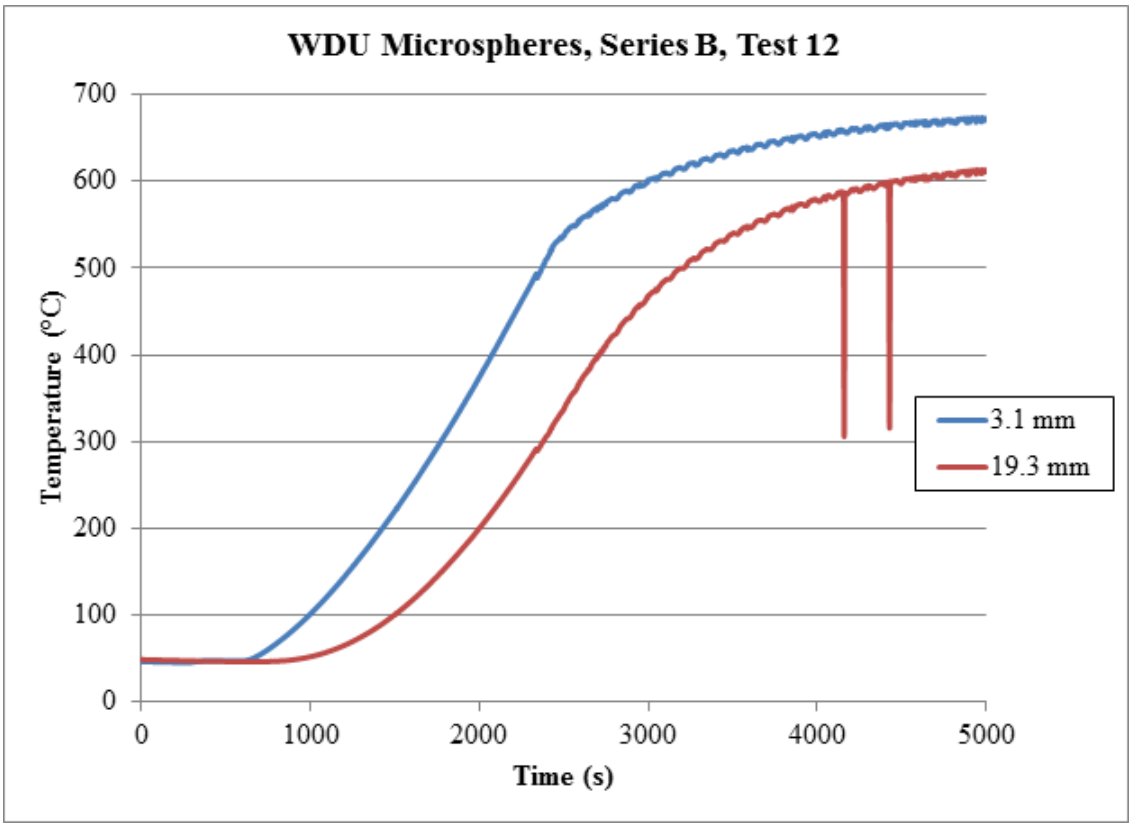

Fig. 4.22. Time dependent temperature data from CHTA testing, Series B, Test 12.

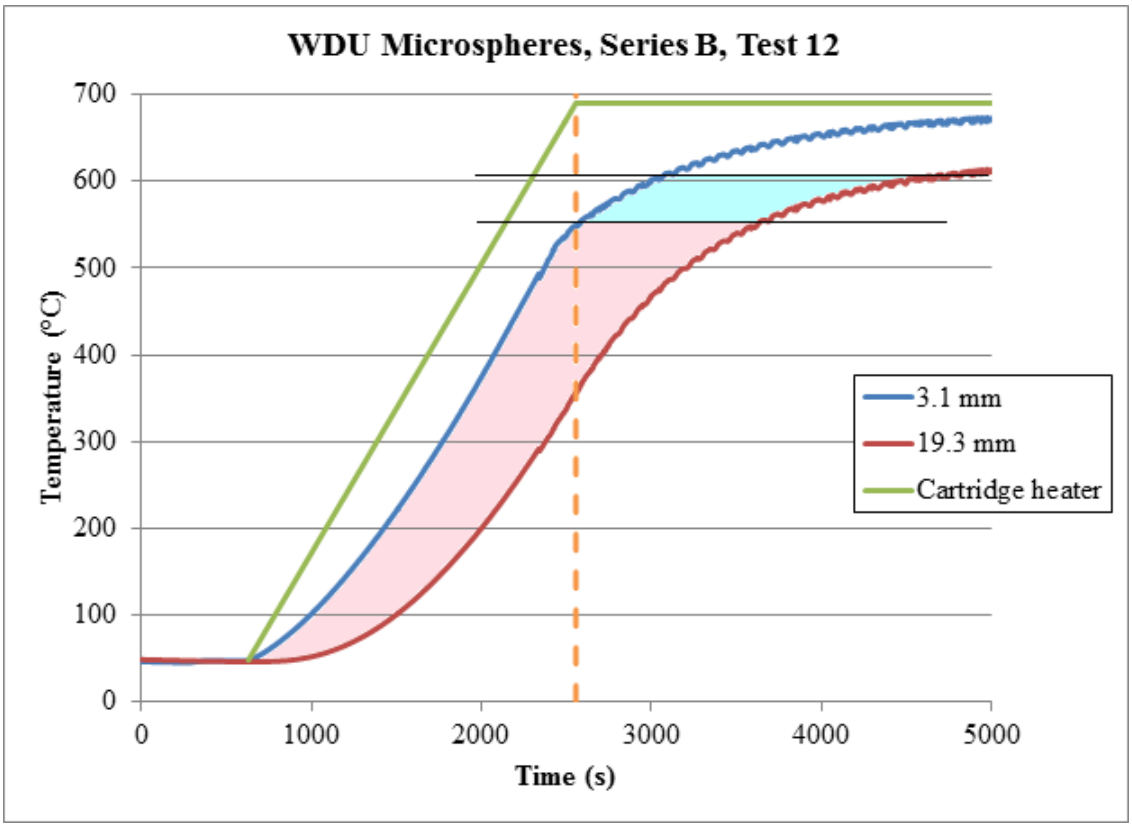

Fig. 4.23. Time dependent temperature data from CHTA testing, Series B, Test 12 with regions of data analysis shown.

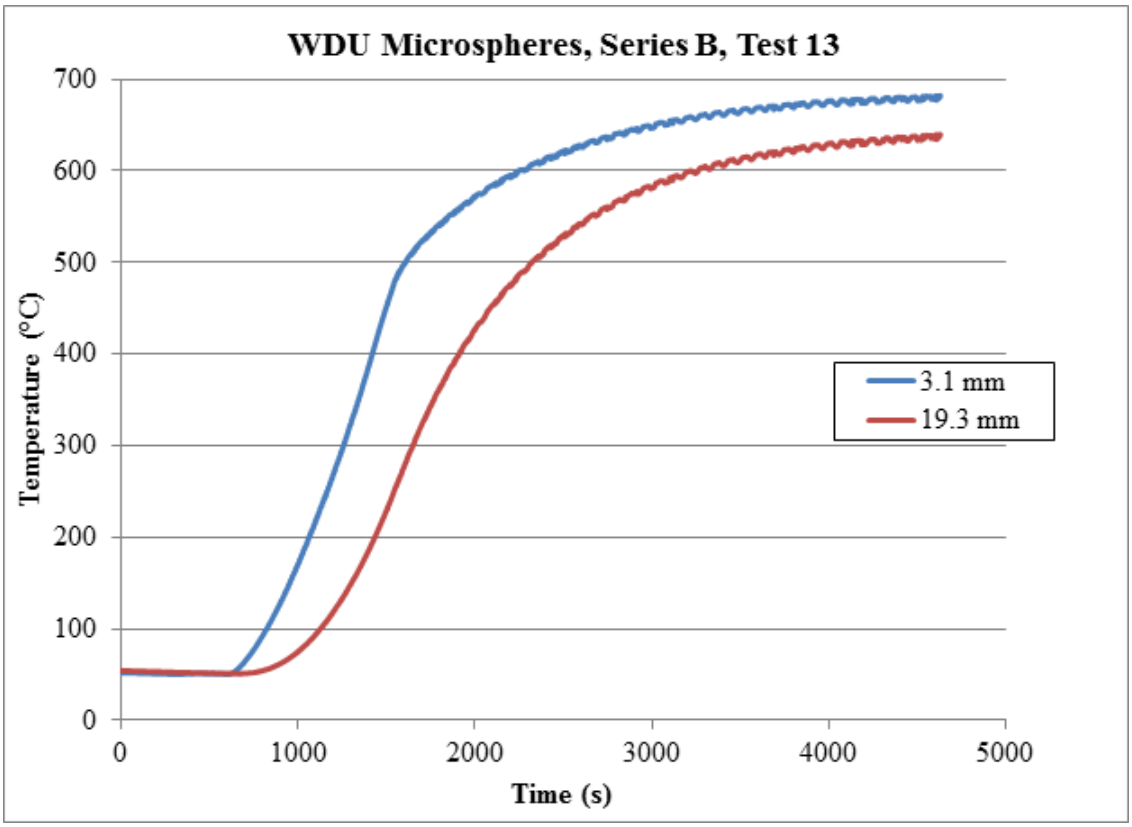

Fig. 4.24. Time dependent temperature data from CHTA testing, Series B, Test 13.

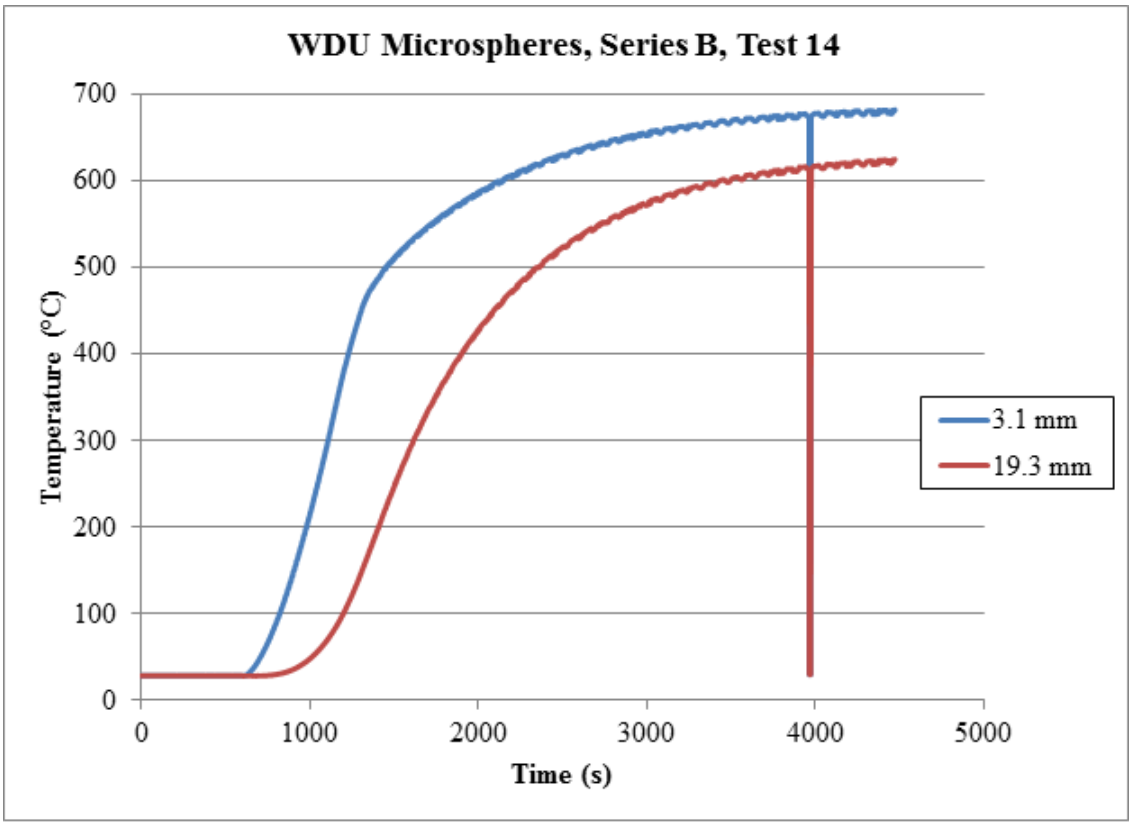

Fig. 4.25. Time dependent temperature data from CHTA testing, Series B, Test 14.

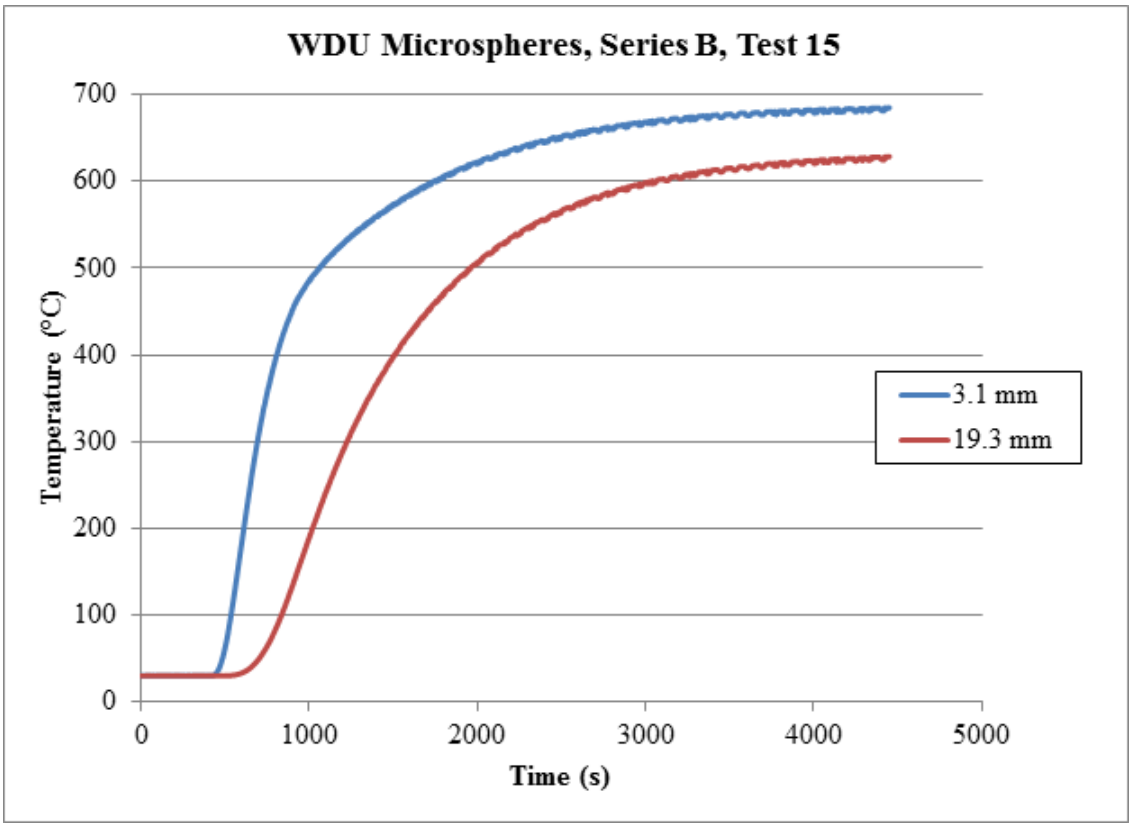

Fig. 4.26. Time dependent temperature data from CHTA testing, Series B, Test 15.

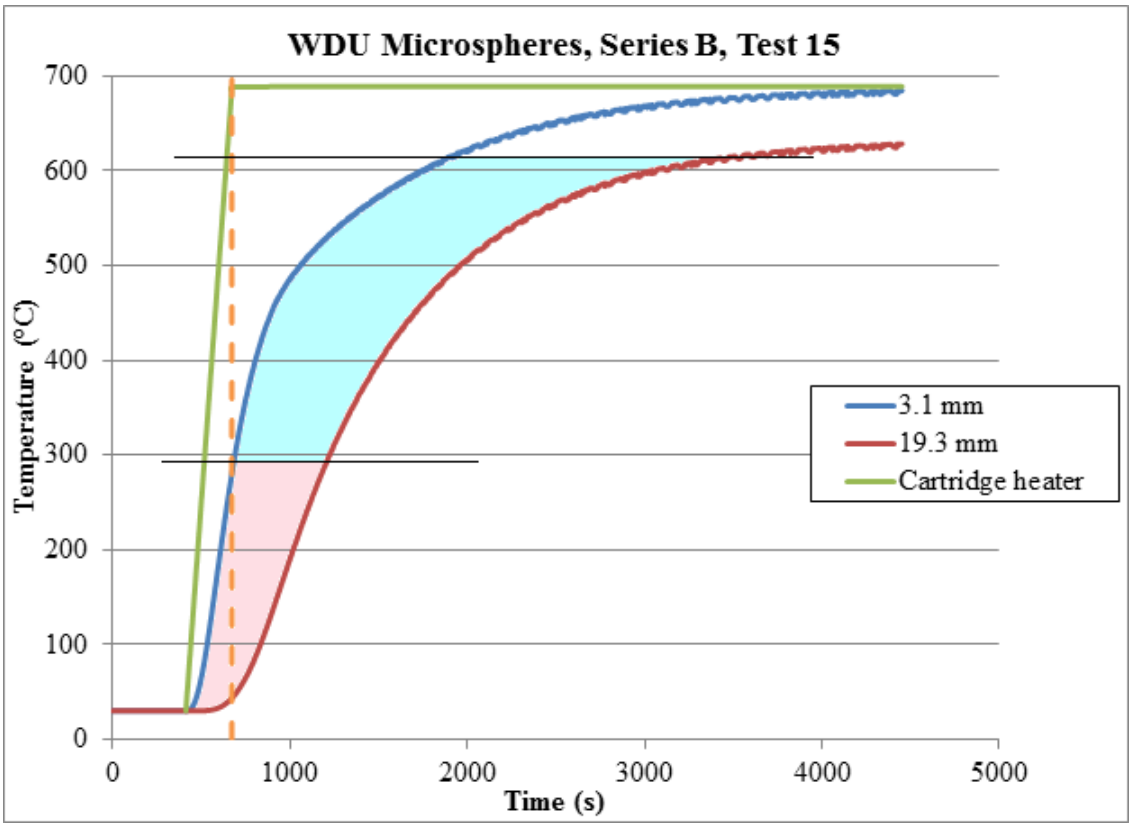

Fig. 4.27. Time dependent temperature data from CHTA testing, Series B, Test 15 with regions of data analysis shown.

5. DISCUSSION

5.1 Interpretation of LFA Data

Two samples of ODU were characterized within the LFA. The program automatically shutdown at 225°C and after opening the machine, it was apparent that the sapphire pan containing the ODU had shattered allowing microspheres to accumulate on the lower plate within the LFA. It was suggested that this incident may have been a result of further oxidation within the LFA. By examining the data, it was evident that at approximately 150°C the thermal diffusivity began a rapid decrease. It is proposed here that the elevated temperature in an oxygen atmosphere allowed oxidation of the microspheres creating a heat source within the sample and possibly allowing a slight volume change. These factors combined to increase the stress on the sapphire pan, causing it to fail. Following this test, it became apparent that no further testing of uranium microspheres should occur within the LFA. It was previously known that the microspheres were oxidized but the thickness of the oxide layer was not analyzed. Previous work has shown that the oxide thickness on these microspheres was between 1 and 5 microns [34].

For the one test that was initiated with the ODU microspheres, the duration of time between the flash firing and detection of the heat pulse by the infrared detector was approximately 30 seconds. Also, the packing density of the microspheres within the sapphire pan was estimated to be 70-75% by considering the mass of microspheres added versus the maximum theoretical mass if the sample pan had been filled with solid uranium metal. The higher packing factor between the two samples resulted in a higher thermal diffusivity. This was expected because it reduced the void space in the sample. This data supported the expectation that greater void space results in lower thermal diffusivity, and, consequentially, lower thermal conductivity.

5.1.1 LFA Challenges

Internal algorithms in the Netzsch LFA software analysis package for the LFA are designed for flat, parallel surfaces positioned perpendicularly to the flash bulb and infrared detector. With the powder and liquid sample holder, this was closely approximated for a liquid or a tightly packed powder with very small particle diameter. In the case of a powder with minuscule particle diameter, the illusion of a smooth, perpendicular surface can be maintained by the difference in scale between the sapphire pan diameter and the particle diameter. However, in the case of the microspheres utilized throughout these experiments, the 250 μm particle diameter may have been too large to ignore the rough surface effects resulting in significant light scattering from the curved surface of the microspheres. Additionally, per the directions of the sample holder, the sample was treated as a single layer. In reality, the sample was contained between two layers of sapphire with non-trivial thickness. Transmission of the light and thermal pulse through the sapphire pan and the sapphire lid may have interfered with an accurate measurement of the microspheres.

Immediately after the light pulse, there was frequently a spike of heat that reached the infrared detector. This spike was representative of the light which transmitted through voids or around the sample. Additionally, due to slight variations of the thickness of the sample, the signal to the infrared detector was frequently obscured by a high noise level. Despite the noise level, a peak in the maximum heat detected by the infrared sensor was still evident and analyzable. The noise significantly contributed to the error in the thermal diffusivity measurement. The high void fraction and rounded surfaces (as opposed to a single, smooth, and flat surface) was the source of the high noise level. Microspheres of other materials (zirconia and assorted steels) evidenced elevated noise levels; an attribute not noticed with solid samples (steels and glasses).

Results were further skewed when a graphite coating was lightly applied to the microspheres. It was common practice to thinly coat solid samples with carbon for

use in the LFA. When this practice was attempted with microspheres, the LFA analysis program tended to fail and the data were meaningless. Coating was attempted on zirconia and stainless steel microspheres in an attempt to maximize the absorption of light from the flash lamp. It was found that the coating drastically increased the noise level; so much so that the actual transmitted heat pulse was undetectable. Alternatively, a coating was applied to the sapphire pan and lid instead of the sample of microspheres. This again increased the noise level and the duration of the shot. In this case, the flash had to essentially navigate through five layers; graphite spray, sapphire, sample, sapphire then graphite spray. However, the sample was still treated as one layer in the thermal diffusivity calculation through the software.

5.2 Interpretation of the CHTA Method

5.2.1 Range of Analyzable Data

It was determined that the ramp rate of the cartridge heater during the heating phase impacted the calculated thermal diffusivity (see Fig. 5.1, 5.2, 5.3, and 5.4). This is due to the realization that the equation for thermal diffusivity does not include a flux-dependent term. Therefore, data from transient region one (during the ramping time of the cartridge heater) does not accurately describe thermal diffusivity. Instead, data during the second transient (after ramping, while the cartridge heater is maintaining a steady-state) produced the most desirable data. The best region for analysis is bordered by the point when the cartridge heater switched from the ramping stage to steady-state and the maximum temperature of the outermost thermocouple. Before the cartridge heater stopped ramping, data analysis was possible but data is questionable.

Additionally, the range of analyzable data was extended by increasing the maximum system temperature. This is shown if comparison is made of Fig. 5.1 and 5.3. Thus, in order to obtain the maximum range of analyzable data, a fast ramp rate

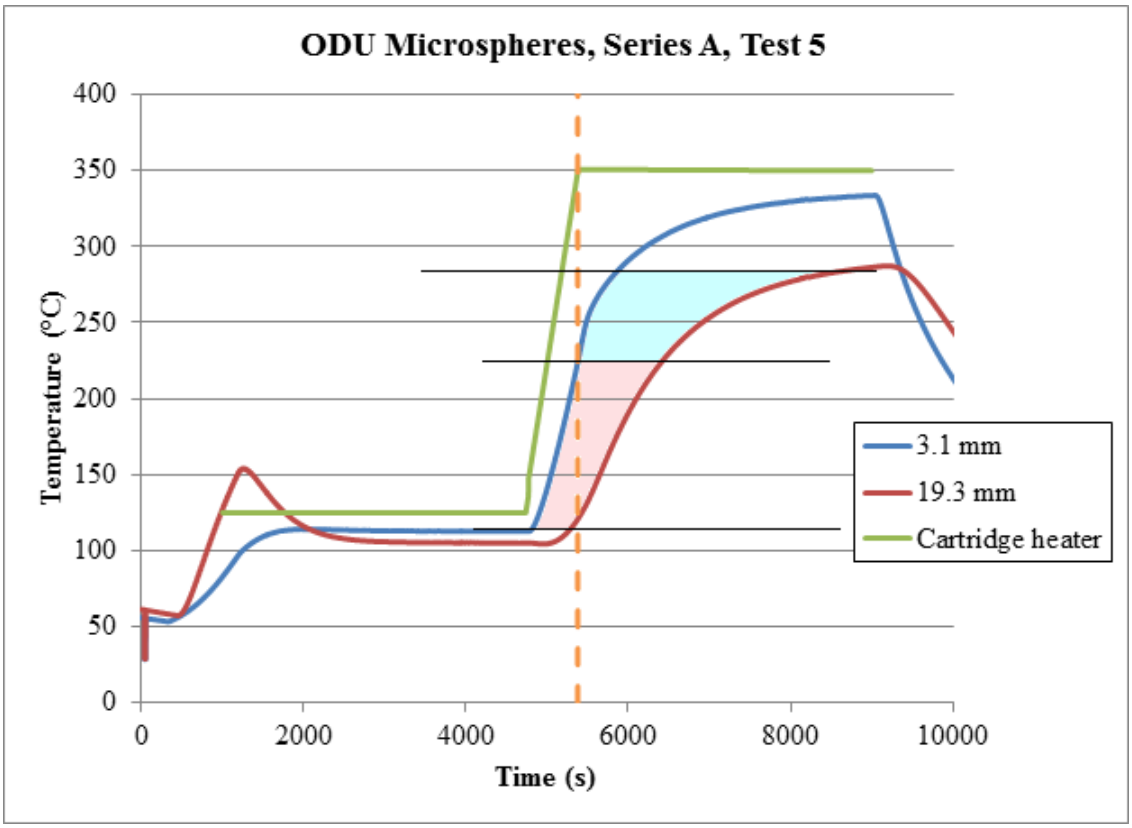

Fig. 5.1. Time-Temperature information for a ramp rate of 20°C/min with a maximum temperature of 350°C. The shaded regions represent the range of analyzable (after dashed line) and questionable (before dashed line) data.

and high maximum temperature are required. This approaches the ideal situation for both the flash and the hot-wire methods discussed in Section 2.2.

5.2.2 Interpretation of the ODU Microsphere Data

For tests where the maximum temperature was 350°C (Series A, Tests 2, 5, and 8), data was analyzable for thermal diffusivity from 125 to 275°C. From the discussion in Section 3.2.3, this is transient phase two. A knee was noticed in the data set near 200°C; after which point the thermal diffusivity seemed to linearly

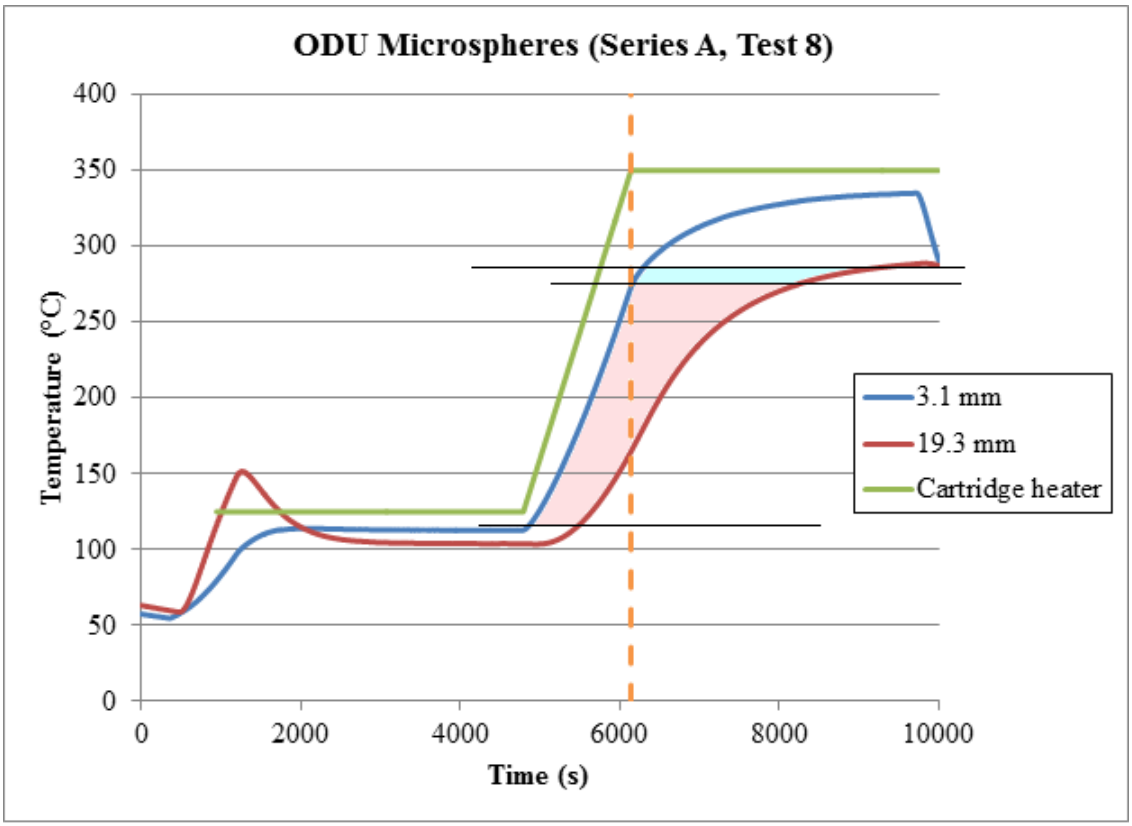

Fig. 5.2. Time-Temperature information for a ramp rate of 10°C/min with a maximum temperature of 350°C. The shaded regions represent the range of analyzable (after dashed line) and questionable (before dashed line) data.

decrease. This data is presented as Fig. 5.5 which depicts the three data sets with a maximum temperature of 350°C for the cartridge heater with ramp rates of 10, 15, and 20°C/min. For the calculated thermal diffusivity values presented from 200 to 275°C, the average was calculated and a line of best fit was applied to the combined data from all three tests. This line is presented in the figure as Linear (Average) and the equation of the line is also presented. It was noticed that there was a convergence in data points between the three initial data sets beginning at 200°C while values above this appeared to be impacted by the ramp rate of the central cartridge heater.

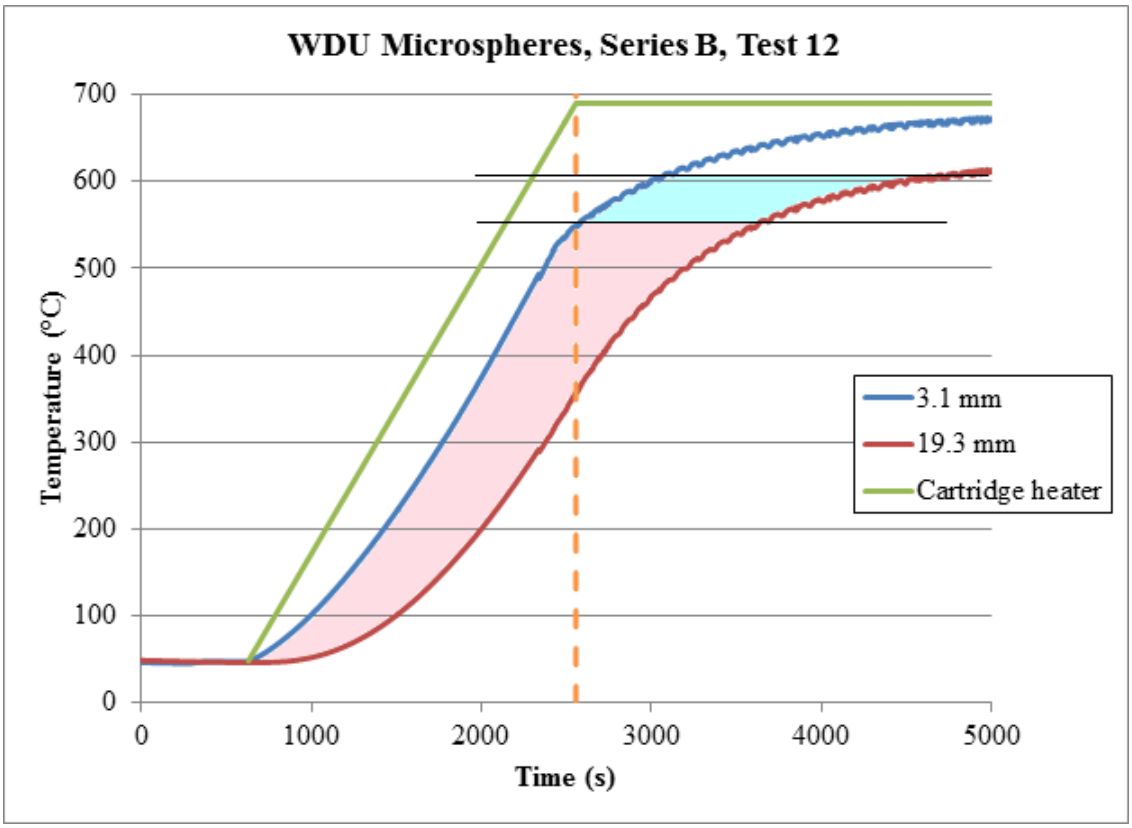

Fig. 5.3. Time-Temperature information for a ramp rate of 20°C/min with a maximum temperature of 650°C. The shaded regions represent the range of analyzable (after dashed line) and questionable (before dashed line) data.

For the 450°C tests (Test Series A, Tests 3, 6, and 9) with ramp rates of 10, 15, and 20°C/min, data was analyzed from 125 to 400°C. A convergence point seemed to occur within the data at 275°C; prior to which there was a significant scattering of calculated thermal diffusivity values. Following this convergence, a linear trend was exhibited between 275 and 375°C which was fitted to the average value of thermal diffusivity for the three data sets. These data sets are presented in Fig. 5.6.

The equations determined in the two series with maximum temperatures of 350 and 450°C (Series A, Tests 2, 3, 5, 6, 8, and 9) were plotted to compare the extrapolated and predicted thermal diffusivities of the different fits. As the temperature

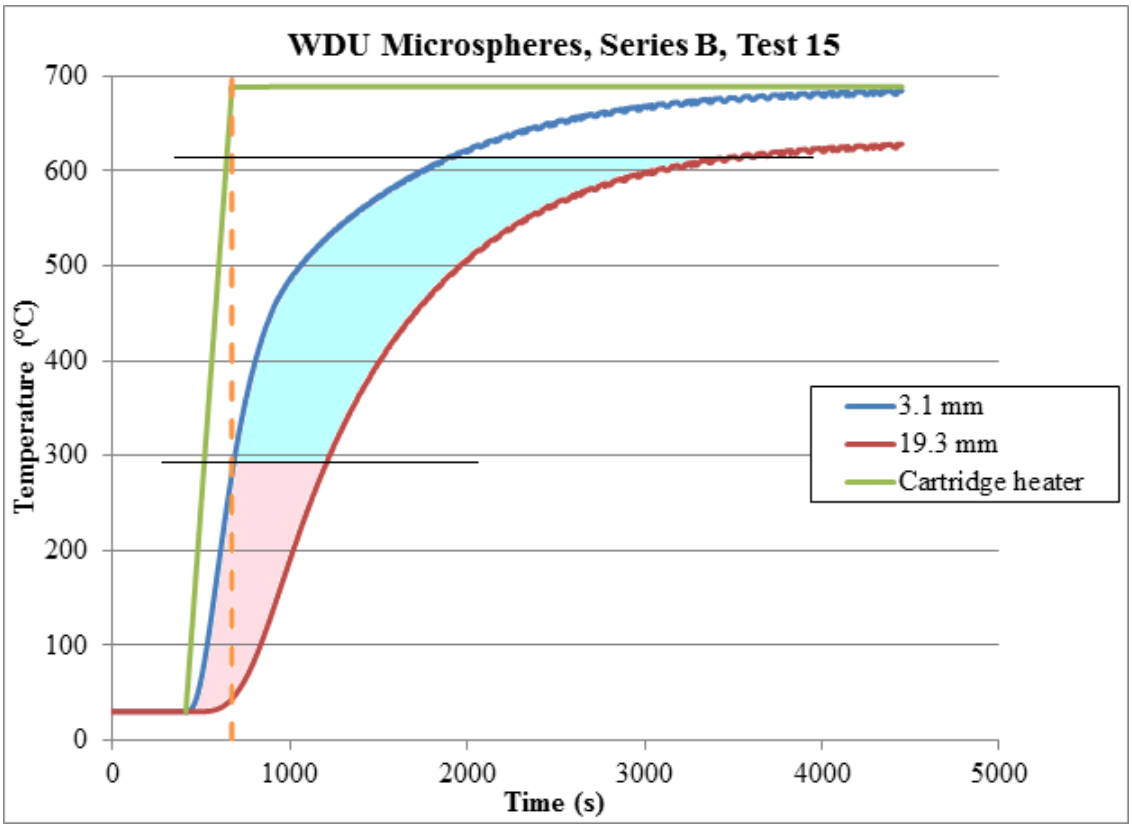

Fig. 5.4. Time-Temperature information for a ramp rate of 150°C/min with a maximum temperature of 650°C. The shaded regions represent the range of analyzable (after dashed line) and questionable (before dashed line) data.

increased, a greater discrepancy between the two data series emerged. Fig. 5.7 presents the extrapolated thermal diffusivities as a function of temperature for the 350 and 450°C tests in Test Series A.

5.2.3 Interpretation of WDU Microsphere Data

Uranium was initially washed with nitric acid in a glovebag within a fume hood. In the glovebag, the uranium turned a bright silver hue while in the nitric acid solution. It was noticed that the nitric acid washing solution created an exothermic

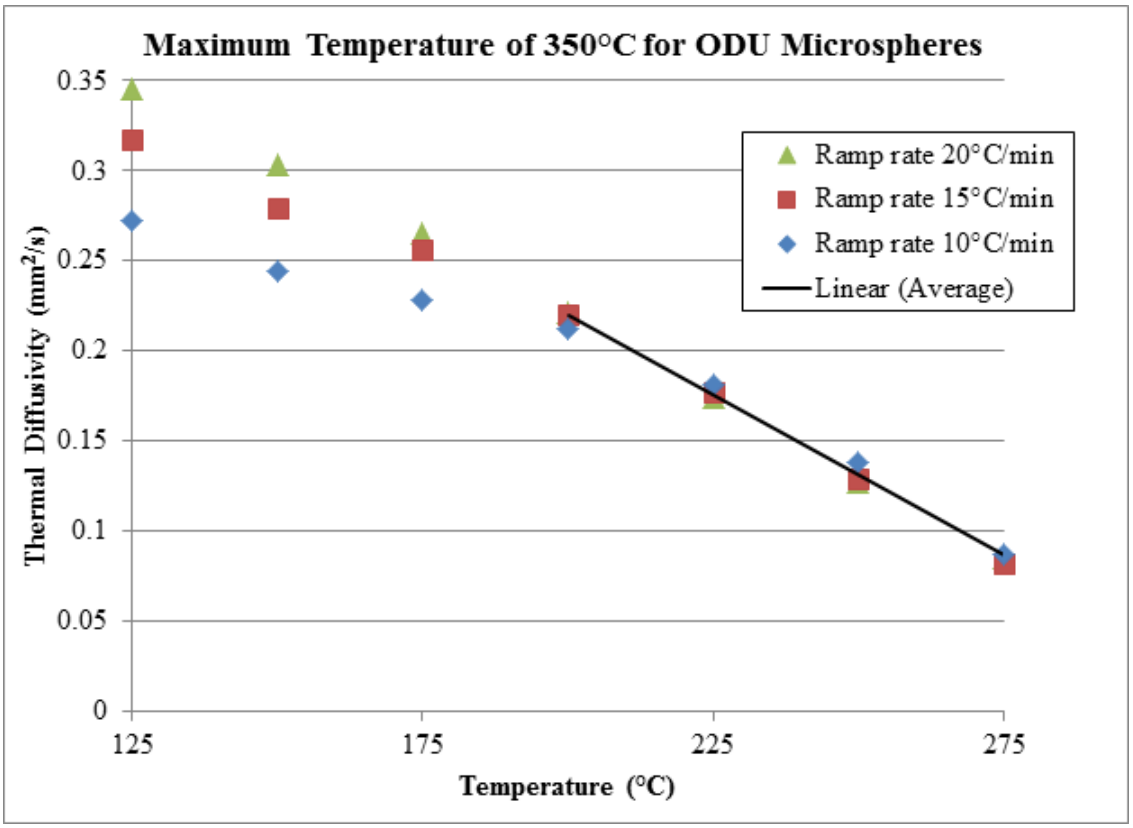

Fig. 5.5. ODU data for maximum temperature of 350°C (Test Series A, Tests 2, 5, and 8).

reaction and the wash beaker became warm to the touch. As the microspheres were poured out of the nitric acid solution, heat was rapidly released and the uranium turned a very dark brown color within the glovebag. It was hypothesized that the key issue was oxygen contamination within the glovebag. The small glovebox was configured for washing the uranium microspheres. Again, while in solution, the microspheres were a bright silver hue. While still in solution, the microspheres began to shift to a darker color with a slight brown hinge. Since the microspheres were entirely submerged in solution, it was suspected that either a thin uranium nitride or uranium oxide layer formed on the exposed surface of the microspheres; with uranium nitride seeming more feasible. Due to the inability to remove this surface

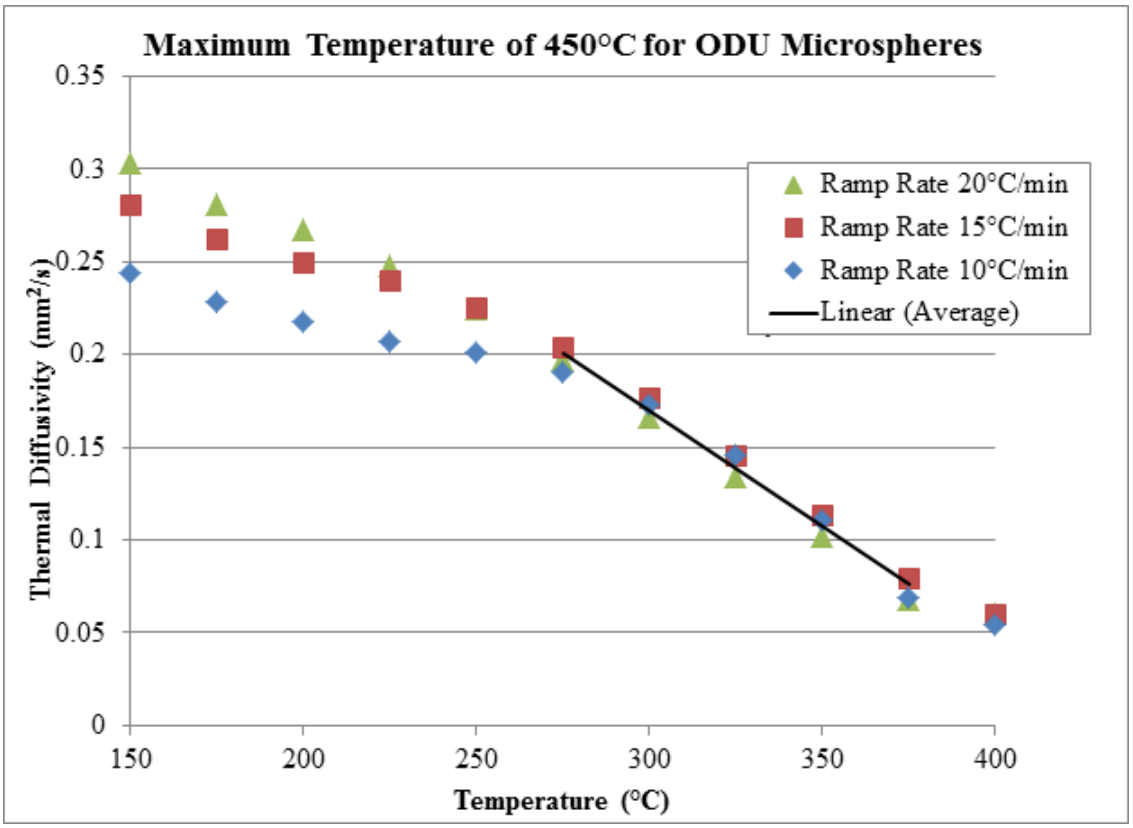

Fig. 5.6. ODU data for maximum temperature of 450°C (Test Series A, Tests 3, 6, and 9).

contamination, the WDU microspheres were tested in the CHTA with a newly formed layer of surface oxidation or nitridation.

Based upon the data collected from the ODU microsphere tests in Series A, the settings for the WDU tests were altered. The runs with a 250°C cartridge heater maximum temperature were not completed due to the lack of analyzable data. Tests at 350°C and above were completed with ramp rates of 20, 40, and 60°C/min (Series B, Tests 1, 2, 5, and 9). The calculated thermal diffusivity for the three data sets consistently converged by 150°C, with very similar calculated values from 250 to 300°C. An average thermal diffusivity was calculated for values between 125 and 275°C and a linear trend-line was fit to the average to determine

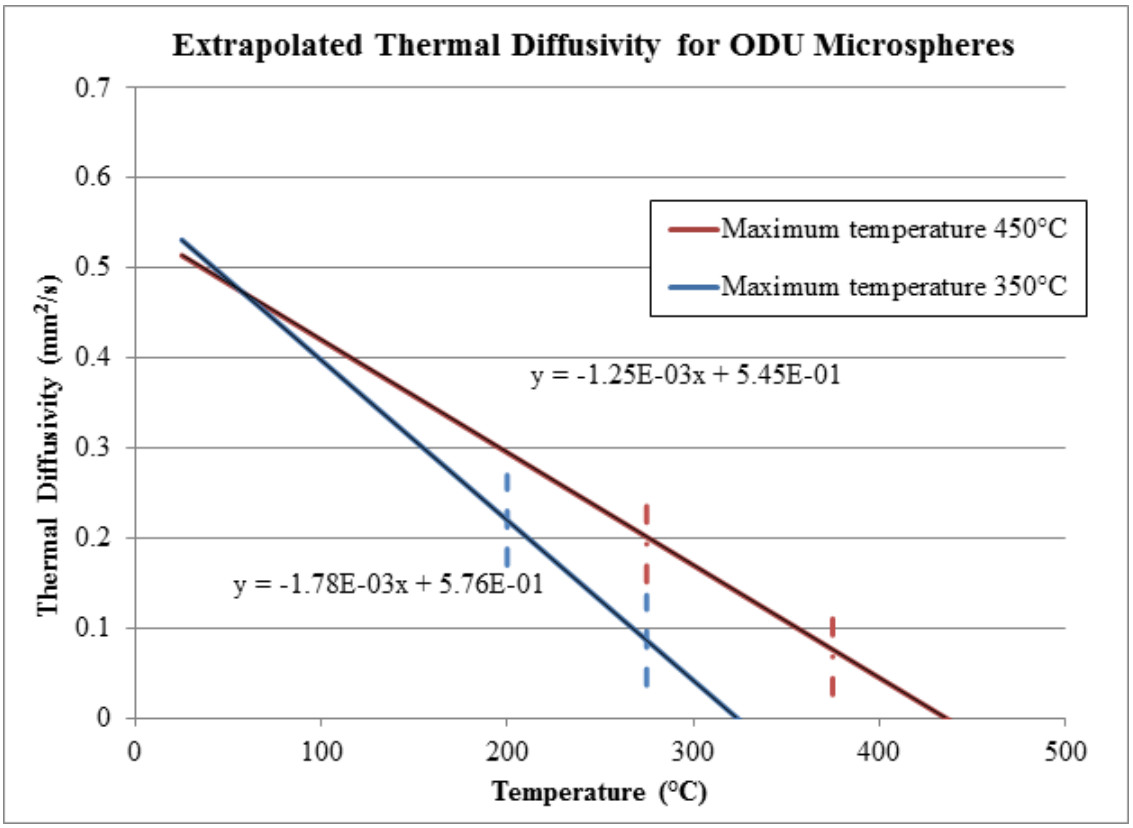

Fig. 5.7. Extrapolation of ODU microspheres data (Series A).

a linear approximation of the thermal diffusivity with regards to temperature. Data from the 350°C series is presented in Fig. 5.8. During the first test with the WDU microspheres, a significant peak in thermal diffusivity was observed that was not observed with the ODU microspheres, for more discussion, see Section 5.2.3.

In the cases with a maximum temperature of 450°C, four tests were run with different parameters and ramp rates (Series B, Tests 3, 4, 6, and 10). A single test was completed with a starting hold temperature of 125°C for direct comparison to ODU microspheres (Series A, Test 6 and Series B, Test 3). At low temperatures, the 60°C/min ramp rate consistently calculated a higher thermal diffusivity as compared to the lower ramp rates. Data sets converged around 175°C. The average of the four

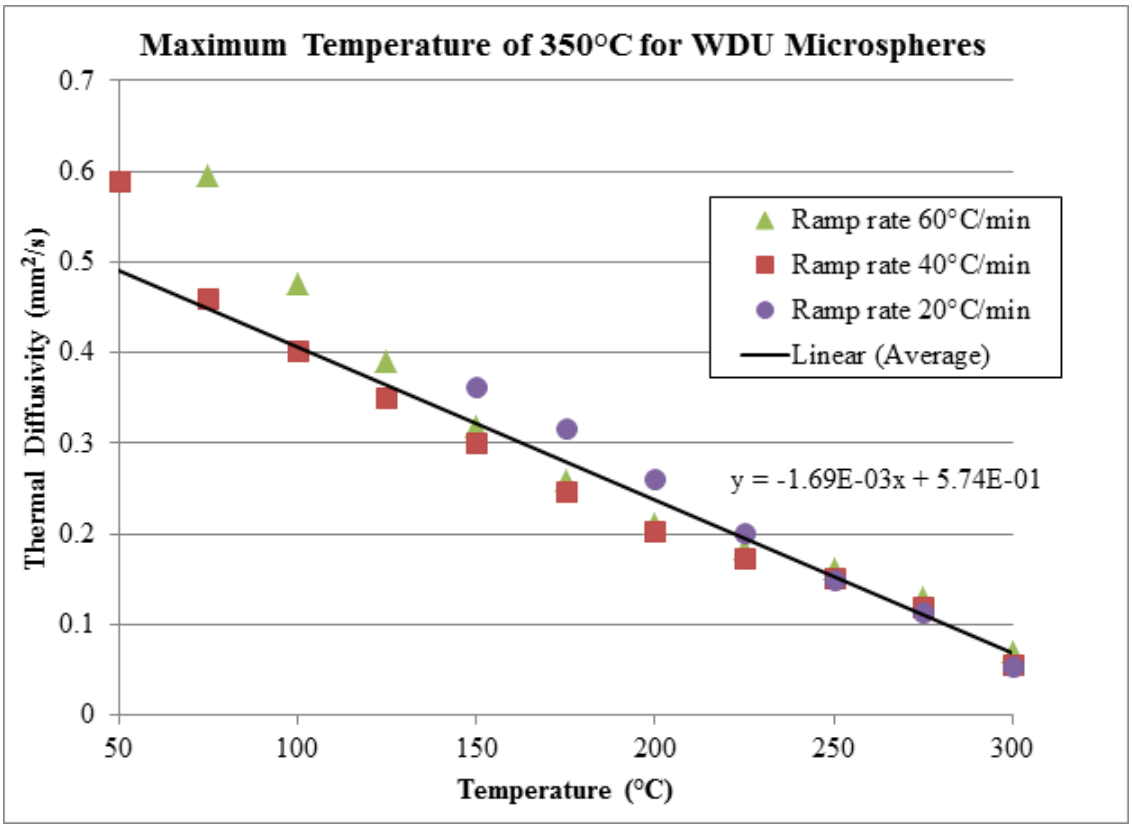

Fig. 5.8. WDU data for maximum temperature of 350°C (Series B, Tests 2, 5, and 9).

data sets was calculated from 125°C to 375°C and was used to create a linear trend-line for the thermal diffusivity. These data sets are presented in Fig. 5.9.

A greater variation of calculated thermal diffusivity data was observed in the cases with a maximum temperature of 550°C (Series B, Tests 7, 8, and 11). Three different data runs were completed with this maximum temperature and ramp rates of 20, 40, and 60°C/min with an initial hold temperature of 50°C. It appeared that data began to converge around 275°C. In the 20°C/min ramp rate case, the calculated thermal diffusivity did not follow the same trend as the other ramp rates and the shape of the curve is significantly different. An average value of thermal diffusivity was calculated from the three data runs for 200 to 475°C and was fitted with a linear equation of

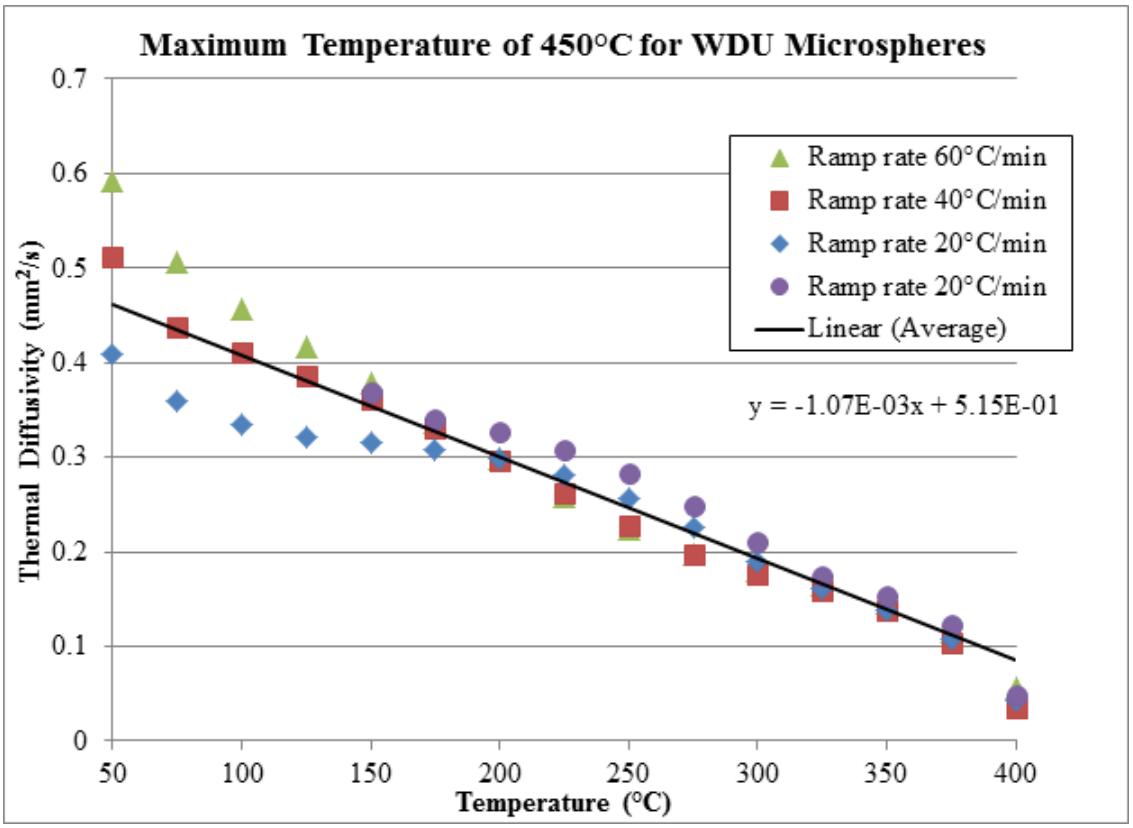

Fig. 5.9. WDU data for maximum temperature of 450°C (Series B, Tests 3, 4, 6, and 10).

best fit. The data collected for a maximum temperature of 550°C is presented in Fig. 5.10.

The highest maximum temperature tested was 650°C with programmed ramp rates of 20, 40, 60, and 200°C/min (Series B, Tests 12, 13, 14, and 15). In the case of the ramp rate of 200°C/min, the cartridge heater consistently maintained a ramp rate of 150°C/min instead of the desired 200°C/min (see Fig. 4.2). At low temperatures, the calculated thermal diffusivity decreased with slower ramp rates; the thermal diffusivity from the 150°C/min ramp rate was consistently higher than all others. Convergence of data runs occurred in order of ramp rate as well; for example, the 60°C/min ramp rate data converged with the 150°C/min data run

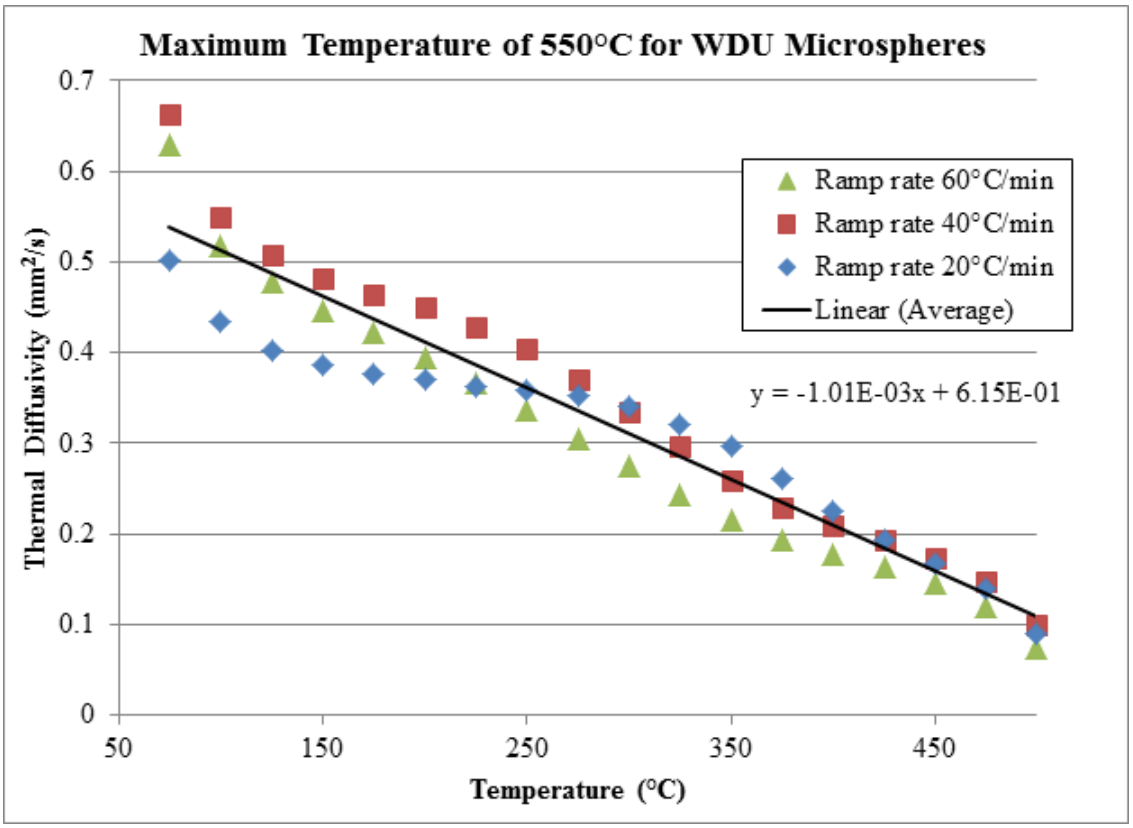

Fig. 5.10. WDU data for maximum temperature of 550°C (Series B, Tests 7, 8, and 11).

before the 40°C/min data run. With the exception of the 20°C/min data run, all data sets converged by 250°C; the 20°C/min ramp rate converged with the rest of the data sets at 325°C. The average thermal diffusivity was calculated from 150°C to 600°C to determine a line of best fit. All data from this series of testing is presented in Fig. 5.11.

As mentioned previously in the description of each of the maximum temperature series, a linear trend-line was fit to the average calculated thermal diffusivity for each data series. The corresponding equations for each line of best fit were extrapolated and plotted for the range of 0°C to 800°C; presented as Fig. 5.12. Vertical dashed lines depict the temperature region to which the line was originally fit. A note-

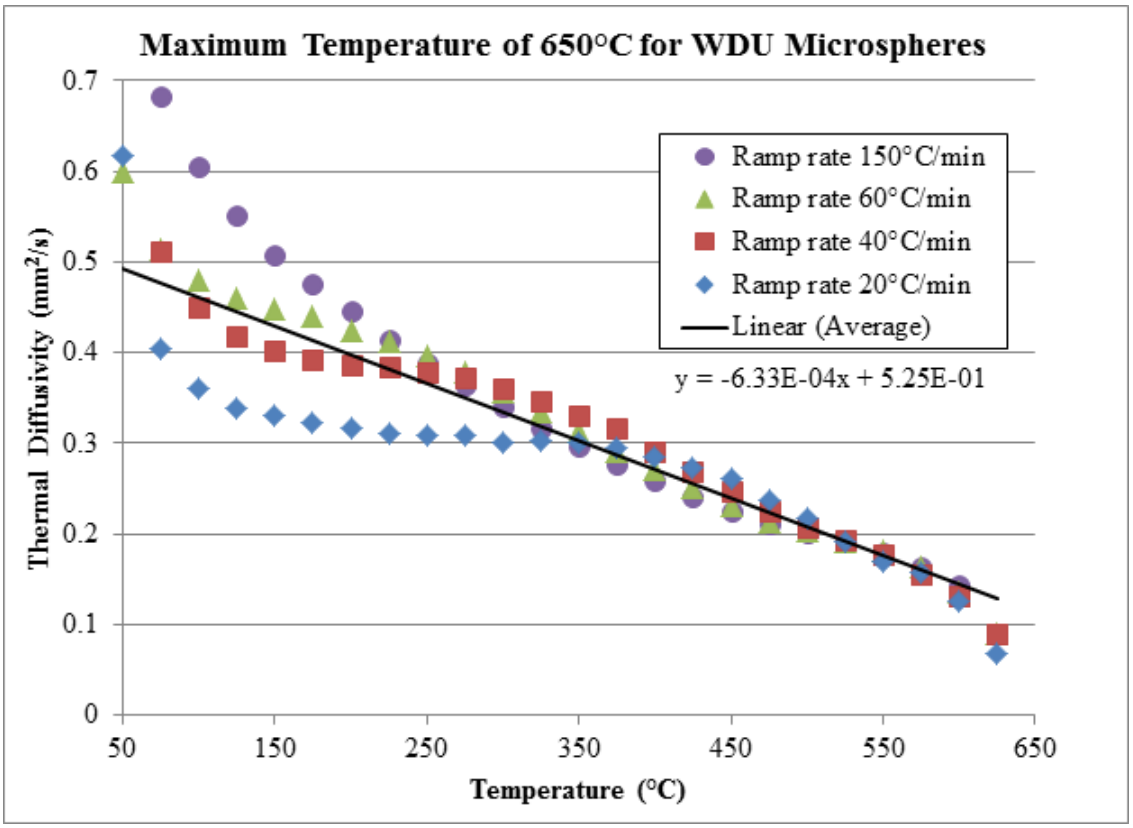

Fig. 5.11. WDU data for maximum temperature of 650°C (Series B, Tests 12 to 15).

worthy effect, depicted predominately with the lower temperature series, was that the thermal diffusivity was expected to go to zero near the maximum temperature peak. This was exemplified by the 350°C maximum temperature data series, the thermal diffusivity was extrapolated to zero at 350°C based upon the equation of the line of best fit. Intersection of lines indicates an agreement in the expected thermal diffusivity; a situation that rarely occurs.

A comparison of a constant 20°C/min ramp rate with different maximum temperature is illustrated in Fig. 5.13. The first test run with a maximum temperature of 350°C was the first run completed with the WDU and, as a result, shows an abnormal spike in thermal diffusivity resulting from the formation of an oxide layer.

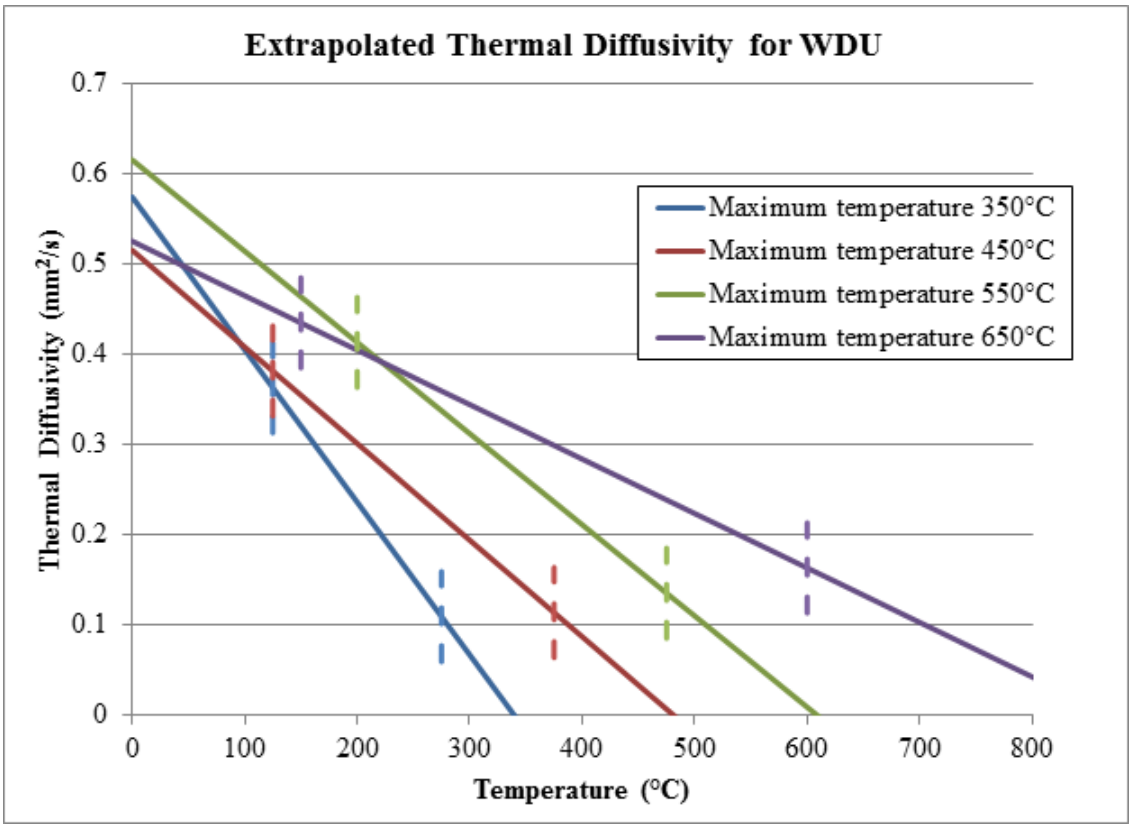

Fig. 5.12. Extrapolated thermal diffusivity for WDU.

The other four data runs presented show a steep downward initial plummet followed by a plateau region which then leads to a gradual decrease in thermal diffusivity (Series B, Tests 1, 2, 3, 4, 7, and 12). The initial plummet appears to be an edge effect caused by the initiation of the cartridge heater. It is within the downward slope region at the higher temperatures that previous data has suggested the true thermal diffusivity values lie; which creates a significant issue in that the values of thermal diffusivity for a specific temperature do not agree.

Similar to the 20°C/min ramp rate scenario, data collected for a ramp rate of 60°C/min with different maximum temperature settings predicted different thermal diffusivity values; shown in Fig. 5.14 (Series B, Tests 9, 10, 11, and 14). As seen in the 20°C/min scenario, there was an initial plummet in thermal diffusivity, which led

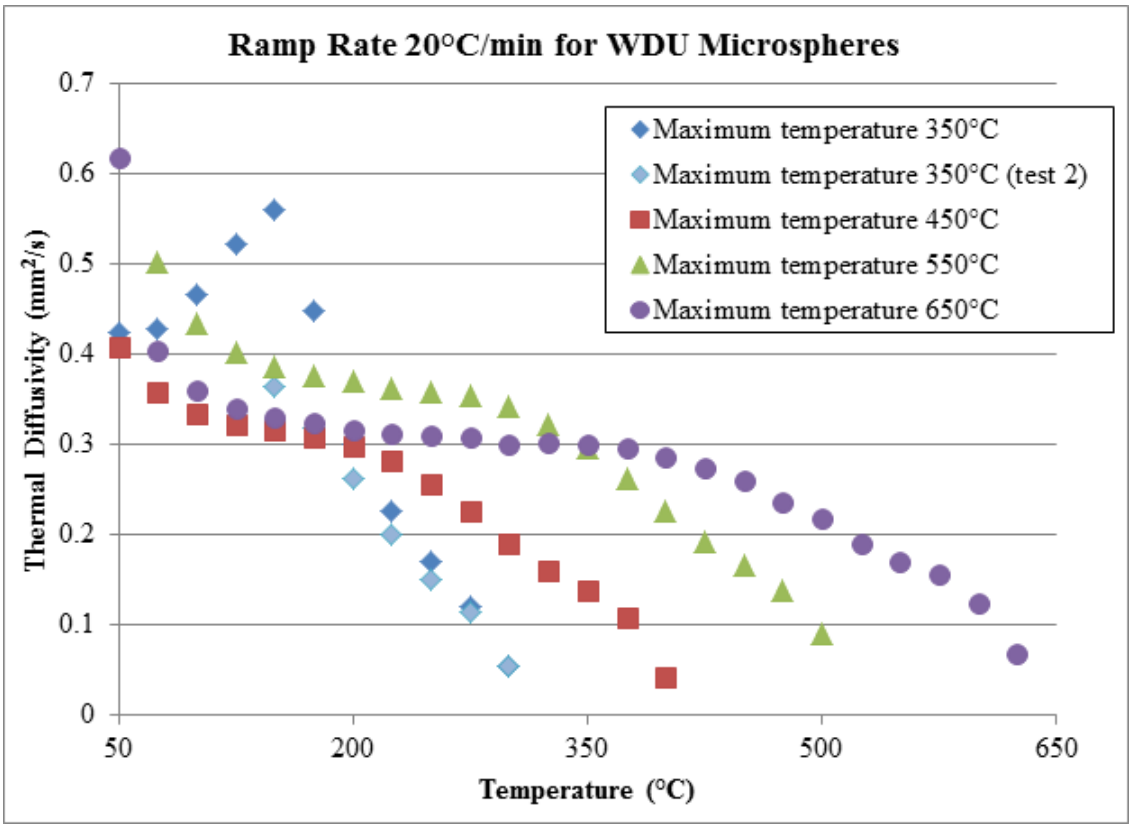

Fig. 5.13. WDU data for a ramp rate of 20°C/min (Series B, Test 1, 2, 3, 7, and 12).

directly into a gradual descent and seemed to end in a sharp drop-off at the highest temperature for each data run. As the ramp rate increased, a higher thermal diffusivity was calculated for any given temperature during the gradual descent portion of the data run.

As discussed in Section 3.2.4, the error inherent to the apparatus was approximately ±13%. This was applied to the data from the test run with a maximum temperature of 650°C and a ramp rate of 150°C/min (Series B, Test 15). Fig. 5.15 shows the data previously presented in Fig. 5.11 with error bars.

Several factors were considered in the setup for Series B; the ramp rate of the cartridge heater and the maximum temperature of the cartridge heater were the two

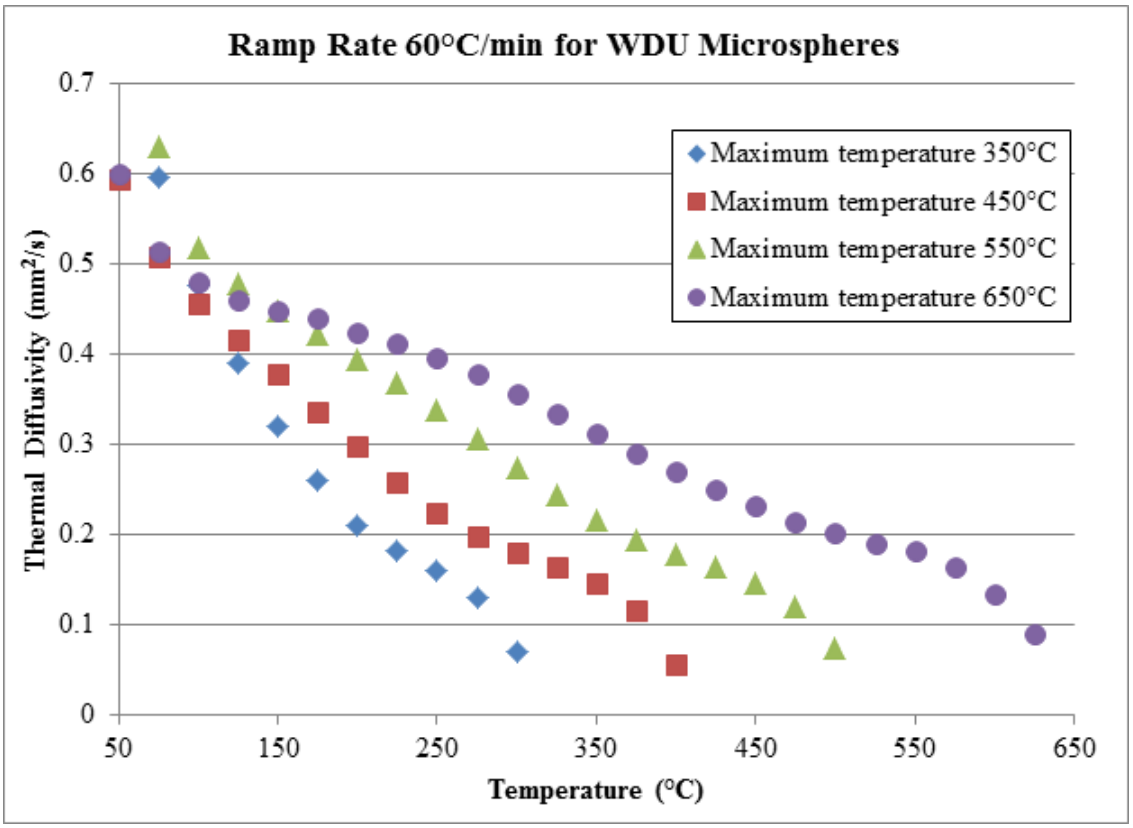

Fig. 5.14. WDU data for a ramp rate of 60°C/min (Series B, Test 9, 10, 11, and 14).

key issues. Data collected showed a wide range in thermal diffusivity dependent upon both of these settings. The highest calculated thermal diffusivity resulted from the fastest ramp rate and the greatest maximum temperature; similarly, the lowest calculated thermal diffusivity resulted from the slowest ramp rate and the lowermost maximum temperature. Equations of best fit produced for each of the maximum temperature series were not in good agreement for predicting extrapolated thermal diffusivity values. This discrepancy was amplified with the comparison of a constant ramp rate to differing maximum temperatures.

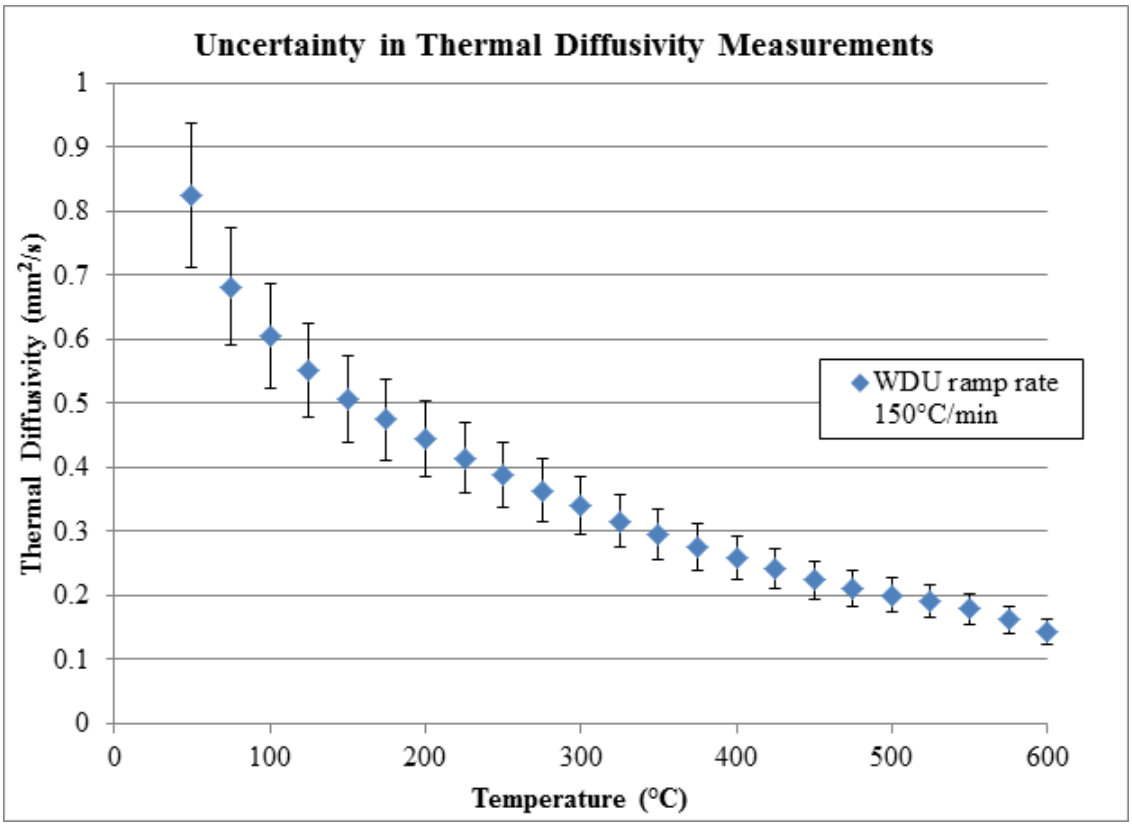

Fig. 5.15. Uncertainty in thermal diffusivity measurement (Series B, Test 15).

5.2.4 Comparison of ODU and WDU Data from the CHTA Method

Analysis of the data collected in the ODU runs indicated that there was an apparent "knee" (i.e. slope change) in the measured thermal diffusivity. This knee varied in placement depending upon both the maximum temperature and the ramp rate of the cartridge heater. It was determined that the equation used for analysis was valid only when a constant temperature hold (phase 2 of the transient discussed in Section 3.2.3) was in effect since it takes no account of the heat flux into the sample. It seems likely, then, that the lower portion of the knee contained the most accurate estimations of thermal diffusivity. The upper portion of the knee was during the heating time of the cartridge heater. Based upon this observation, it was

determined that the quickest ramp rate possible would produce the most accurate results in order to quickly reach the lower knee portion.

Since the data during the cartridge heater ramping time was deemed to be inaccurate, the maximum temperature needed to be set higher to broaden the thermal diffusivity temperature range. The temperatures selected were 350 and 450°C, for comparison to the ODU data, and, 550 and 650°C to optimize thermal diffusivity ranges. With the higher maximum temperature and ramp rate, the linear post-knee region of the thermal diffusivity calculation was extended; an indication that the accurate data range increased.

A linear trendline was calculated and applied to the post-knee data for data sets with the same maximum temperature and like-material (see **??**, **??**, **??**, **??**, **??**, and **??**). The linear equation describing the line was determined and plotted for each data set. When compared, the maximum cartridge heater set-point consistently resulted in a higher thermal diffusivity value; an issue which proves to be quite problematic. Essentially, during the comparison of different data sets for the same material, four different values of thermal diffusivity were predicted at any given temperature. For example, at 200°C, the thermal diffusivity predicted by the linear equation for the 350°C set was different than that from the 450, 550, and 650°C sets; none of the sets agreed on a single value of thermal diffusivity. It was conjectured that the best estimate for thermal diffusivity resulted from the highest maximum temperature because the data set was the most comprehensive and minimized edge effects. There were two key edge effects in play: the period of time in which the cartridge heater was ramping and the period of time after the innermost thermocouple had reached thermal equilibrium with the cartridge heater resulting in no net change. The thermal diffusivity calculation seemed to be only accurate after the source of the wave had steadied (not during the transient heating stage) and before the wave flattened at the innermost thermocouple.

Over time, the radial temperature profile of the system was designed to equalize. This indicates that, by design, the innermost thermocouple will eventually achieve thermal equilibrium with the cartridge heater. However, this was achieved by the innermost thermocouple well before the outer thermocouples. When a steady-state is achieved by the innermost thermocouple, the thermal diffusivity calculation method is no longer valid. This is because the innermost thermocouple exists at a steady-state while the outermost thermocouples remains in a transient-state. The derived analysis method only functions when both the innermost and outermost measurement points are experiencing transients.

Also, during the heating stage, the greatest discrepancy between the thermal diffusivity calculations of the three ramp rates was noticed. The quickest ramp rate, 60°C/min, consistently produced a higher calculated thermal diffusivity during the cartridge heater ramping period. This indicated that the data obtained during this time period was not valid; as previously suspected. As time, and subsequently temperature, increased, the thermal diffusivity calculations converged; data from 60°C/min converged with data from 40°C/min before finally converging with data from 20°C/min. After the data sets converge, they closely follow nearly identical behavior. This was the point in time at which the linear trend was strongly observed. After thermal equilibrium had been achieved between the cartridge heater and the innermost thermocouple, the calculated thermal diffusivity decreased rapidly and approached zero. This was due to the difference in state between the innermost and outermost thermocouples (i.e. steady-state versus transient-state).

When the equations defined by the maximum temperature data sets were compared between the ODU and WDU data series, the trends displayed for the same maximum temperature were nearly identical. This indicated a comparable level of oxidation on the microspheres. Since results for the ODU and WDU were extremely similar, regardless of history, this suggested two main possibilities; either the microspheres oxidized very rapidly with the formation of a quick oxygen passivation layer

or, any oxidation on the surface of the microspheres drastically reduced the thermal diffusivity. One possible explanation is that the thermal energy may traverse solely through the microsphere circumference in the oxygen passivation layer instead of through the diameter of the microsphere. Since the concentration of oxygen within the glovebox was monitored, it was evidenced that the oxygen level did not rapidly decrease.

Upon comparison of the ODU microspheres to the WDU microspheres, it was apparent that oxidation must have occurred within the first test run of the WDU. Data from the first test run showed a dramatic spike in thermal diffusivity followed by a rapid descent. After the descent, the thermal diffusivity was slightly higher than that of the microspheres before the nitric acid washing step.

During the first run with the WDU microspheres, a sharp initial peak was noticed in the data. The maximum of this peak occurred at 150°C. In accordance with the test plan, the first two tests in Test Series B were both at a maximum temperature of 350°C with a ramp rate of 20°C/min, however, test 1 began at 30°C and test 2 began at 125°C to mimic the testing of the ODU. Data from these two test runs is presented in Fig. 5.16, along with the 350°C maximum temperature, 20°C/min ramp rate test (Series A, Test 5) with ODU. At all temperatures, the calculated thermal diffusivity from the WDU was greater than that obtained from the ODU test. By 200°C, the initial drop-off evidenced in the first WDU test run had subsided and the data nearly converged with the calculated thermal diffusivity of both the other WDU and ODU tests. In test 2, the thermal diffusivity was continuously calculated to be a value less than that determined from test 1 but greater than that from the ODU test run. Combining these observations led to the conclusion that minor oxidation must have occurred during the first WDU test but the level of oxidation may still have been reduced to less than that of the original ODU microspheres.

In the case of a maximum temperature of 450°C, the WDU tests were consistently slightly higher than the ODU test. All of the data sets seemed to follow the same

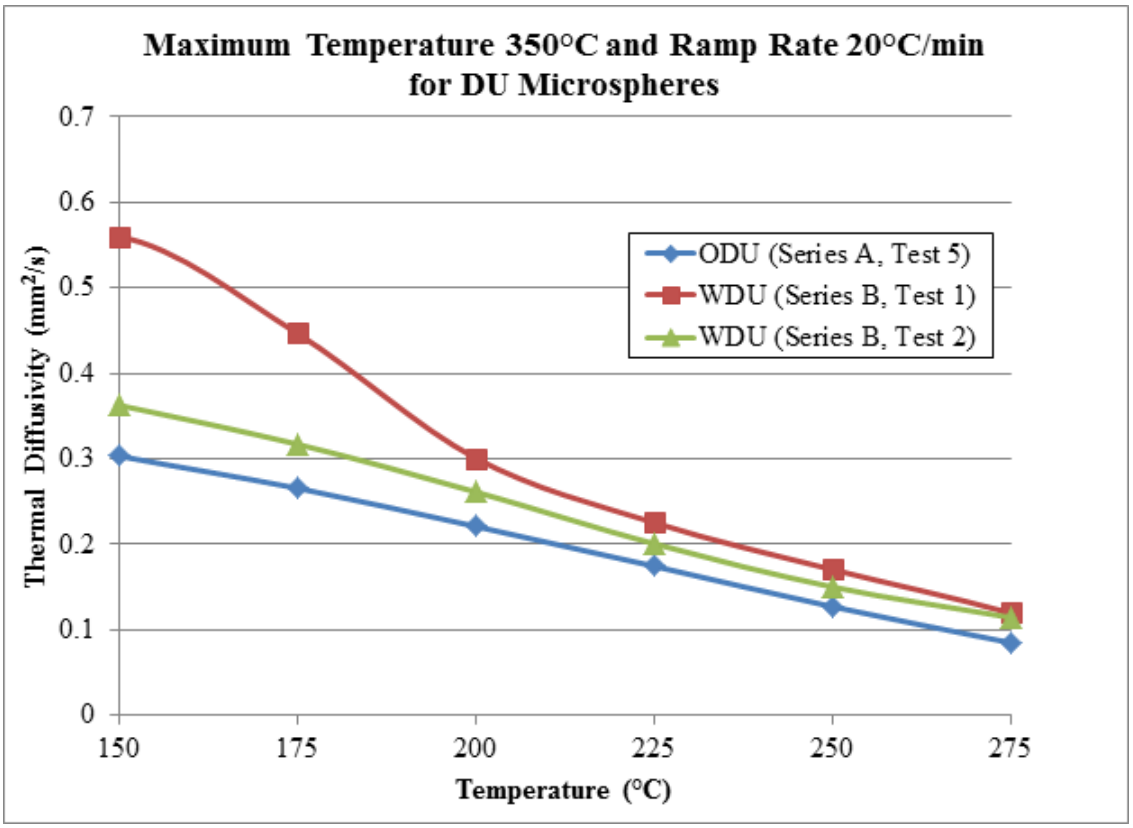

Fig. 5.16. WDU and ODU data for a maximum temperature of 350°C (Series A, Test 5 and Series B, Tests 1 and 2).

trend. The only difference between the two WDU data runs was the initial start temperature; one of which was 30°C and the other was 125°C. The case of 125°C was completed to allow direct comparison between the WDU and ODU using identical heater parameters. Data is presented in Fig. 5.17.

From the previous sections on the separate results of ODU and WDU, equations representing the line of best fit were formulated. These equations were compared for the 350°C and 450°C tests with ODU and WDU. The extrapolated thermal diffusivity values are presented from 0°C to 500°C in Fig. 5.18. Nearly all lines intersect at 100°C. Lines tended to go to zero thermal diffusivity at the maximum temperature programmed for the cartridge heater; i.e. the 350°C data series predicted a ther-

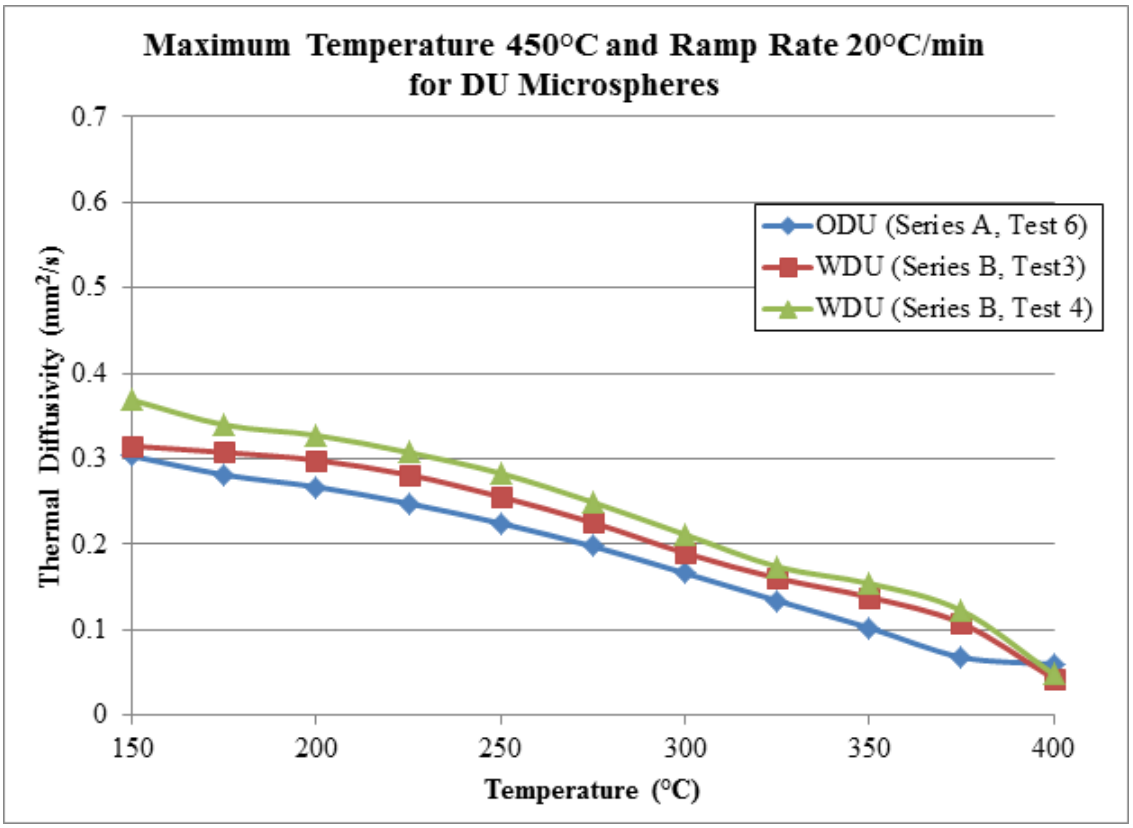

Fig. 5.17. WDU and ODU data for a maximum temperature of 450°C (Series A, Test 6 and Series B, Tests 3 and 4).

mal diffusivity of 0.00 mm^2/s between 300°C and 350°C; which reveals a physical impossibility.

5.2.5 CHTA Challenges

With the CHTA, it was difficult to determine which thermal diffusivity calculations were valid due to significant edge effects and the variations between data generated at different thermal fluxes. This was illustrated through the problematic characteristic that as the maximum temperature setting increased, so did that thermal diffusivity calculation. Additionally, since the CHTA analysis method was only valid during the second transient phase, it was best to have a very quick, high-

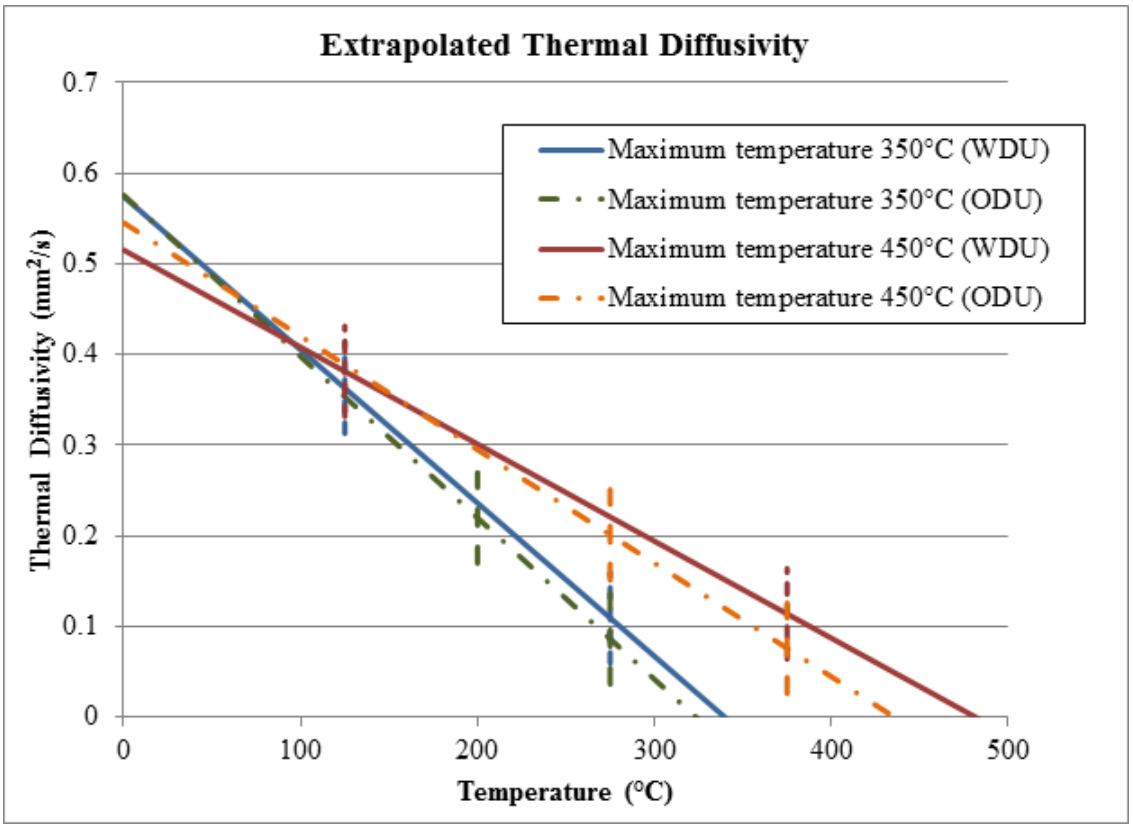

Fig. 5.18. Extrapolation of data from ODU and WDU test cases.

temperature pulse from the cartridge heater compared to a gradual temperature increase. The key recommendation for future work with a CHTA-type system was to ramp the cartridge heater to a high maximum set point temperature at the quickest ramp rate possible. For the cartridge heater selected in this study, those values were 150°C/min and greater than 650°C.

Future studies could eliminate the band heater and instead simply use a secondary containment system. The yttrium oxide crucibles selected in this study were quite fragile and tended to break in nearly every test run. An alternate crucible selection is recommended. Crucible selection should be based upon thermal characteristics of the material; metals may be problematic due to increased heat transfer and may skew the outermost thermocouple readings. It was suggested that a more durable ceramic

crucible may be desirable to act as insulation to the system and minimize radial heat loss; this may simply mean a yttrium oxide crucible with a thicker crucible wall.

5.3 Comparison of CHTA to LFA

Shown in Fig. 5.19 is a chart of calculated thermal diffusivity values for the ODU microspheres based on the CHTA and LFA methods. The data available to form a comparison between the LFA method and the CHTA method was very limited in this study since the LFA sample holder proved ineffective. Since the ODU seemed to undergo significant oxidation within the LFA resulting in shattered sample holders, data was only collected from room temperature up to 200°C. With the CHTA, this was frequently the temperature range in which the cartridge heater was ramping to the set point so calculated thermal diffusivity was less reliable. However, when the two data sets were compared, it was determined that the thermal diffusivity average of the two LFA samples was within approximately 10% that of the CHTA for the temperatures available. This temperature range was within the CHTA ramping zone, a region in which considerable edge effects were noticed.

5.4 Thermal Conductivity Calculations

Using the interpolated density presented in Fig. 2.2, in combination with the extrapolated specific heat shown in Fig. 2.1, the thermal conductivity of the WDU microspheres was calculated using the measured data in the previous section. The thermal diffusivity values used were those obtained with the 150°C/min ramp rate with a maximum temperature of 650°C. Thermal conductivity was calculated using the relation $k = \alpha \rho c_p$. Thermal conductivity of the WDU microspheres exhibited a decreasing trend as temperature increased. The density was scaled to consider an estimated packing factor of 70%, accomplished by multiplying the temperature-

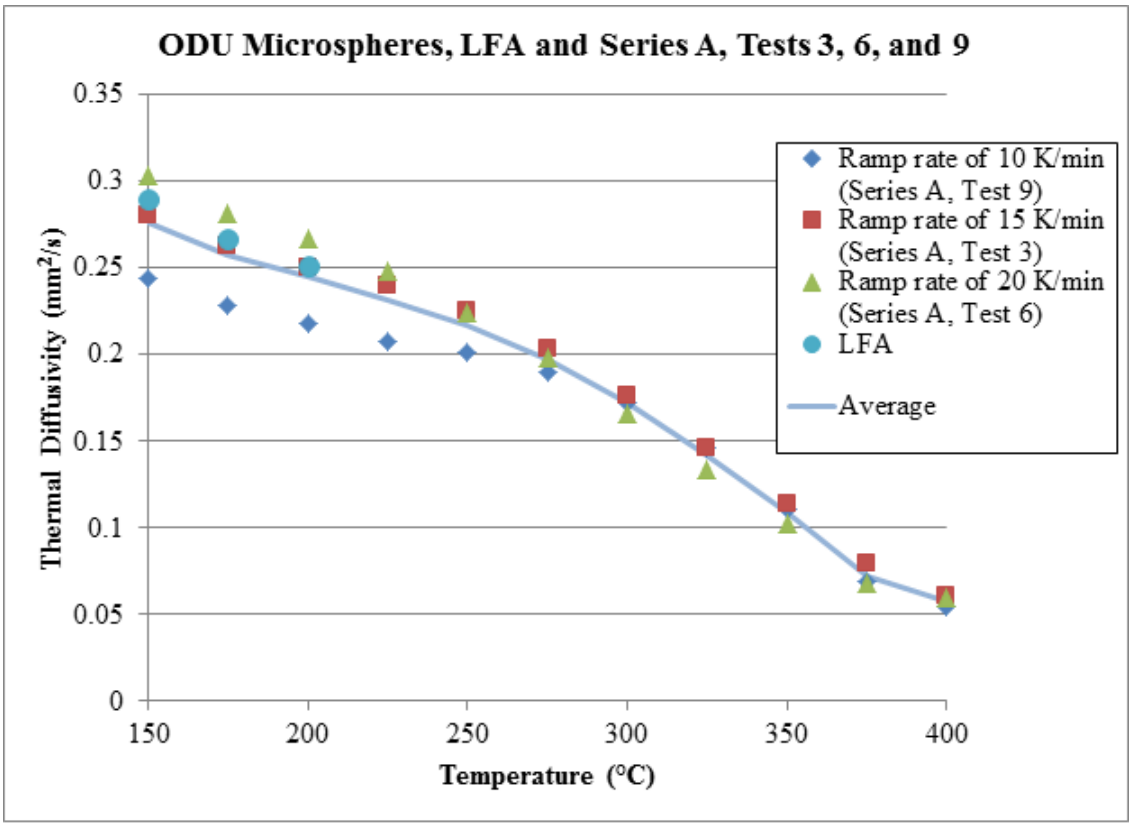

Fig. 5.19. Comparison of data from the CHTA and LFA methods.

dependent density by a constant factor of 0.7. These values are presented in Table 5.1 and depicted in Fig. 5.20.

Thermal conductivity values for uranium metal microspheres and uranium dioxide microspheres [29] are compared in Fig. 5.21. Reference data for the thermal conductivities of solid uranium metal [13] and uranium dioxide [35] are presented in Fig. 5.22.

5.5 Thermal Conductivity Interpretation

Thermal diffusivity values used in the calculation of thermal conductivity were obtained from the 150°C/min ramp rate and 650°C maximum temperature because

Table 5.1
Key thermal properties of WDU microspheres (Series B, Test 15).

Temperature (°C)	Thermal Diffusivity (mm^2/s)	Density (g/cm^3)	Specific Heat (J/g/K)	Thermal Conductivity (W/m-K)
175	0.475	18.9	0.128	0.804
200	0.446	18.8	0.131	0.771
225	0.414	18.8	0.134	0.731
250	0.388	18.7	0.137	0.698
275	0.364	18.7	0.140	0.669
300	0.341	18.7	0.143	0.638
325	0.316	18.6	0.146	0.603
350	0.296	18.6	0.149	0.575
375	0.277	18.5	0.152	0.547
400	0.259	18.5	0.155	0.521
425	0.242	18.4	0.158	0.494
450	0.225	18.4	0.161	0.467
475	0.212	18.4	0.164	0.448
500	0.201	18.3	0.167	0.431
525	0.192	18.3	0.170	0.419
550	0.179	18.2	0.173	0.396
575	0.163	18.2	0.176	0.365

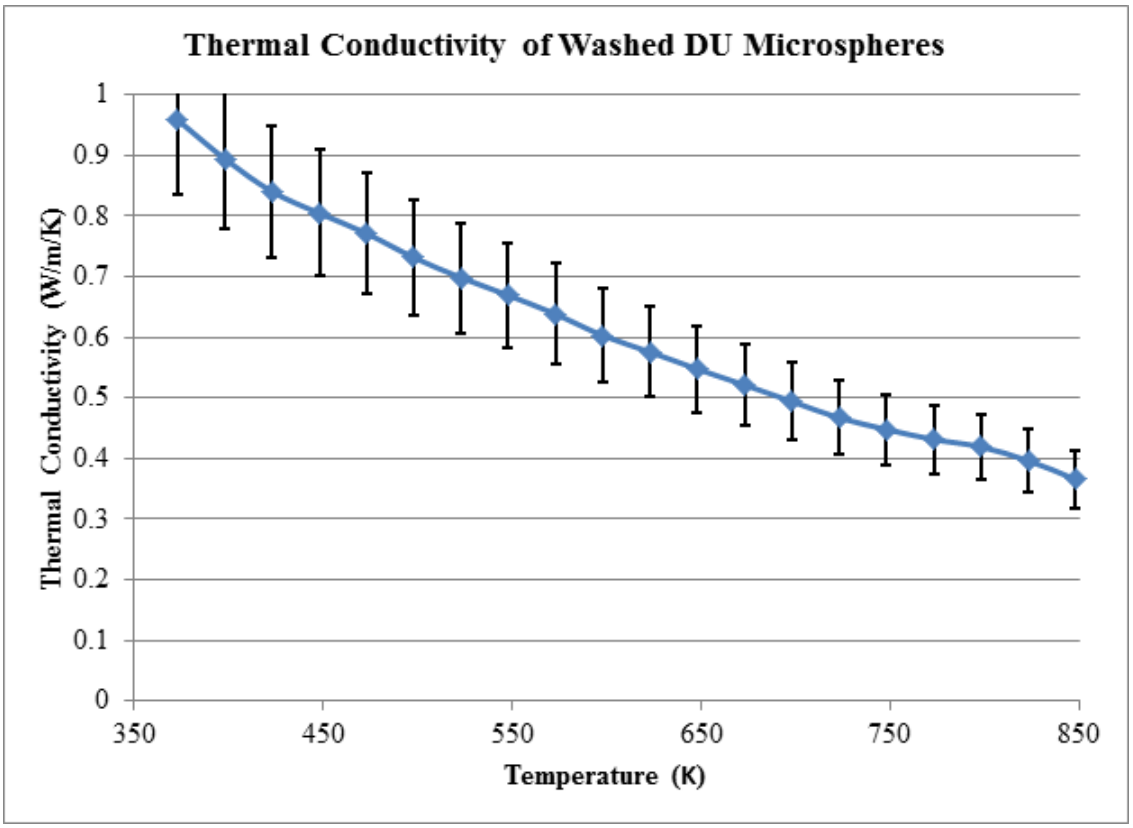

Fig. 5.20. Calculated thermal conductivity of WDU microspheres (Series B, Test 15).

this test likely had minimal edge effects. Both LFA samples measured had packing factors between 72 and 76%; for this reason, a packing factor of 70% was assumed for the samples in the CHTA. Additionally, literature [10] suggested that the density of uranium decreased at a rather linear rate between room temperature and the melting point (1132°C); due to this, a linear interpolation was utilized for determining the temperature-dependent density of the sample. Additionally, within the temperature range analyzed, specific heat followed a nearly linear trend and an extrapolation and interpolation combination from literature values [11] was utilized to determine the temperature-dependent specific heat.

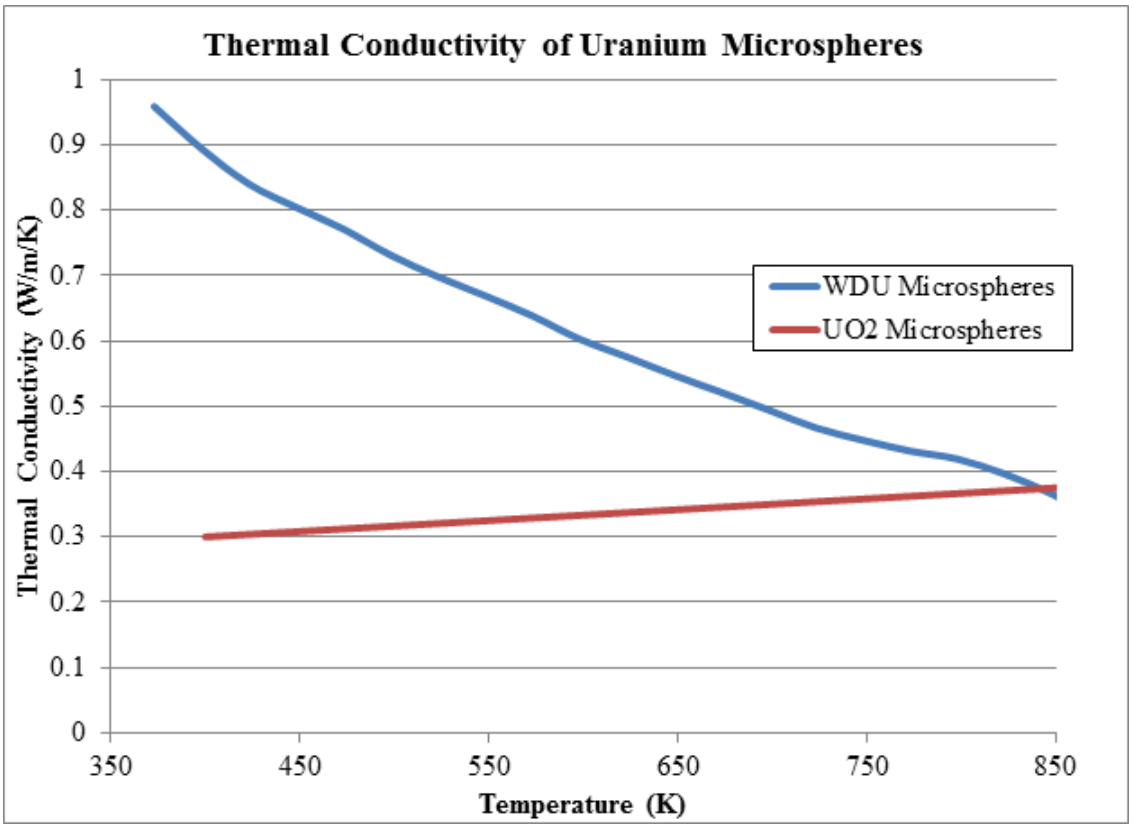

Fig. 5.21. Thermal conductivity of WDU and UO_2 [29] microspheres.

The resulting thermal conductivity was significantly lower than an unirradiated UO_2 pellet; at 600 K the UO_2 pellet had a thermal conductivity of about 5 W/m-K [36] while the WDU microspheres had a thermal conductivity of about 0.65 W/m-K. For packed microspheres of UO_2, the thermal conductivity of 200 μm spheres at 600 K in argon was approximately 0.3 W/m-K [30]; for the same microspheres this jumped to 1.1 W/m-K in helium. The U metal microspheres tested throughout this work were always minimally packed in an argon atmosphere. If the packing fraction was increased or the fill gas or liquid was changed, the effective thermal conductivity may increase significantly.

In ceramics, thermal conductivity is expected to decrease with temperature due to phonon heat transfer and the impedance of phonon vibrations with increased tem-

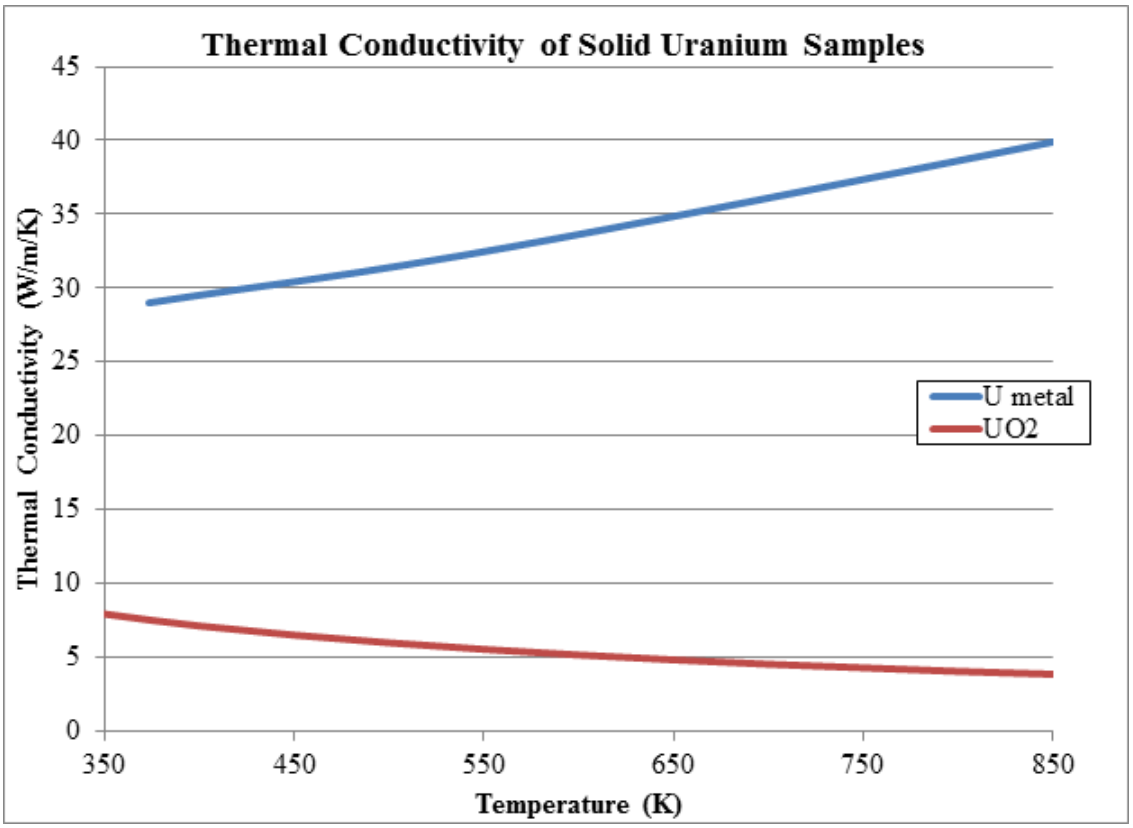

Fig. 5.22. Thermal conductivity of solid U metal [13] and UO_2 [35].

perature. In metals, the scenario is complicated due to contributions from electron-electron and electron-phonon heat transfer modes. At low temperatures, electron-electron heat transfer is the dominant mode of heat transfer for metals. However, as temperature increases electron-phonon interactions can increase for metals which causes a reduction in thermal conductivity. The effects of electron-electron and electron-phonon interactions are in competition with one another to produce either a downward or upward thermal conductivity trend. For these metal microspheres, it is not surprising that a downward trend in thermal diffusivity was noticed due to surface effects on the microspheres and electron-phonon interactions.

5.6 Error Sources

Primary sources of error may have resulted from either measurement of thermal diffusivity, determination of density and specific heat values, estimation of the packing factor or sample loading. With the exception of the PID control box, all equipment was calibrated by the manufacturer. The PID controllers were auto-tuned to the appropriate heater (either the band or cartridge heater dependent upon the port), additionally, settings were changed to control the high temperature limit and ramping method. The data logger was calibrated and certified by the manufacturer for type K thermocouples. The type of thermocouple, crucible, insulation, stainless steel, and activated channels on the data logger remained constant throughout all test runs. Two different cartridge and band heaters were used throughout the study and were differentiated between in notes. There was no noticeable difference between results for the different heaters.

The density and specific heat values used in calculation were based upon literature values with a linear interpretation between available data points. Prior literature suggested that these properties had a linear trend at temperatures below the melting point of uranium. This linear assumption may have resulted in an unquantifiable error. The packing factor estimate was based upon the calculated packing factor for the LFA samples which was determined by weighing the mass of the microspheres as they were loaded into a LFA sample holder of known volume.

6. SUMMARY

The findings of this thesis are summarized here as a list with references to sections within the thesis for more information.

- The thermal conductivity of the depleted uranium metal microspheres was of the same order of magnitude as that previously found for comparable UO_2 microspheres. At 750 K, the thermal conductivity of WDU was about 0.45 W/m-K, UO_2 microspheres were about 0.35 W/m-K, solid uranium metal was about 38 W/m-K and monolithic UO_2 was about 4 W/m-K (see Sections 5.4 and 5.5).

- The LFA method posed inadequate for the analysis of depleted uranium metal microspheres. The ODU samples did not react in air until elevated temperatures. Based on data presented in 4.1 and the discussion in 5.1, it is probable that further oxidation began to occur at 150°C. This low temperature data is not satisfactory for characterizing potential nuclear fuel. Low temperature data collected from the LFA for ODU microspheres is in agreement with low temperature data from the CHTA (Section 5.3 and Fig. 5.19).

- A systematic uncertainty of 13% was calculated for the CHTA method of analysis (see Section 5.6). This uncertainty is primarily due to the level of precision in thermocouple placement. Bore holes were drilled with a diameter slightly greater than that of the thermocouple creating issues for precise placement. Uncertainty that can not be quantified is attributed to system assumptions and reference values used in the calculation of thermal conductivity. System assumptions were that thermal energy progressed radially through a sample with a uniform flux, thermal effects from the stainless steel blocks were mitigated by the use of an insulation sheet, and that packing throughout the microsphere sample was uniform. The values used for density and specific heat were based

on sparse reference data and relied on interpolation and extrapolation to obtain data points (see Fig. 2.1 and 2.2).

- During the nitric acid washing procedure, which occurred in a glovebox, the depleted uranium metal microspheres developed either a surface oxidation or nitridation layer. The layer was first noticed while the microspheres were still in the nitric acid wash. The material referred to as WDU did have some surface characteristic and was not pure uranium metal. The ODU microspheres were completely black; WDU was initially a brown-green hue but after testing was noticed to be black. This color change supports the claim that Series B, Test 1 resulted in oxidation on the WDU microspheres (see Fig. 5.16).

- Based on the body of data presented in this thesis, the CHTA produces the most analyzable data with a quick ramp rate and a high maximum temperature. This allows the system to quickly pass through the first transient phase and progress into the second transient phase (see Section 3.2.3). For this reason, the data deemed most accurate from this study is that which resulted from Series B, Test 15 which had a maximum temperature of 650°C with a ramp rate of 150°C/min.

Suggestions for additional testing of the CHTA and uranium metal microspheres are as follows.

- Further investigation should be completed on characterizing the CHTA to determine why different maximum temperatures effect the calculated thermal diffusivity values. It is currently assumed that this is an edge effect due to the reduced range of analyzable data points for tests with a lower maximum temperature. For illustration of the issue, see Fig. 5.7, 5.12, and 5.18.

- Methods to improve the thermal conductivity of uranium metal microspheres are to increase the pressure of the packed bed, change the fluid that fills the

void spaces (for example helium or liquid sodium), and remove surface contamination in a high-purity inert atmosphere.

- Different packing factors of the uranium metal microspheres could also be tested. As the packing factor increases, it is theorized that better contact will result between microspheres thus elevating the thermal conductivity. Microspheres of varying diameters could be used to increase the packing factor.

- A good way to characterize the accuracy of the CHTA may be to use a liquid with known thermal conductivity to establish optimal temperature measurement points. With a solid material, thermocouples would have to be embedded into the sample at specific locations which may prove to further complicate the analysis method.

- Recommended changes to the CHTA include eliminating the outer band heater, adding a secondary containment system, and selecting an alternate crucible type.

REFERENCES

[1] K.L. Peddicord, R.W. Stratton, and J.K. Thomas, Prog. Nuc. Energy, 18, (1986), 265.

[2] L.C. Walters, D.L. Porter, and D.C. Crawford, Prog. Nuc. Energy, 40, (2002), 513.

[3] W.D. Callister Jr., Materials Science and Engineering, An Introduction, 7^{th} Edition, Wiley, 2007, p.41.

[4] A.S. Icenhour, and D.F. Williams, Sphere-pac Evaluation for Transmutation, in: Oak Ridge National Laboratory Report ORNL/TM-2005/41, (2005), p. 3.

[5] J.P. Holman, Heat Transfer 7^{th} Edition, McGraw-Hill, 1990, p. 139.

[6] E.R.G. Eckert, and R.J. Goldstein, Measurements in Heat Transfer, Hemisphere Pub. Corp., 1976.

[7] N. Wakao, and S. Kaguei, Heat and Mass Transfer in Packed Beds, Gordon and Breach, 1982, p. 161.

[8] J.E. Parrott, and A.D. Stuckes, Thermal Conductivities of Solids, Pion Limited, 1975, p. 90.

[9] K.D. Maglic, A. Cezairliyan, and V.E. Peletsky, Compendium of Thermophysical Property Measurement Methods 1, Plenum Press, 1984, p. 299.

[10] I. Iosilevskiy, and V. Gryaznov, J. Nuc. Mat., 344, (2005), 30.

[11] Tables of Physical & Chemical Constants, 2.3.6 Specific Heat Capacities, Kaye & Laby Online. Version 1.0 (2005) `http://www.kayelaby.npl.co.uk`.

[12] Tables of Physical & Chemical Constants, 2.2.1 Properties of the Elements, Kaye & Laby Online. Version 1.1 (2008) `http://www.kayelaby.npl.co.uk`.

[13] Tables of Physical & Chemical Constants, (16^{th} edition 1995), 2.3.7 Thermal Conductivities, Kaye & Laby Online. Version 1.0 (2005) `http://www.kayelaby.npl.co.uk`.

[14] Tables of Physical & Chemical Constants, 3.1.2 Properties of the Elements, Kaye & Laby Online. Version 1.0 (2005) http://www.kayelaby.npl.co.uk.

[15] W.J. Parker, R.J. Jenkins, C.P. Butler, and G.L. Abbott, J. Appl. Phys. 32 (1961) 1679.

[16] P.B. Jacovelli, and O.H. Zinke, J. Appl. Phys. 37 (1966) 4117.

[17] E.L. Woisard, J. Appl. Phys. 32 (1961) 40.

[18] S. Polesek-Karczewska, Int. J. Heat Mass Transfer 39 (2003) 375.

[19] G.S.C Beveridge, and D.p. Haughey, Int. J. Heat Mass Transfer 14 (1971) 1093.

[20] Y. Nagasaka, and A. Nagashima, Rev. Sci. Instrum. 52 (1981) 229.

[21] S.E. Gustafsson, E. Karawacki, and M.N. Khan, J. Phys. D: Appl. Phys. 12 (1979) 1411.

[22] W. Kaminski, J. Heat Transfer 112 (1990) 555.

[23] C. Bai, and A.S. Lavine, Trans. ASME, 117 (1995) 256.

[24] E.F. Jaguaribe, and D.E. Beasley, Int. J. Heat Mass Transfer 27 (1984) 399.

[25] S. Masamune, and J.M. Smithi, I&EC Fundamentals 2 (1963) 136.

[26] S. Yagi, and D. Kunii, A.I.Ch.E J. 3 (1957) 373.

[27] A.B. Duncan, G.P. Peterson, and L.S. Fletcher, Trans. ASME 111 (1989) 830.

[28] M. Bahrami, M.M. Yovanovich, and J.R. Culham, Int. J. Heat Mass Transfer 49 (2006) 3691.

[29] R.O.A. Hall, and D.G. Martin, J. Nuc. Mat. 101 (1981) 172.

[30] R.O.A. Hall, D.G. Martin, and M.J. Mortimer, J. Nuc. Mat. 173 (1990) 130.

[31] R.L. Beatty, R.E. Norman, and K.J. Notz, *Gel-sphere-pac Fuel for Thermal Reactors - Assessment of Fabrication Technology and Irradiation Performance*, in: Oak Ridge National Laboratory Report ORNL-5469 (1979), p. 27.

[32] C. Hellwig, et al., in: Atalante 2004, Nimes, France, 2004, p. O14.

[33] Netzsch Analyzing and Testing, *Thermal Diffusivity - Thermal Conductivity: LFA 447 NanoFlash* [brochure], `http://www.netzsch-thermal-analysis.com/download/LFA447_E_0811w%20(2)_en_180.pdf`.

[34] S.M. McDeavitt, and A.A. Solomon, Ad. in Powder Met. & Par. Mat. 6 (1992) 109.

[35] C.G.S. Pillai, and A.M. George, J. Nuc. Mat. 200 (1993) 78.

[36] C. Ronchi, M. Sheindlin, M. Musella, and G.J. Hyland, J. Appl. Phys. 85 (1999) 776.

APPENDIX A
OPTICAL MICROSCOPE IMAGES OF MICROSPHERES

A.1 WDU Microspheres

After testing was completed, images of the WDU microspheres were taken using a Digital Optical Microscope (HiRox KH-1300 with and MX-5040SZ lens). The microspheres were found to have a diameter of approximately 100 μm instead of the 250 μm originally anticipated. Figures A.1, A.2, and A.3 show the microspheres at increasing magnification with a consistent 100 μm scale bar.

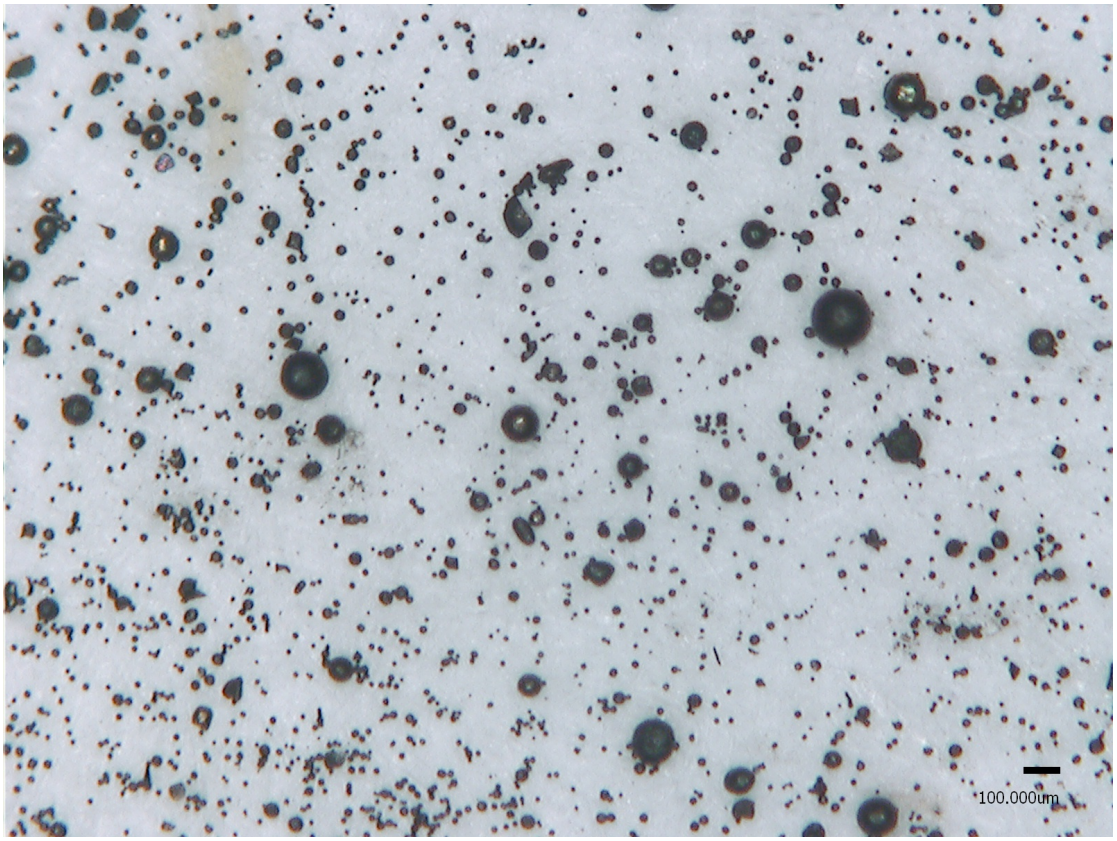

Fig. A.1. Low magnification microscope image of WDU microspheres after testing was completed in the CHTA.

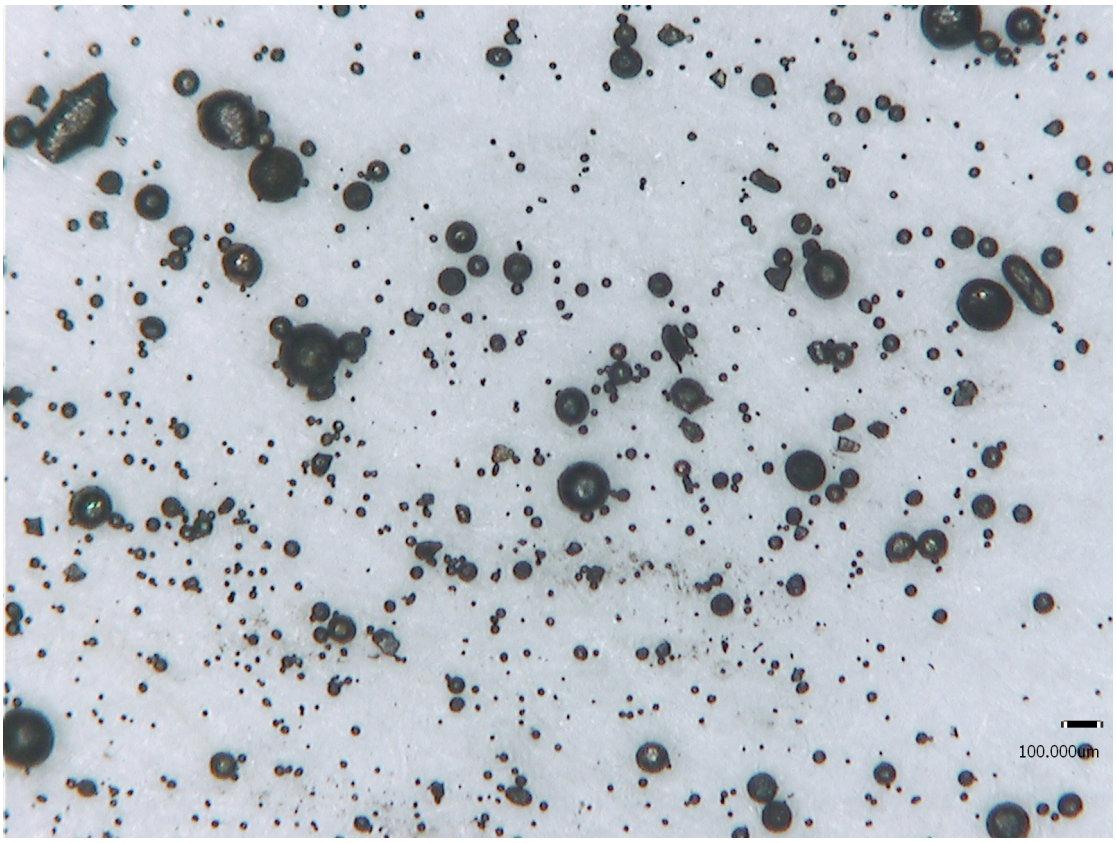

Fig. A.2. Low magnification microscope image of WDU microspheres after testing was completed in the CHTA.

A.2 LFA Microspheres

Images (Fig. A.4 and A.5) were also taken of the microspheres after the failed testing in the LFA. These microspheres show drastic deterioration likely due to oxidation effects.

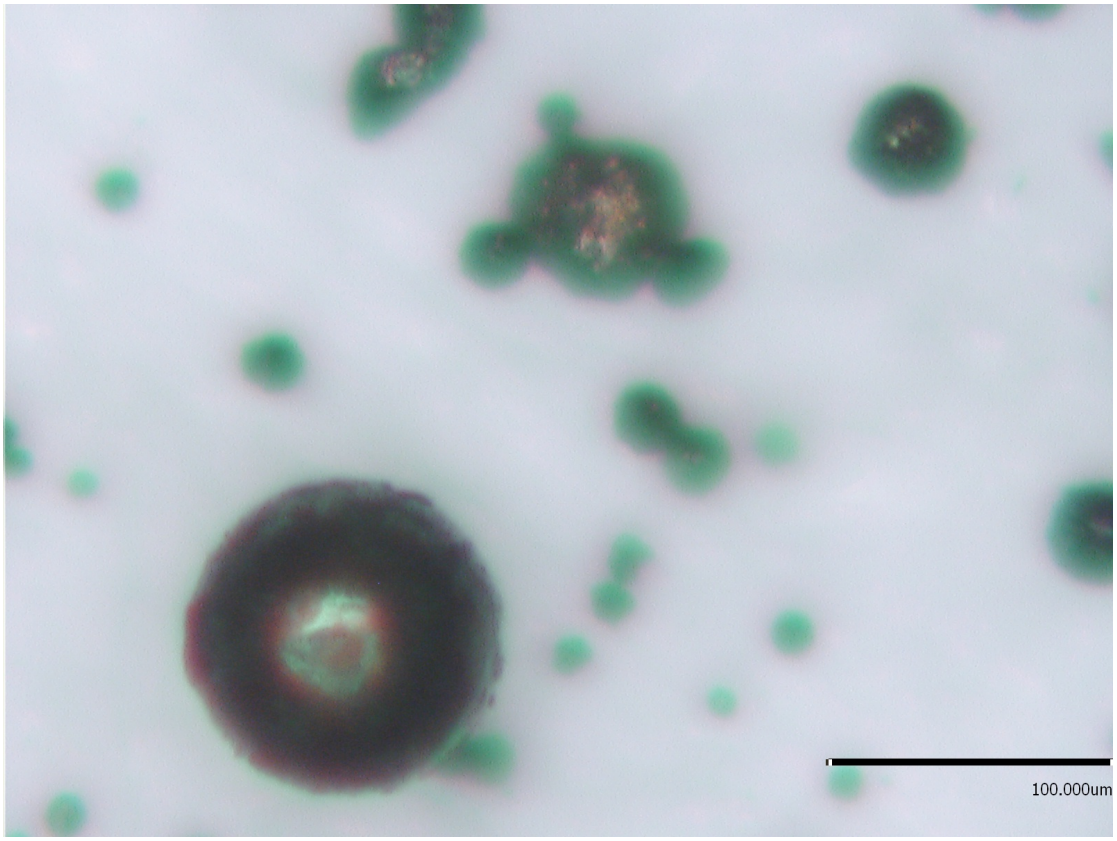

Fig. A.3. High magnification microscope image of WDU microspheres after testing was completed in the CHTA.

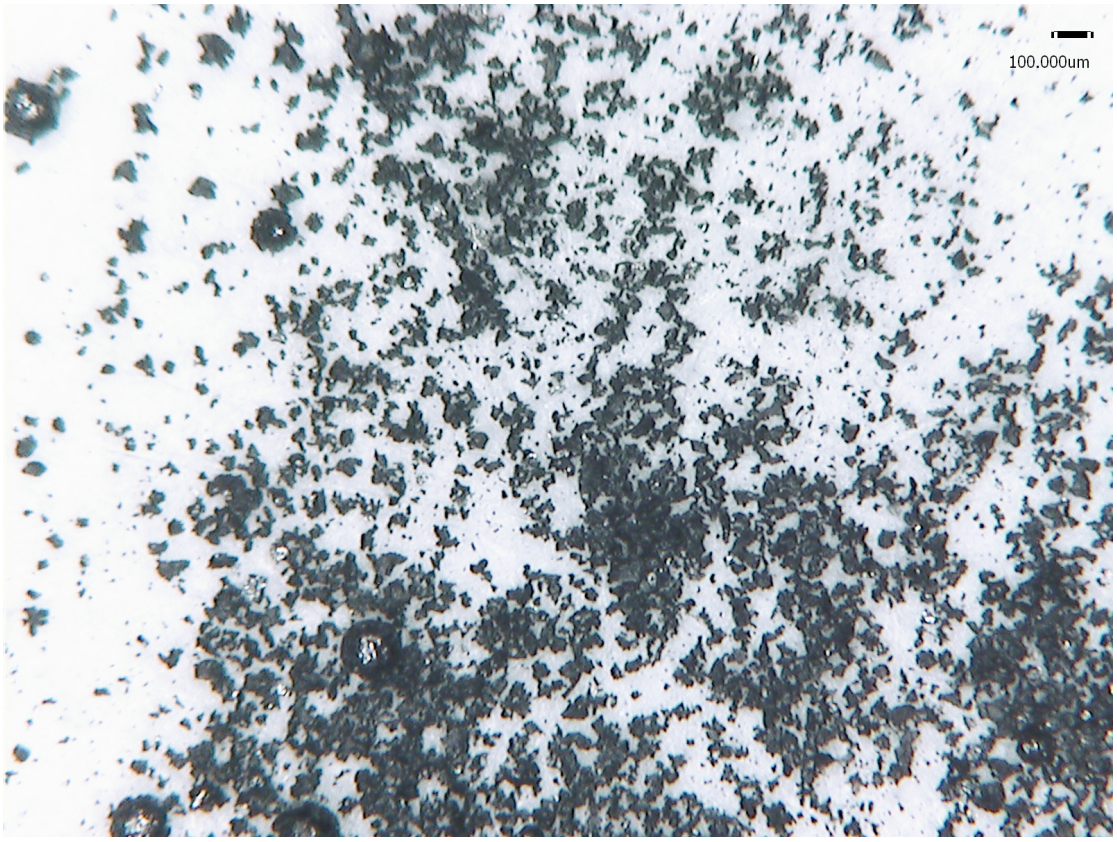

Fig. A.4. Low magnification microscope image of ODU microspheres after testing was completed in the LFA; these microspheres were not used in any further testing.

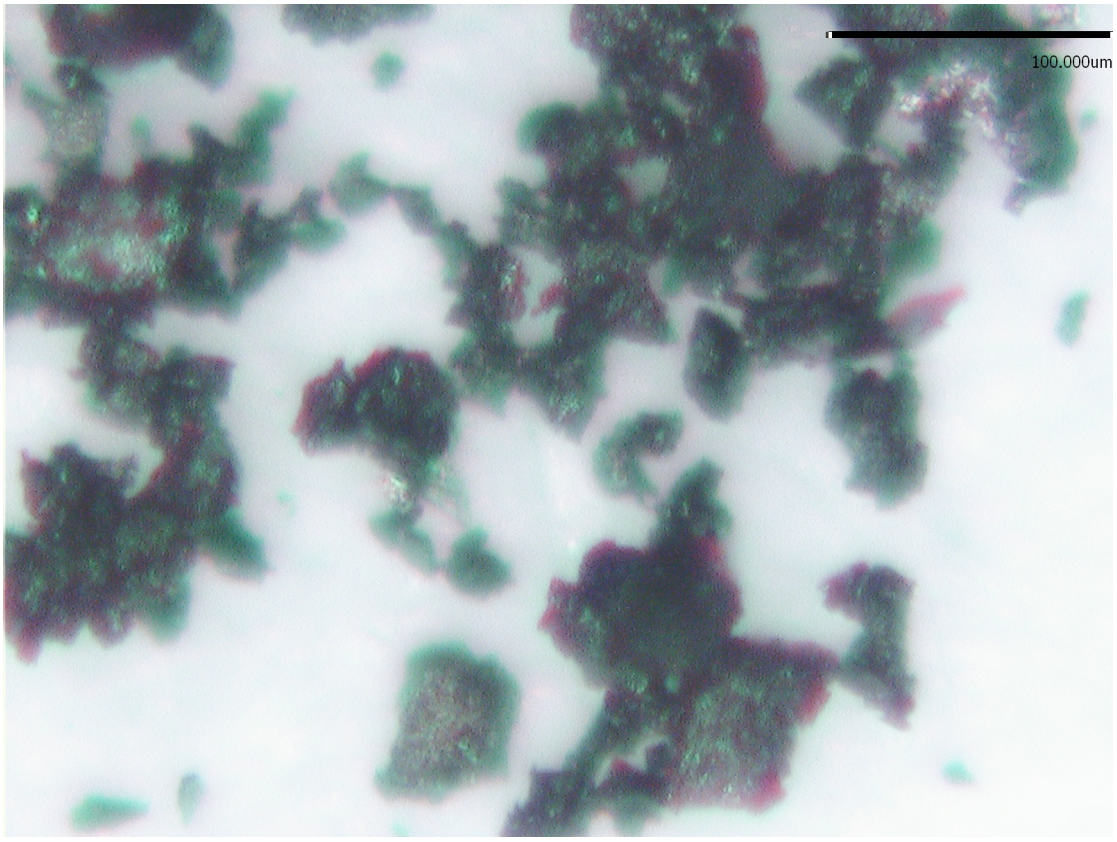

Fig. A.5. High magnification microscope image of ODU microspheres after testing was completed in the LFA; these microspheres were not used in any further testing.

VITA

Carissa Joy Humrickhouse

Texas A&M University, Department of Nuclear Engineering

3133 TAMU, College Station, TX

(509) 961-6614 • c.humrickhouse@gmail.com

Education

Texas A&M University College Station, TX, USA • Master of Science in Nuclear Engineering, 2012 • Cumulative GPA: 3.8/4.0 • Selected Coursework:

Nuclear Engineering Nuclear Materials · Nuclear Fuel Performance · Radiation Interactions & Measurements · Nonproliferation

Whitworth University Spokane, WA, USA • Bachelor of Arts in Physics, 2008 • Cumulative GPA: 3.6/4.0 • Selected Coursework:

Physics Thermodynamics · Quantum Mechanics · Nuclear Physics · Electricity & Magnetism · Electronics · Chemistry

Mathematics Calculus · Linear Algebra · Complex Variables

Work History

Texas A&M University - Department of Nuclear Engineering (2009 - present), ***Graduate Assistant Researcher***

- Research assistant in the Fuel Cycle & Materials Laboratory.

TerraPower, LLC. (summer 2011), ***Nuclear Fuel Cycle Intern***

- Implement ORIGEN, MCNP, and MC**2 to analyze melt refined U-Zr fuel.

Pacific Northwest National Laboratory - Glass Development Laboratory (2008 - 2009), ***Post-Bachelors Research Assistant***

- Conduct laboratory experiments designed to improve nuclear waste vitrification.
- Contribute to research papers published by P. Hrma and M. Schweiger.

Awards

- Golden Neutron Award, ATR NSUF User's Week, June 2011.